CONTRACTOR REPORT

SAND86–7130
Unlimited Release
UC–70

Nevada Nuclear Waste Storage Investigations Project

Laboratory Determination of the Mechanical, Ultrasonic and Hydrologic Properties of Welded Tuff From the Grouse Canyon Heated Block Site

M. P. Board, M. L. Wilson, M. D. Voegele
Science Applications International Corp.
Las Vegas, NM 87109

Prepared by Sandia National Laboratories Albuquerque, New Mexico 87185
and Livermore, California 94550 for the United States Department of Energy
under Contract DE-AC04-76DP00789

Printed August 1987

"Prepared by Nevada Nuclear Waste Storage Investigations (NNWSI) Project participants as part of the Civilian Radioactive Waste Management Program (CRWM). The NNWSI Project is managed by the Waste Management Project Office (WMPO) of the U. S. Department of Energy, Nevada Operations Office (DOE/NV). NNWSI Project work is sponsored by the Office of Geologic Repositories (OGR) of the DOE Office of Civilian Radioactive Waste Management (OCRWM)."

Issued by Sandia National Laboratories, operated for the United States Department of Energy by Sandia Corporation.

Printed in the United States of America
Available from
National Technical Information Service
U.S. Department of Commerce
5285 Port Royal Road
Springfield, VA 22161

NTIS price codes
Printed copy: A05
Microfiche copy: A01

Distribution
Category UC-70

SAND86-7130
Unlimited Release
Printed August 1987

LABORATORY DETERMINATION OF THE MECHANICAL, ULTRASONIC AND HYDROLOGIC PROPERTIES OF WELDED TUFF FROM THE GROUSE CANYON HEATED BLOCK SITE

M. P. Board
M. L. Wilson
M. D. Voegele

Science Applications International Corp.
Las Vegas, NV 89109

Contract Monitor
Roger M. Zimmerman
NNWSI Geotechnical Projects Division
Sandia National Laboratories
Albuquerque, NM 87185

ABSTRACT

The results of a laboratory testing program conducted to determine the mechanical, ultrasonic, and hydrologic properties of samples from the Grouse Canyon Member of the Belted Range Tuff exposed in the GTUF Heated Block Alcove, U12G Tunnel, Nevada Test Site are described. These results tend to reinforce similar measurements made earlier at Sandia National Laboratories.

CONTENTS

ILLUSTRATIONS

ILLUSTRATIONS (Continued)

ILLUSTRATIONS (Concluded)

TABLES

1.0 INTRODUCTION

This report describes the results of a laboratory testing program conducted to support the findings of the G-Tunnel Heated Block Experiment. The heated block experiment was performed in G-Tunnel by Sandia National Laboratories (SNL) under sponsorship of the Nevada Nuclear Waste Storage Investigations (NNWSI) for the purpose of obtaining a variety of field scale data for model applications, developments, and comparisons applicable to radioactive waste repository design and performance assessment functions (Zimmerman et al., 1986). Jointed welded tuffs at Yucca Mountain, on and near the boundary of the Nevada Test Site (NTS), are being considered for the repository storage host rock. G-Tunnel, which is located some 40 km away on the NTS, contains both jointed welded tuffs and a stress state that are similar to the proposed repository conditions at Yucca Mountain. Rock mechanics type testing has been conducted in G-Tunnel until later in situ scale testing can be conducted at Yucca Mountain under a site characterization program.

The heated block testing was established to evaluate the behavior of jointed-welded tuffs under stress and temperature conditions appropriate for the early stages of repository designs and analyses. On the field scale, the single experiment provided data on thermal, mechanical, thermomechanical, and hydrologic properties of jointed welded tuff occupying a volume in excess of 8 m^3. The heated block experiment was located in the Heated Block Alcove near the back end of G-Tunnel. The alcove was part of the Grouse Canyon Member of the Belted Range Tuff.

The testing was conducted with SNL having overall technical and operational responsibilities. Science Applications International Corporation (SAIC) was placed under contract to perform field testing activities at G-Tunnel and laboratory testing in supporting facilities. The SAIC laboratory testing discussed in this document consisted of performing intact rock strength, ultrasonics, and permeability measurements and joint shear strength evaluations. This report describes the sample selection process and provides results of the different types of measurements and evaluations. A summary of all of the findings is included in Table 1 to facilitate referencing and to provide a scope of the laboratory testing activities. The topics in the table provide the organization about which this report is written.

TABLE 1

SUMMARY OF THE AVERAGE PROPERTIES
OF GROUSE CANYON MEMBER WELDED TUFF

PROPERTY	CONDITIONS	AVERAGE VALUE	COMMENTS
Bulk Density	Muck Pile Samples	2.21 g/cm^3	
Moisture Content	Fresh Muck Pile Samples (wrapped and protected)	5.75%	
Percent Saturation	Fresh Muck Pile Samples (wrapped and protected)	79%	
Porosity	Fresh Muck Pile Samples (wrapped and protected)	16.9%	
Uniaxial Compressive Strength	Dry Saturated	134.4 MPa 95.9 MPa	No apparent temperature dependence
Elastic Moduli			
■ Young's Modulus	Dry Saturated Combined	27.7 GPa 23.0 GPa 25.6 GPa	Little temperature dependence
■ Poisson's Ratio	Combined	0.24	
Tensile Strength (Brazilian)		9.6 MPa	Possible temperature dependence
Mohr-Coulomb Properties of Intact Rock			
■ Cohesion	Dry Saturated	27.7 MPa 19.5 MPa	Little temperature effect
■ Angle of Friction	Dry Saturated	47° 48°	
Saw-Cut Joint Frictional and Stiffness Properties			
■ Angle of Friction	Dry Saturated	20° 26°	Little temperature effect

TABLE 1 (Cont.)

SUMMARY OF THE AVERAGE PROPERTIES
OF GROUSE CANYON MEMBER WELDED TUFF

PROPERTY	CONDITIONS	AVERAGE VALUE	COMMENTS
■ Normal Stiffness	Dry	42.5 GPa/m	Function of normal stress
Wave Velocities			
■ P Wave	Saturated, 20°C	4.14 km/s	250 kHz
	Saturated, 55°C	4.21 km/s	
	Saturated, 90°C	4.23 km/s	
	Unsaturated, 20°C	3.93 km/s	250 kHz
	Unsaturated, 120°C	3.98 km/s	
	Unsaturated, 220°C	4.03 km/s	
■ S Wave	Saturated, 20°C	2.49 km/s	250 kHz
	Saturated, 55°C	2.48 km/s	
	Saturated, 90°C	2.46 km/s	
	Unsaturated, 20°C	2.43 km/s	250 kHz
	Unsaturated, 120°C	2.44 km/s	
	Unsaturated, 220°C	2.44 km/s	

INTACT SPECIMEN PERMEABILITY

CONFINING PRESSURE (MPa)	TEMPERATURE (°C)	GAS PERMEABILITY ($\times 10^{-13}$ cm^2)
1.7	20	3.16
10.0		2.39
20.6		1.94
1.7	50	2.89
10.0		1.81
20.6		1.75
1.7	90	3.32
10.0		1.66
20.6		1.62

2.0 SAMPLE SELECTION AND PREPARATION

A total of 52 EW (37.9-mm diameter), 6 AW (48.2-mm diameter), 39 NQ (47.6-mm diameter), and other miscellaneous-size cores were selected by M. Voegele from G-Tunnel heated block diamond drill holes and shipped by REECO to the SAIC Salt Lake City facility. All of the cores were of welded tuff from the Grouse Canyon Member and were from diamond drilled holes located in the immediate vicinity of the Heated Block Test Alcove. After arrival at the laboratory, core samples for individual tests were chosen, for the most part, from homogeneous sections of core that contained minimal fracturing or large vesicles. Although this selection biases the results of testing to some extent, it is unavoidable for standard testing methods.

The length of each sample and an identification number were marked on the core prior to sample preparation. The samples were cut to lengths approximately 0.6 cm greater than the final required length. Sample ends were cut with a diamond saw and finished flat and parallel to within 0.025 mm using a surface grinder. The sample designation, along with original drill hole location and specimen dimensions for each test, is given in Table 2.

After preparation, samples were stored in the laboratory. Either in an oven, if dry testing was to be conducted, or in air-tight polyethylene bags, after saturation, for saturated testing. Samples to be tested dry were placed in an oven at 100°C for several days prior to testing. All samples designated for testing under saturated conditions were immersed in water and subject to 635-mm Hg (85-kPa) vacuum for a minimum of 1 week prior to testing in an attempt to fully saturate the pore space. Each sample and container was marked with the sample number (Table 2) and was accompanied by a test documentation form that detailed the test type and parameters to be controlled for that particular sample.

The procedures for the testing programs were, in general, derived from two sources: The Manual of Technical Practice: Laboratory Rock Mechanics Testing, prepared for the Office of Nuclear Waste Isolation (ONWI) by Foundation Sciences, Inc. and the International Society for Rock Mechanics Standards for Laboratory and Field Testing (Brown, 1981). The specific procedures are discussed in each of the following chapters; laboratory equipment calibration is reviewed in the appendix.

TABLE 2

SUMMARY OF SPECIMENS
(Grouse Canyon Welded Tuff)

HOLE ID	FOOTAGE ft (m)	SAMPLE NUMBER	DIMENSIONS OF SAMPLE (mm)	TESTS PERFORMED
TC-11	1.31-1.71 (0.400-0.521)	EW-35	47.00 x 21.03	UCS,SAT,20°C
		EW-36	40.67 x 21.29	UCS,DRY,220°C
		EW-37	48.08 x 21.21	UCS,SAT,20°C
TC-15	1.25-1.71 (0.381-0.521)	EW-38	40.56 x 21.11	CCS,20 MPa,SAT,90°C
		EW-39	45.87 x 21.03	CCS,10 MPa,DRY,20°C
		EW-40	51.00 x 21.11	CCS,20 MPa,SAT,55°C
		EW-41	45.70 x 21.08	CCS,20 MPa,SAT,55°C
		EW-42	43.46 x 21.08	CCS,10 MPa,SAT,55°C
		EW-43	43.23 x 21.11	UCS,SAT,90°C
TC-6	1.31-1.71 (0.400-0.521)	EW-44	50.42 x 21.18	CCS,20 MPa,DRY,20°C
		EW-45	46.69 x 21.16	UCS,DRY,20°C
		EW-46	49.05 x 21.11	CCS,10 MPa,DRY,120°C
		EW-47	48.41 x 20.98	CCS,10 MPa,DRY,220°C
		EW-48	48.82 x 21.18	UCS,DRY,20°C

*Test Nomenclature:

UCS = Uniaxial Compressive Strength
CCS = Confined Compressive Strength
UCMOD = Uniaxial Compression Elastic Moduli Determination
SAT = Saturated
DRY = Oven-Dried
JS = Joint Shear
PERM = Gas Permeability

The following code is used to characterize a test:

Test Type (e.g., CCS), Pressure (e.g., MPa), Saturation (e.g., Dry), Temperature (Celsius)

where Pressure = Confining Pressure for Confined Compressive Strength
= Normal Pressure for Joint Shear

TABLE 2 (Cont.)

SUMMARY OF SPECIMENS

HOLE ID	FOOTAGE ft (m)	SAMPLE NUMBER	DIMENSIONS OF SAMPLE (mm)	TESTS PERFORMED
TC-6	0.61-1.31 (0.156-0.400)	EW-49	47.75 x 21.18	CCS,10 MPa,SAT,90°C
		EW-50	49.53 x 21.11	CCS,20 MPa,DRY,120°C
		EW-51	46.00 x 20.90	UCS,SAT,20°C
		EW-52	41.45 x 21.21	CCS,10 MPa,DRY,120°C
		EW-53	50.19 x 21.11	UCS,DRY,220°C
		EW-54	49.12 x 21.18	CCS,20 MPa,SAT,55°C
		EW-55	49.58 x 21.08	UCS,SAT,90°C
		EW-56	44.15 x 21.18	CCS,20 MPa,SAT,90°C
GH-2	2.29-2.59 (0.698-0.789)	EW-57	45.67 x 21.08	UCS,DRY,20°C
		EW-58	48.44 x 21.11	CCS,20 MPa,DRY,120°C
		EW-59		
GH-1	2.29-2.35 (0.698-0.716)	EW-10	41.63 x 21.18	CCS,10 MPa,SAT,90°C
		EW-11	47.90 x 20.98	USC,DRY,120°C
		EW-12	44.76 x 21.16	CCS,10 MPa,DRY,120°C
		EW-13	40.16 x 21.08	UCS,DRY,220°C
		EW-14		
		EW-15	41.17 x 21.16	CCS,20 MPa,SAT,90°C
		EW-16		
		EW-17	44.65 x 21.13	CCS,10 MPa,SAT,55°C
		EW-18	42.65 x 21.18	UCS,SAT,90°C
		EW-19	46.38 x 21.18	CCS,20 MPa,DRY,220°C
		EW-20	48.13 x 21.26	CCS,20 MPa,SAT,20°C
		EW-21	49.81 x 21.21	CCS,20 MPa,DRY,120°C
		EW-22	47.22 x 21.16	CCS,10 MPa,SAT,90°C
		EW-23	44.04 x 21.11	CCS,20 MPa,DRY,220°C
		EW-24	48.62 x 21.16	UCS,DRY,120°C
		EW-25	40.59 x 21.13	UCS,DRY,120°C
		EW-26		
		EW-27	41.50 x 21.11	UCS,SAT,55°C
		EW-28	48.11 x 21.11	CCS,10 MPa,DRY,220°C
		EW-29	45.34 x 21.11	CCS,10 MPa,SAT,55°C
		EW-30	48.82 x 21.11	CCS,20 MPa,DRY,20°C
		EW-31	49.89 x 21.21	UCS,SAT,55°C
		EW-32	50.83 x 21.19	CCS,10 MPa,SAT,20°C
		EW-33	47.73 x 21.06	UCS,SAT,20°C
		EW-34	48.41 x 21.11	UCS,SAT,55°C

TABLE 2 (Cont.)

SUMMARY OF SPECIMENS

HOLE ID	FOOTAGE ft (m)	SAMPLE NUMBER	DIMENSIONS OF SAMPLE (mm)	TESTS PERFORMED
		EW-60	53.39 x 20.96	CCS,20 MPa,DRY,220°C
		EW-61	47.93 x 20.96	CCS,10 MPa,DRY,220°C
US-1	1.28-1.34 (0.390-0.400)	NQ-18		
	1.52-1.95 (0.463-0.594)	NQ-22	101.88 x 47.63	UCMOD,DRY,20°C, 100°C,220°C
US-2	3.02-3.32 (0.920-1.012)	NBQ-19		
		NBQ-20		
		NBQ-21	95.81 x 47.63	UCMOD,SAT,50°C,90°C
		NBQ-23	95.73 x 47.55	UCMOD,DRY,20°C
		NBQ-24	96.52 x 47.63	ULTRASONICS
		NBQ-25	96.52 x 47.63	ULTRASONICS
		NBQ-26	96.52 x 47.63	ULTRASONICS
		NBQ-27	96.52 x 47.63	ULTRASONICS
	1.40 (0.427)	NQ-14		JS
	1.55 (0.472)	NQ-15	96.32 x 47.63	UCMOD,DRY,20°C, 100°C,220°C
	1.83 (0.558)	NQ-16	93.88 x 47.63	UCMOD,DRY,20°C, 100°C,220°C
	2.07 (0.631)	NQ-17		ULTRASONICS
US-3	1.98-2.20 (0.634-0.671)	NQ-29	47.63 Diam.	JS,5 MPa,DRY,20°C
		NQ-30		
US-4	1.40-1.86 (0.427-0.567)	NQ-20	95.81 x 47.63	UCMOD,SAT,20°C
		NQ-21	95.86 x 47.63	UCMOD,SAT,20°C
P-3	1.37-1.71 (0.418-0.521)	NQ-27		PERM
		NQ-28		PERM
RMP-2	4.94-5.15 (1.506-1.570)	NQ-31	47.63 Diam.	JS,5 MPa,SAT,20°C
		NQ-32		
		NQ-34	47.63 Diam.	JS,10 MPa,DRY,20°C
	12.59-12.80 (3.837-3.901)	NQ-35		JS
		NQ-36		JS

TABLE 2 (Cont.)

SUMMARY OF SPECIMENS

HOLE ID	FOOTAGE ft (m)	SAMPLE NUMBER	DIMENSIONS OF SAMPLE (mm)	TESTS PERFORMED
MPBX-1	3.29-3.72 (1.003-1.134)	NQ-1	47.63 x 78.94	CCS,20 MPa,DRY,20°C
		NQ-2	47.63 Diam.	JS
		NQ-3	47.63 Diam.	JS
		NQ-4	47.63 Diam.	JS
		NQ-5	47.63 Diam.	JS
		NQ-6	91.90 x 47.32	CCS,10 MPa,DRY,120°C
		NQ-7	47.63 Diam.	JS
	2.16-2.29 (0.658-0.698)	NQ-8	47.63 Diam.	JS
		NQ-9	146.30 x 47.63	UCMOD,20°C
		NQ-10	96.52 x 47.63	ULTRASONICS
		NQ-11	95.81 x 47.63	UCMOD,SAT,50°C,90°C
		NQ-12	95.00 x 47.63	UCMOD,SAT,20°C
MPBX-2	2.13-2.16 (0.649-0.658)	NQ-13	98.07 x 47.55	CCS,10 MPa,DRY,120°C
	2.29-2.32 (0.698-0.707)	NQ-14	47.63 Diam.	JS,5 MPa,DRY,20°C
U12G HBTIA (FRAC. TEST HOLE)	0.55-0.64 (0.168-0.195)	BRAZ-1	22.91 x 54.61	BRAZILIAN
		BRAZ-2	22.07 x 54.61	BRAZILIAN
		BRAZ-3	25.15 x 54.61	BRAZILIAN
		BRAZ-4	17.58 x 6.38	BRAZILIAN
U12G HB-WTLS TC-10	0.95-1.13 (0.290-0.344)	AW-11	60.662 x 28.68	CCS,20 MPa,DRY,20°C
		AW-12	59.77 x 28.73	CCS,10 MPa,DRY,20°C
		AW-13	54.25 x 28.78	CCS,20 MPa,DRY,120°C
		AW-14	56.79 x 28.80	CCS,10 MPa,DRY,120°C
		AW-4	55.68 x 28.83	CCS,10 MPa,SAT,20°C
		AW-5	54.86 x 28.88	CCS,20 MPa,SAT,20°C

3.0 PHYSICAL PROPERTIES

Bulk density, moisture content, percent saturation, and porosity were determined from samples collected from a freshly blasted muck pile of Grouse Canyon Member welded tuff in the extensometer drift in U12G Tunnel. These samples were wrapped in air-tight polyethylene to prevent moisture loss. Physical property measurements were conducted within 3 days of the sampling.

3.1 Bulk Density

The bulk density of two Grouse Canyon Member tuff samples was determined using standard mercury immersion and displaced volume methods. All weights were determined to the nearest 0.01 g. The two samples yielded results of 2.26 and 2.16 g/cm^3.

3.2 Moisture Content/Percent Saturation

Moisture content (mass water/mass solids) and saturation (volume water/volume pores) were determined for two samples of the Grouse Canyon Member tuff. These were initially weighed to an accuracy of 0.01 g on an Ohaus triple-beam balance. The samples were then placed in a vacuum oven at 100°C and weighed periodically until no further weight loss was registered. On the average, the samples were maintained under these conditions for 7 days.

The moisture content and saturation for these two samples are listed in Table 3.

3.3 Porosity

An approximate porosity was calculated by the following technique:

A weighed and dried tuff sample was immersed in water and a vacuum of 635 mm of Hg (85 kPa) was maintained for a minimum of 7 days in an attempt to fully saturate the sample. The sample was reweighed and porosity calculated assuming 100% saturation. The porosity of the sample was calculated to be 16.9%.

TABLE 3

MOISTURE CONTENT AND PERCENT SATURATION
OF GROUSE CANYON MEMBER TUFF
FROM EXTENSOMETER DRIFT MUCK PILE

SAMPLE NUMBER	MOISTURE CONTENT (%)	SATURATION (%)
1	5.6	77
2	5.9	81

4.0 STRENGTH PROPERTIES

The compressive strength of the Grouse Canyon Welded Tuff was determined using standard uniaxial and triaxial compression methods. Tensile strength was determined using the Brazilian indirect method.

4.1 Uniaxial Compression

A total of 18 uniaxial compressive strength tests were run under a variety of temperature and saturation conditions. Three temperatures were used with air-dried samples (20°, 120° and 220°C) and with saturated samples (20°, 55° and 90°C). Air-dried samples were left open to the atmosphere for a minimum of 1 month prior to testing; saturated samples were placed in water and maintained at a vacuum of 635 mm of Hg (85 kPa) for a minimum of 2 weeks prior to testing. Table four lists the uniaxial compressive strengths and specifies the test conditions.

4.1.1 Equipment and Procedure

A schematic of the load frame and pressure vessel used for this testing is shown in Figure 1. The hydraulic system consisted of a 10-gal/min (0.6-l/s), 3000-psi (21 MPa) power supply with a 200-ton (1780-kN), 6-inch (15.24-cm) stroke Enerpac ram. The power supply was servo-controlled using displacement feedback from a 6-inch (15.24-cm) stroke Schaevitz Direct Current Linear Variable Differential Transformer (DCDT) attached to the ram piston. Load was sensed by either a 100-ton (890-kN) capacity Terrametrics or 200-ton (1780-kN) capacity Sensotec calibrated load cell. Axial load change versus axial displacement was plotted continuously during testing on a Houston Instruments analog X-Y recorder. Failure load was scaled directly from the plots using the calibrated voltage output of the load cell.

Prior to each test series, the data acquisition system (DAS) was calibrated using traceable load and displacement instruments. Typical calibration procedures are given in Appendix B. In addition to DAS calibration, the system stiffness was determined to allow correction for machine deformation. This was done by compression of samples of materials with well-known mechanical properties, as described in Appendix B.

The procedures for the uniaxial compression tests were as follows:

1. Samples were prepared with a 2:1 length-to-diameter ratio, ends parallel to within 0.025 mm.

TABLE 4

RESULTS OF UNIAXIAL COMPRESSIVE STRENGTH TESTS

SAMPLE ID	TEMPERATURE (°C)	SATURATION	COMPRESSIVE STRENGTH (MPa)
EW-11	120	DRY	198.9
EW-13	220	DRY	110.5
EW-18	90	SATURATED	76.5
EW-24	120	DRY	136.0
EW-25	120	DRY	123.2
EW-27	55	SATURATED	65.9
EW-31	55	SATURATED	112.6
EW-33	20	SATURATED	63.7
EW-34	55	SATURATED	89.2
EW-35	20	SATURATED	142.4
EW-36	220	DRY	106.3
EW-37	20	SATURATED	105.2
EW-43	90	SATURATED	99.9
EW-45	20	DRY	125.6
EW-48	20	DRY	132.6
EW-51	20	SATURATED	112.6
EW-53	220	DRY	162.0
EW-55	90	SATURATED	91.4
EW-57	20	DRY	114.8

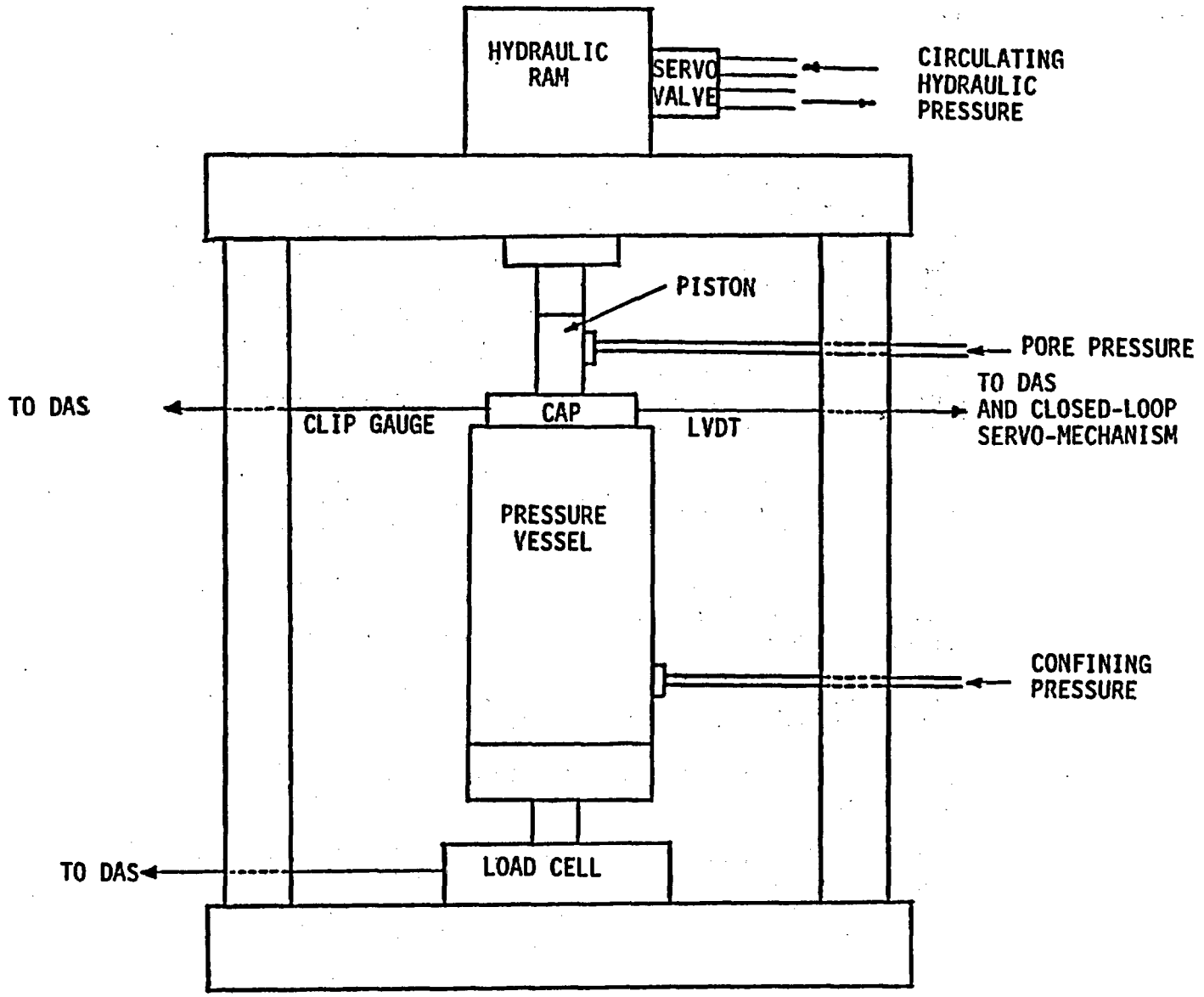

FIGURE 1. Compression Testing System.

2. Calibrated value of axial displacement and load to respective shunt resistors within the servo system was determined.

3. The samples were assembled in the load frame, ends covered with Teflon to reduce friction, and the ram was brought into contact with the specimen using the manual servo set control.

4. Several of the samples were tested at an elevated temperature. The samples were slowly heated (0.5°C/min or less) to the prescribed temperature in a small oven adjacent to the load frame. When the samples had attained the prescribed temperature, they were insulated in a fiberglass blanket and transferred immediately to the load frame. The insulated samples were, in general, out of the oven for no more than 15 min prior to sample failure. The test temperature of an insulated sample was monitored while outside the oven, and minimal temperature loss was noted for the maximum test time (approximately 10 to 15 min).

5. Once the ram contacted the sample, the hydraulic power supply was clamped, the X-Y analog plotter initialized, and both load and displacement shunts for calibration actuated.

6. The function generator ramp rate was configured to load the sample over the prescribed displacement span at a rate of approximately 50 $\mu\epsilon$/s, or failure in approximately 15 min.

7. Loading of the sample was begun, the load displacement curve being recorded with the analog plotter.

8. The test was completed when the sample showed brittle failure by a marked reduction in load.

A typical X-Y plot for a uniaxial test is shown in Figure 2. As seen from this plot, an easily distinguishable failure point was obtained and, in most cases, the use of the displacement-control servo-controller enabled a residual strength to be observed.

The uniaxial compressive strength, σ_C, was calculated as follows:

$$\sigma_C = \frac{F_f}{A}$$

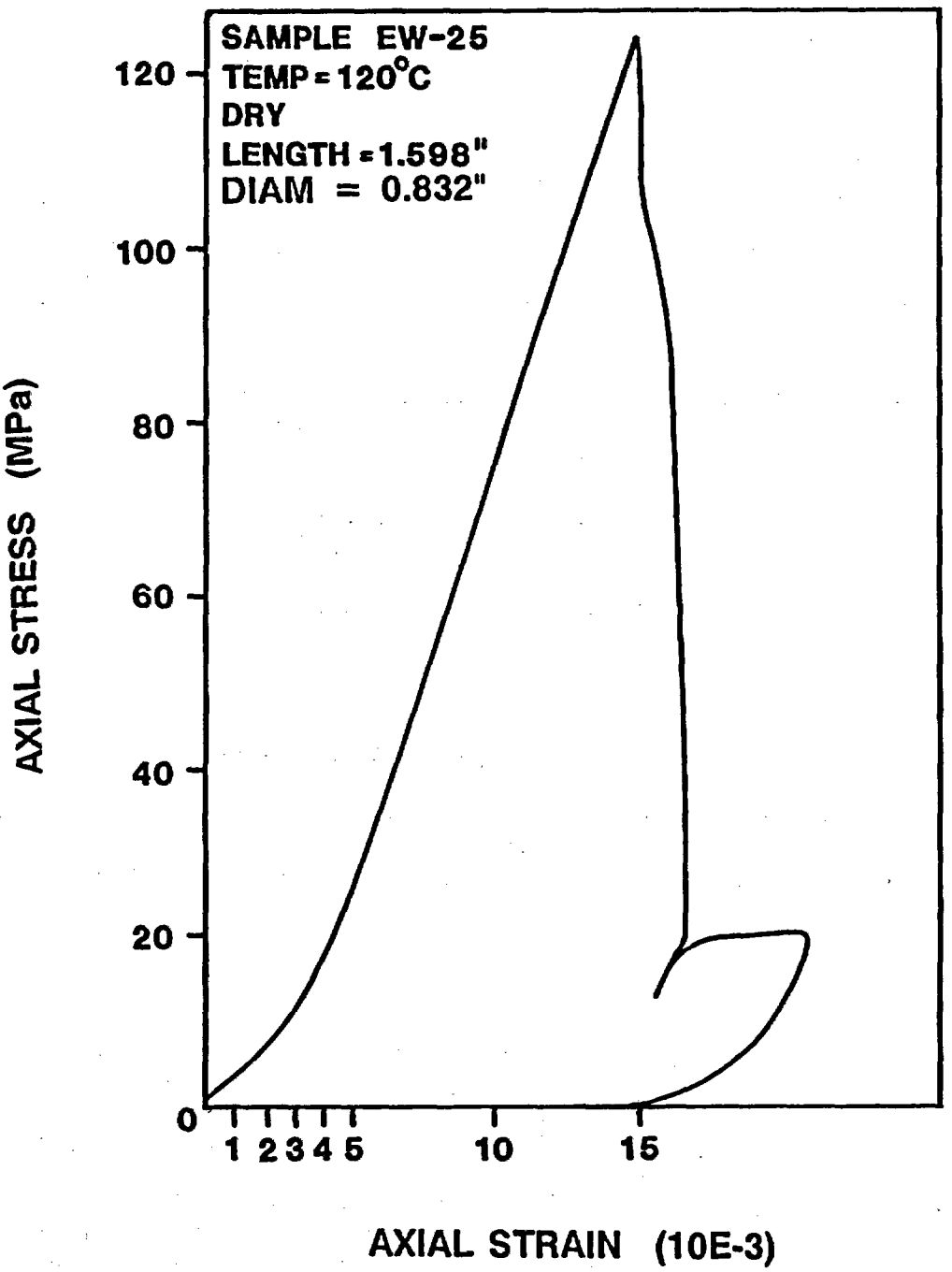

FIGURE 2. Typical Uniaxial Compression Test Stress-Strain Curve.

where F_f = peak load at failure
A = original cross-sectional area of the sample

4.1.2 Results

The test results are summarized in Table 4. The data from Table 4 are plotted as a function of temperature for dry and saturated samples in Figure 3. The following observations can be made:

1. In general, the saturated samples appear to have a lower strength than the dry samples. Averaging the uniaxial compressive strengths for both cases yields the following results:

   Saturated - 95.9 ± 24 MPa
   Dry - 134.4 ± 29.3 MPa

2. No distinct relationship between strength and temperature is evident.

4.2 Elastic Moduli Determined In Uniaxial Compression

A series of uniaxial compression tests were conducted on NQ size, (96 mm long by 48 mm in diameter) cores of welded tuff to determine the elastic moduli (Young's modulus and Poisson's ratio).

4.2.1 Equipment and Procedure

Elastic moduli measurements were made using the apparatus shown in Figure 4. This device consists of upper and lower steel platens that contact each specimen end and provide load transfer from the piston and load cell. Axial displacements are measured using two diametrically opposed Schaevitz DCDTs which are connected to the upper and lower yoke. The axial displacement is determined by averaging the opposing DCDT output to account for any bending effects. Lateral strains are monitored by two opposing pairs of beryllium-copper cantilevers that contact the specimen by means of knife-edge setscrews at the sample midplane. Each cantilever pair is wired for a full Wheatstone bridge output and is calibrated to produce a relationship between output and diametral displacement. Thus, Poisson's ratio can be determined along two directions.

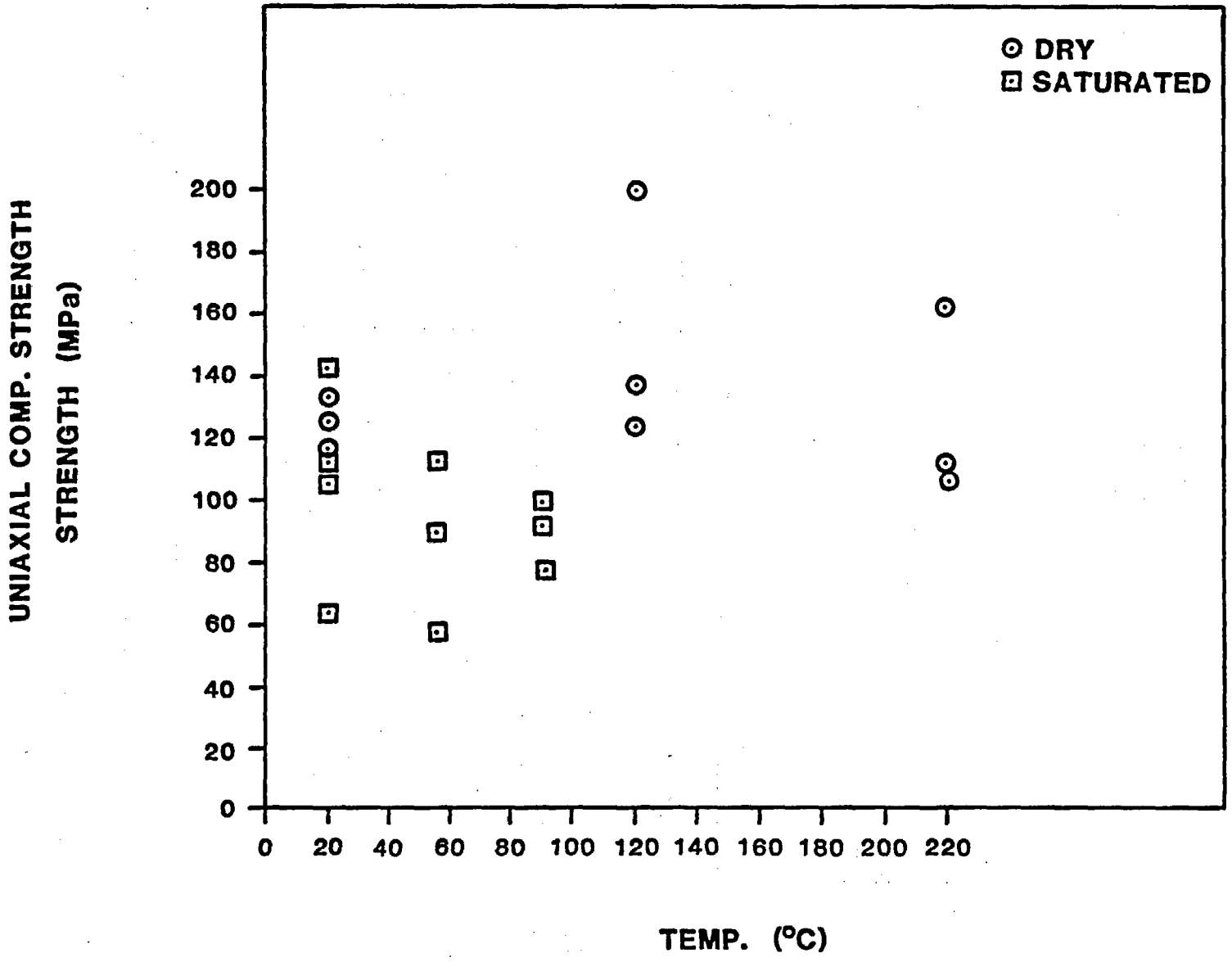

FIGURE 3. Summary of Uniaxial Compressive Strength of Dry and Saturated Welded Tuff versus Temperature.

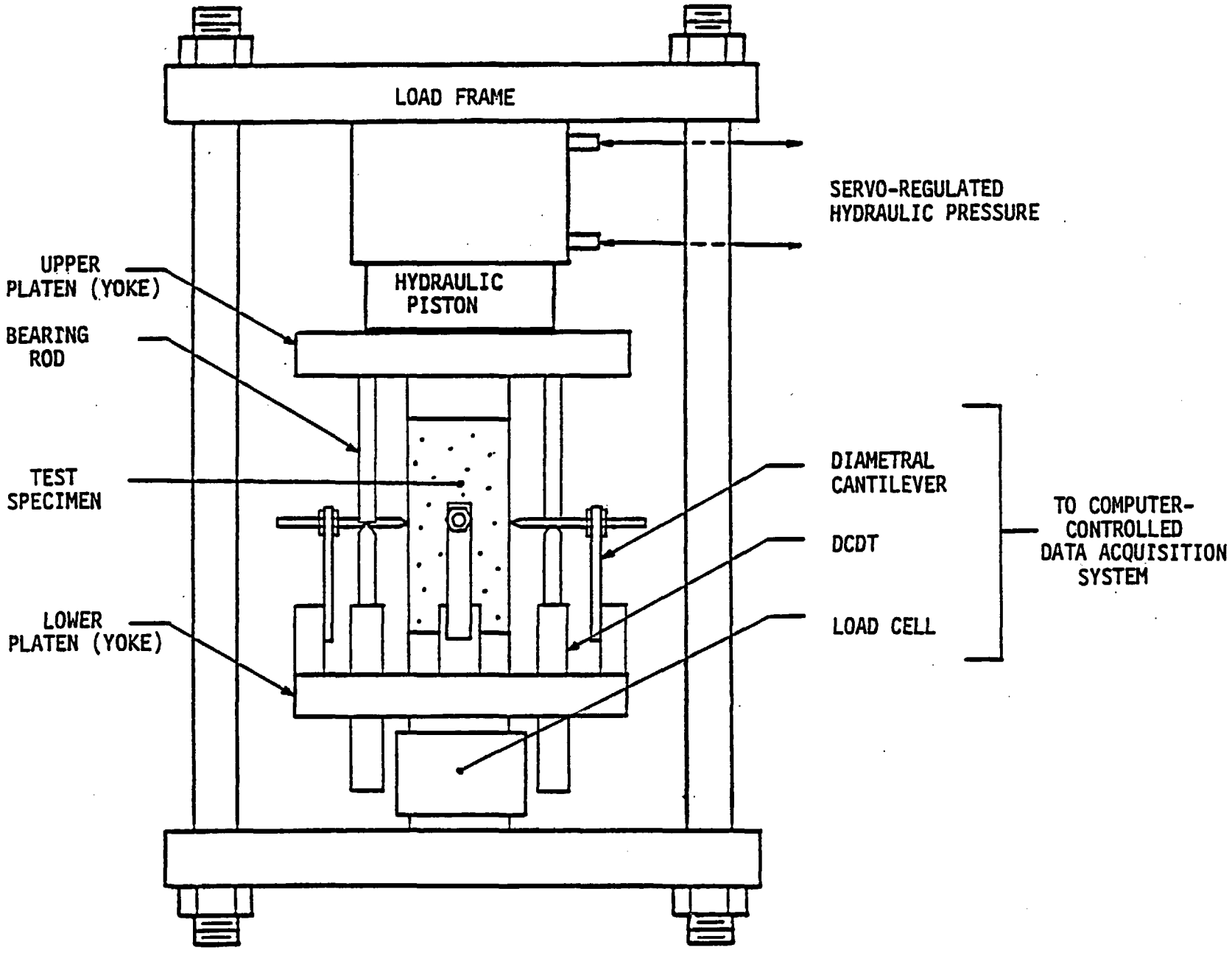

FIGURE 4. Elastic Modulus Apparatus.

A typical test was conducted in the following manner:

1. The elastic moduli apparatus was calibrated with an aluminum sample prior to the test series.

2. A sample was placed in the measurement apparatus.

3. The piston was manually brought into contact with the sample.

4. The recorders were initialized.

5. A load-unload cycle was performed to approximately 20% of the uniaxial compressive strength over the span of approximately 5 min; this gives a loading rate of approximately 0.1 MPa/s).

All instrumentation was continuously monitored in real time using an HP 85/3497 DAS. The software acquired data every 5 s, stored the raw data, and calculated the elastic moduli. For measurements at elevated temperatures, the cores were raised to the desired temperature in an oven over approximately 2 days. The core was then insulated and placed in the elastic moduli apparatus. The measurements were made over a short period of time (typically approximately 5 min). It is believed that insignificant cooling of the core occurred in that time and that the temperature of the elastic moduli apparatus remained unchanged during the testing.

4.2.2 Results

Table 5 summarizes the results of the moduli tests. For each test, an average value for the Young's modulus and Poisson's ratio was taken over the linear portion of the loading curve.

The test program for determination of elastic moduli was conducted under the restriction of having only a few samples to cover a wide range of conditions. As a result, only a small number of repeat tests were possible under any given conditions. The statistical significance of any given parameter was difficult to determine since individual variations in core lithology could significantly influence material properties. The average moduli for all tests (Young's modulus = 25.6 MPa and Poisson's ratio = 0.24) agree well with the previously used heated block test average mechanical properties of 26 GPa and 0.21. Within the dry and saturated groups, there appears to be little, if any, variation in moduli with temperature. There is approximately a 17% difference in the average Young's modulus between the dry and saturated samples. Figure 5 is a summary plot of Young's modulus as a function of temperature for dry and saturated conditions. The dashed lines are linear least square fits to the data for dry and saturated conditions.

TABLE 5

ELASTIC MODULI

SAMPLE NO.	TEMPERATURE (°C)	SATURATION	AVERAGE YOUNG'S MODULUS (GPa)	AVERAGE POISSON'S RATIO
NQ-15	100	DRY	27.6	0.21
NQ-11	50	SATURATED	23.8	0.21
NQ-22	100	DRY	26.3	0.31
NQ-12	50	SATURATED	22.3	-* AXIAL FRACTURE ALONG CORE
NQ-12	90	SATURATED	22.0	0.22
NQ-23	20	DRY	29.1	0.21
NQ-23	20	DRY	28.8	0.23
NQ-16	20	DRY	25.2	0.28
NQ-11	90	SATURATED	26.5	0.29
NQ-21	90	SATURATED	18.9	0.27
NQ-22	220	DRY	25.6	0.28
NQ-21	50	SATURATED	20.0	0.24
NQ-16	220	DRY	28.7	0.23
NQ-15	220	DRY	30.9	0.20
NQ-22	20	DRY	24.5	-* AXIAL FRACTURE ALONG CORE
NQ-15	20	DRY	30.1	0.24
NQ-9	20	SATURATED	23.2	0.27
NQ-11	20	SATURATED	28.1	0.19
NQ-21	20	SATURATED	21.8	0.24
NQ-12	20	SATURATED	25.5	0.26
NQ-16	100	DRY	28.1	0.20

AVERAGE VALUES:

20°C	DRY	27.5 ± 2.5	0.24 ± 0.03	(5 SAMPLES)
100°C	DRY	27.3 ± 0.9	0.24 ± 0.06	(3 SAMPLES)
220°C	DRY	28.4 ± 2.6	0.23 ± 0.04	(3 SAMPLES)
20°C	SATURATED	24.7 ± 2.7	0.24 ± 0.04	(4 SAMPLES)
50°C	SATURATED	22.0 ± 1.9	0.23 ± 0.02	(3 SAMPLES)
90°C	SATURATED	22.4 ± 3.8	0.26 ± 0.04	(3 SAMPLES)
TOTAL OF ALL SAMPLES		25.6 ± 3.3	0.24 ± .03	

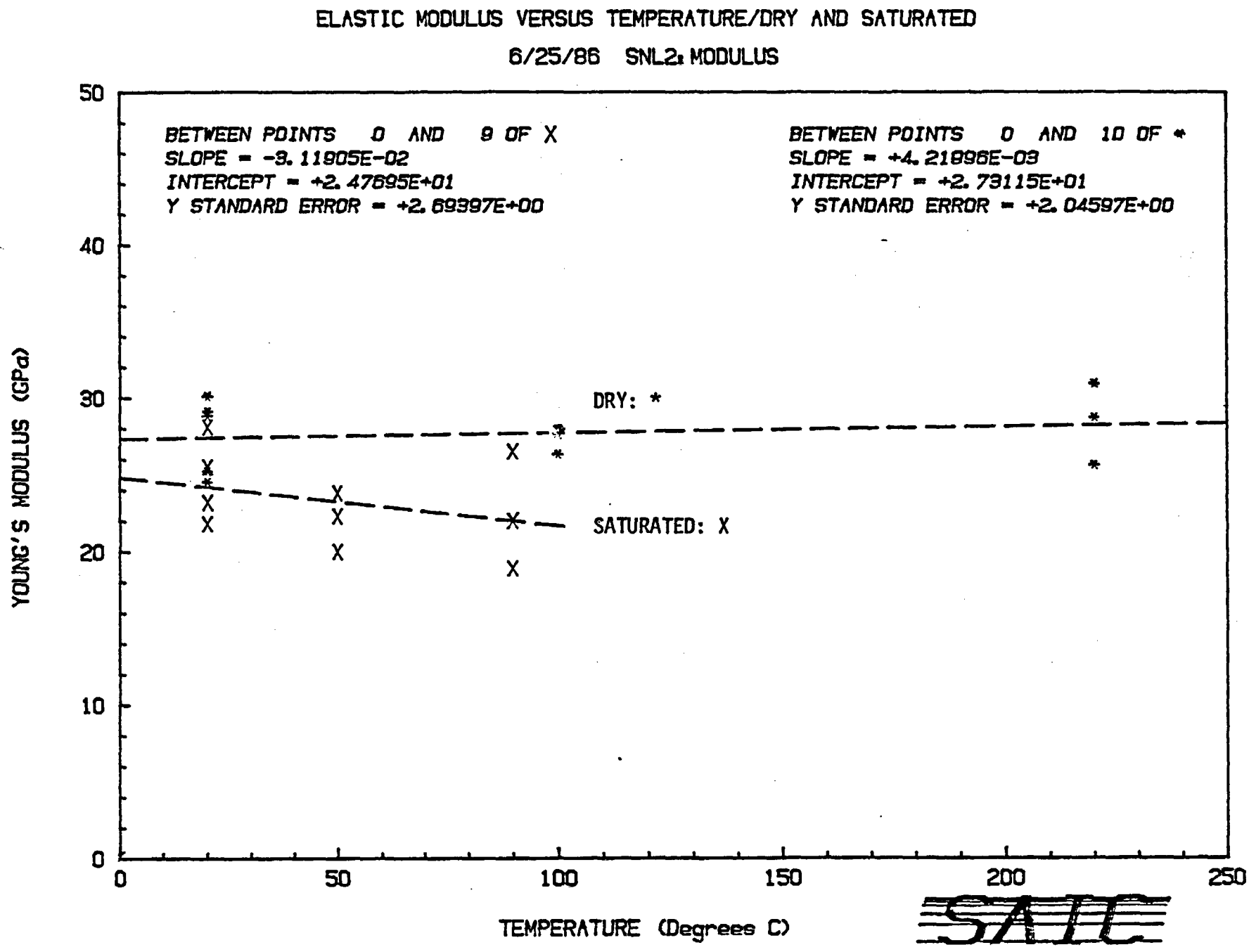

FIGURE 5. Elastic Modulus versus Temperature for Dry and Saturated Samples of Grouse Canyon Welded Tuff.

4.3 Brazilian Tensile Strength

A series of tensile strength tests were run on NQ-sized cores (47.6-mm diameter) using the indirect "Brazilian" method.

4.3.1 Equipment and Procedures

The Brazilian tests were conducted according to standard ISRM procedures (Brown, 1981) using the apparatus shown in Figure 6. A small load frame with a 10-ton (890-kN) single-acting ram actuated by a hand pump was used to load the specimen. Each sample disc was cut with a length-to-diameter ratio of 1:2. Sample load was calculated from the cross-sectional area of the hydraulic piston and the output of a calibrated pressure transducer attached to the hydraulic circuit. Data obtained on a strip chart recorder were used to determine peak load. Failure stress was calculated from the formula:

$$\sigma t = \frac{2P}{\pi D t}$$

where D = diameter (m)
t = thickness (m)
P = failure load (N)

For tests at elevated temperatures, the samples were heated slowly in an oven to the desired level then removed and loaded to failure within 2 to 3 min.

4.3.2 Results

The results of the tensile strength tests are given in Table 6. A plot of the tensile strength as a function of temperature is given in Figure 7.

4.4 Triaxial Compression Testing

A series of triaxial compression tests were conducted at various confining pressures and temperatures. The results of these tests, in combination with the uniaxial compression tests, can be used to determine the Mohr-Coulomb failure criterion parameters of the intact rock.

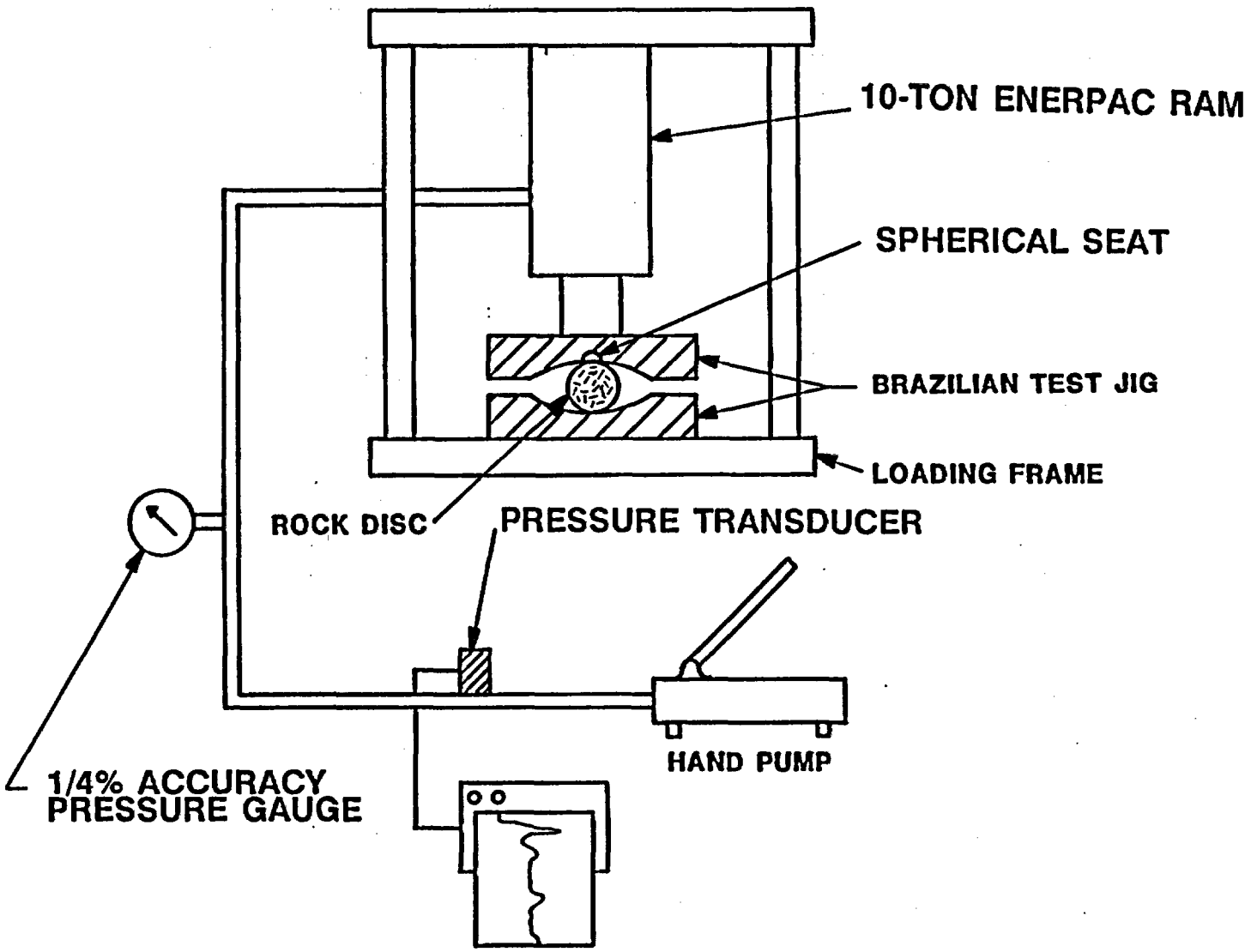

FIGURE 6. Setup for Brazilian Tensile Strength Testing.

TABLE 6

RESULTS OF
BRAZILIAN TENSILE STRENGTH TESTS

SAMPLE ID	TEMPERATURE (°C)	BRAZILIAN TENSILE STRENGTH (MPa)
NQB-1	20	10.9 DRY
NQB-2	20	11.0
NQB-4	20	11.6
US4-1	55	7.6 DRY
US4-3	55	10.1
US4-4	55	8.9
US4-2	90	10.7 DRY
US4-5	90	10.0
US4-7	90	10.6
NQB-3	120	12.3 DRY
NQB-5	120	7.0
NQB-9	120	8.1
NQB-6	220	18.3 DRY
NQB-7	220	13.9
NQB-8	220	13.5
NQB-11	20	9.1 SATURATED
NQB-15	20	13.4
NQB-17	20	14.7
NQB-18	20	7.2

The average of all samples is 11.0 ± 2.9 MPa.

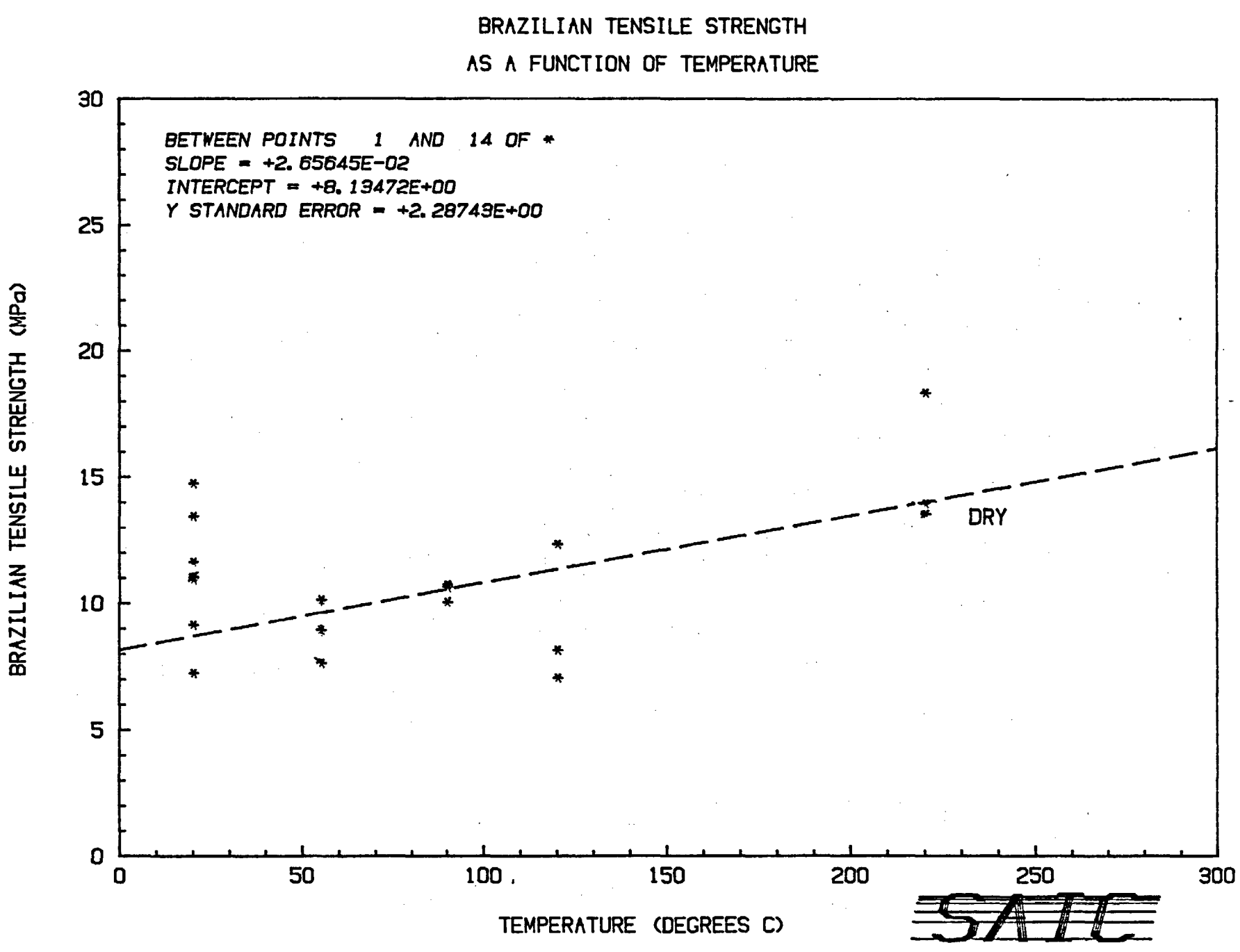

FIGURE 7. Brazilian Tensile Strength As a Function of Temperature.

4.4.1 Equipment and Procedures

All of the triaxial testing discussed here was performed using a Hoek-type triaxial cell (Figure 8). This device allows testing at confining pressures to 70 MPa, while providing an extremely quick and simple sample setup. For ambient temperature testing, the core sample was placed in a neoprene confining jacket, which was, in turn, clamped in the chamber. EW (37.9-mm) and NQ 47.6-mm) sized chambers were used for these tests. At each end of the sample, an end cap was placed in contact with the core, one end cap being equipped with a spherical seat for axial load alignment. With the sample and end caps in place, a slight confining pressure was placed in the chamber using a hand pump with accumulator. The cell was then placed between a Terrametrics 100-ton (890-kN) load cell and a 6-inch stroke, 200-ton (1780-kN) Enerpac ram in a reaction frame. The ram was brought just into contact with the upper end cap using a manual set point control. At this point, a Houston Instruments analog X-Y recorder was centered and calibrated shunt resistors actuated to provide a load and displacement calibration on the chart paper. Next, confining pressure and axial load were increased simultaneously to their prescribed values. The axial load was controlled manually with the servo-controller set point control, and the confining pressure was increased with a hand pump. Once the test confining pressure was reached, the pressure vessel was isolated from the hand pump, the in-line accumulator keeping the confining pressure constant to within 2% during the test. The servo-controller was placed on displacement control and the ramp rate adjusted so that axial pressure would increase at approximately 0.2 MPa/s, producing failure in approximately 15 min. The above procedures conform to the ISRM standards as given by Brown (1981).

For elevated temperature testing, silicone-rubber jackets were used. Three band heaters, 500 W maximum per heater, were placed around the cell and wired in series (Figure 8). An insulating blanket was wrapped around the entire assembly. The power to the band heaters was controlled by an Omega temperature controller, sensing a Type K thermocouple at the sample. Each sample was slowly heated to the desired temperature in an oven prior to testing, then removed and placed in the confining chamber; the chamber placed in the loading frame, the heaters energized, and the sample allowed to equilibrate at the desired temperature. Sample loading and data recording procedures were the same as those used for ambient testing.

4.4.2 Results

A typical triaxial test stress versus strain plot is shown in Figure 9. Brittle failure occurred in each case, producing typical shear fractures. The strength of each sample was calculated by dividing the peak load by the original sample cross-sectional area. The results of all tests are given in Table 7.

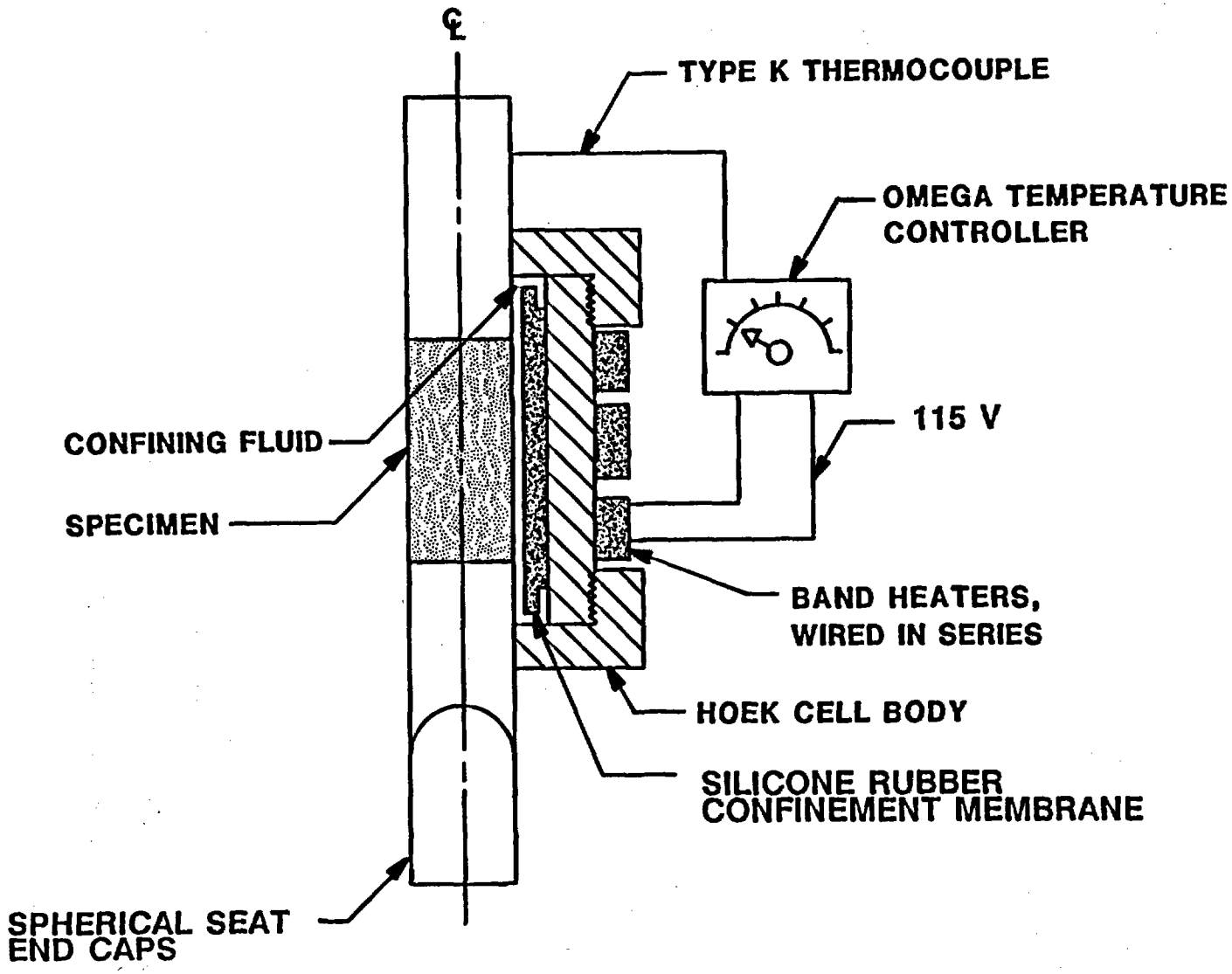

FIGURE 8. High Temperature Hoek Triaxial Cell (insulation removed for clarity). (Not to scale.)

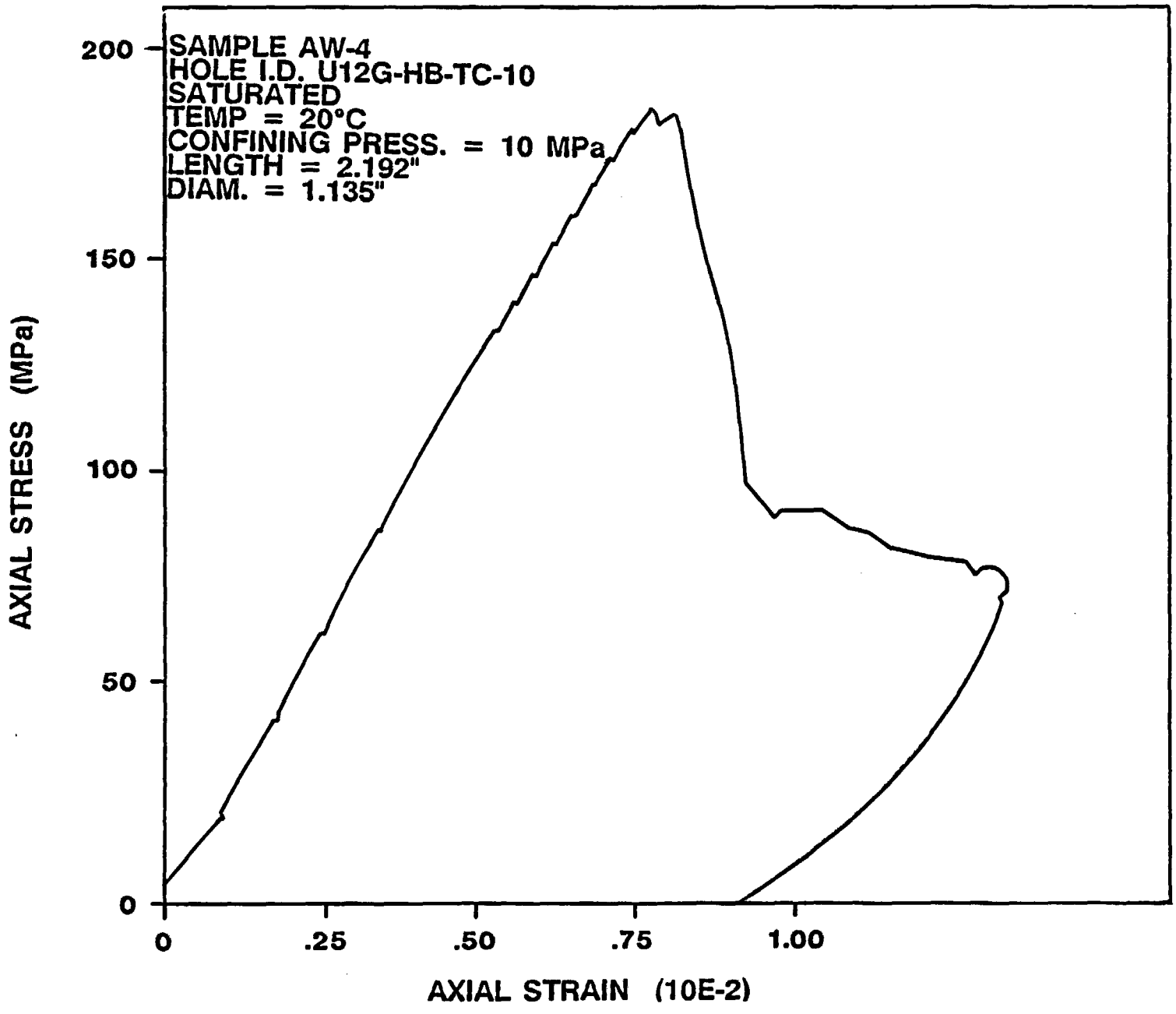

FIGURE 9. Typical Triaxial Stress-Strain Plot from an X-Y Recorder.

TABLE 7

RESULTS OF TRIAXIAL COMPRESSION TESTS

SAMPLE NO.	TEMPERATURE (°C)	SATURATION	CONFINING PRESSURE (MPa)	AXIAL STRESS AT FAILURE (MPa)
EW-7	20	DRY	10	176
EW-9	20	DRY	20	228
AW-4	20	SATURATED	10	183
AW-5	20	SATURATED	20	215
EW-15	20	SATURATED	20	210
EW-6	20	SATURATED	10	141
EW-8	20	SATURATED	10	208
EW-1	20	SATURATED	20	177
NQ-1	20	DRY	20	266
NQ-13	120	DRY	10	182
BW-2	20	DRY	20	82
EW-3	20	DRY	10	232
AW-134	120	DRY	10	216
AW-13	120	DRY	20	253
AW-12	20	DRY	10	193
AW-11	20	DRY	20	296
EW-52	120	DRY	10	229
EW-46	120	DRY	10	262
EW-12	120	DRY	10	175
EW-50	120	DRY	20	338
EW-58	120	DRY	20	292
EW-21	120	DRY	20	347
EW-47	220	DRY	10	234
EW-28	220	DRY	10	189
EW-62	220	DRY	10	292
EW-19	220	DRY	20	163
EW-23	220	DRY	20	191
EW-60	220	DRY	20	317
EW-39	20	DRY	10	177
EW-44	20	DRY	20	285
EW-30	20	DRY	20	213
EW-20	20	SATURATED	20	283
EW-32	20	SATURATED	10	130
EW-29	55	SATURATED	10	179
EW-42	55	SATURATED	10	236
EW-17	55	SATURATED	10	166
EW-40	55	SATURATED	20	219
EW-54	55	SATURATED	20	219
EW-41	55	SATURATED	20	257
EW-10	90	SATURATED	10	243
EW-49	90	SATURATED	10	162
EW-22	90	SATURATED	10	145
EW-56	90	SATURATED	20	279
EW-15	90	SATURATED	20	175
EW-38	90	SATURATED	20	249

To determine the Mohr-Coulomb parameters (ø, the intact angle of internal friction, and c, the cohesion), plots of the axial stress at failure versus the confining stress were made (Figures 10 through 12) after Brace (1981, p. 127). Here, the tests have been divided into three groups: 20°C, dry; 20°C to 90°C, saturated; and 120°C to 220°C, dry. Only one sample size, EW diameter, is used in the statistical analysis to reduce any additional variability caused by different sample sizes. In addition to the triaxial tests, data taken under similar conditions of temperature and moisture are plotted from the uniaxial compression tests. As seen in these plots, the data fall, in general, along a straight line. The slope, m, and intercept, b, of these lines have been computed using a least-squares linear regression analysis. These parameters, m and b, have been used to compute the Mohr-Coulomb parameters, as suggested by the ISRM standards (Brown, 1981):

$$\Phi = \arcsin \frac{m - 1}{m + 1}$$

$$c = b \frac{1 - \sin\phi}{2\cos\phi} \qquad (4.1)$$

Standard deviations of Φ and c have also been calculated from the above equations. The results of these calculations for each test series are given in Table 8. In view of the considerable data scatter, no significant trends can be identified in the data. This scatter is particularly masked in the data for dry samples at elevated temperatures (120° to 220°C).

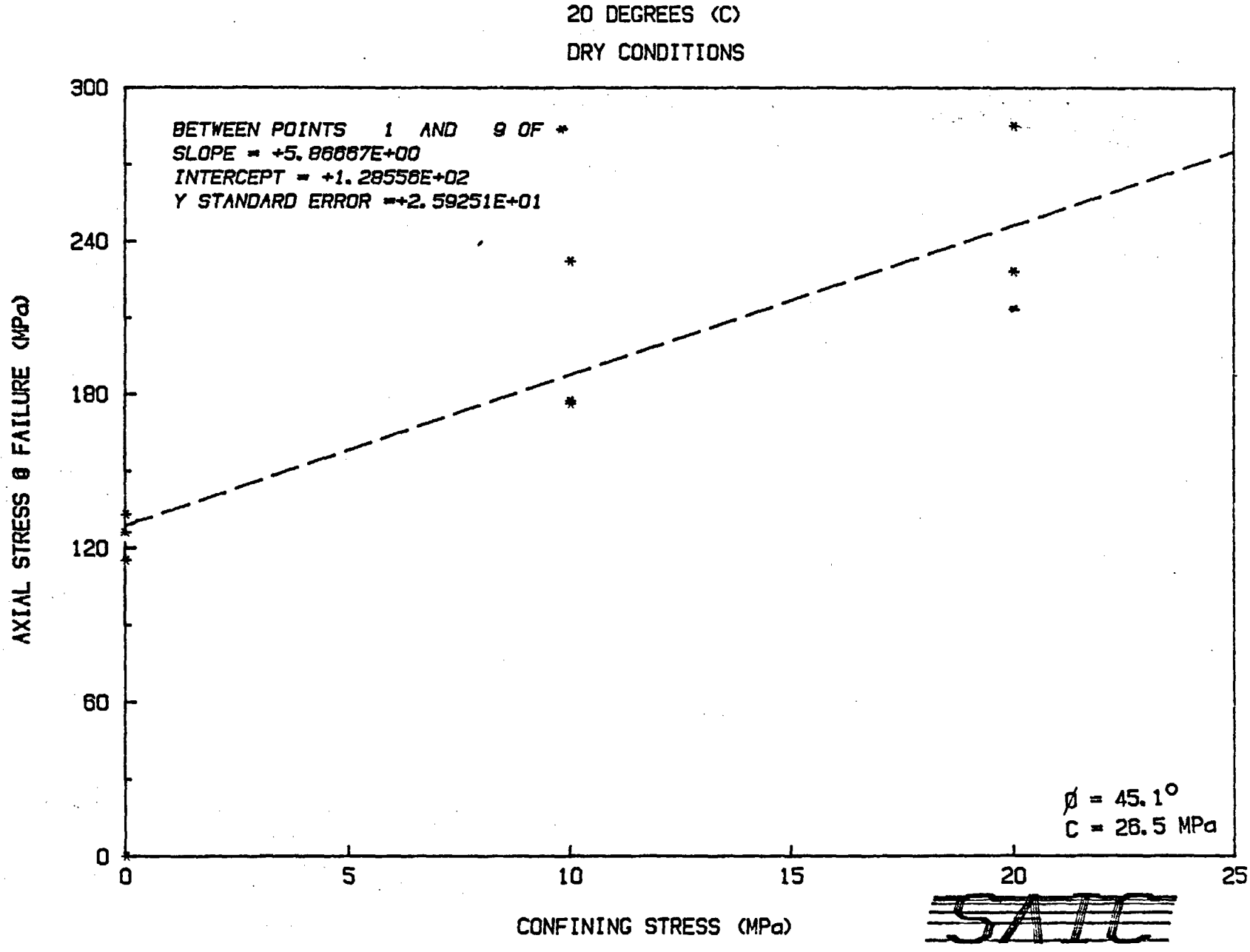

FIGURE 10. Compressive Strength versus Confining Pressure for Triaxial and Uniaxial Tests at 20°C, Dry Conditions.

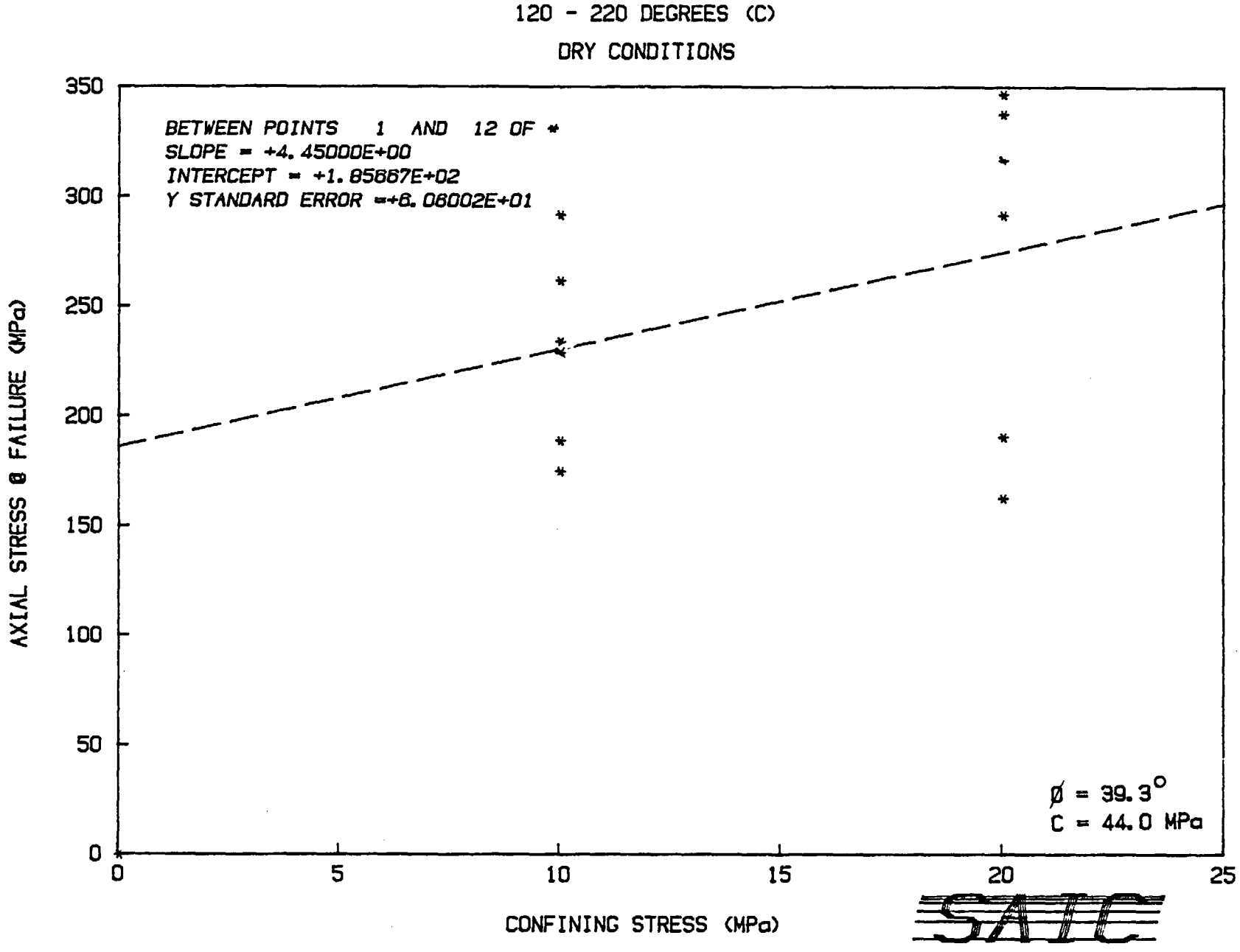

FIGURE 11. Compressive Strength versus Confining Pressure for Triaxial and Uniaxial Tests at 120 to 220°C, Dry.

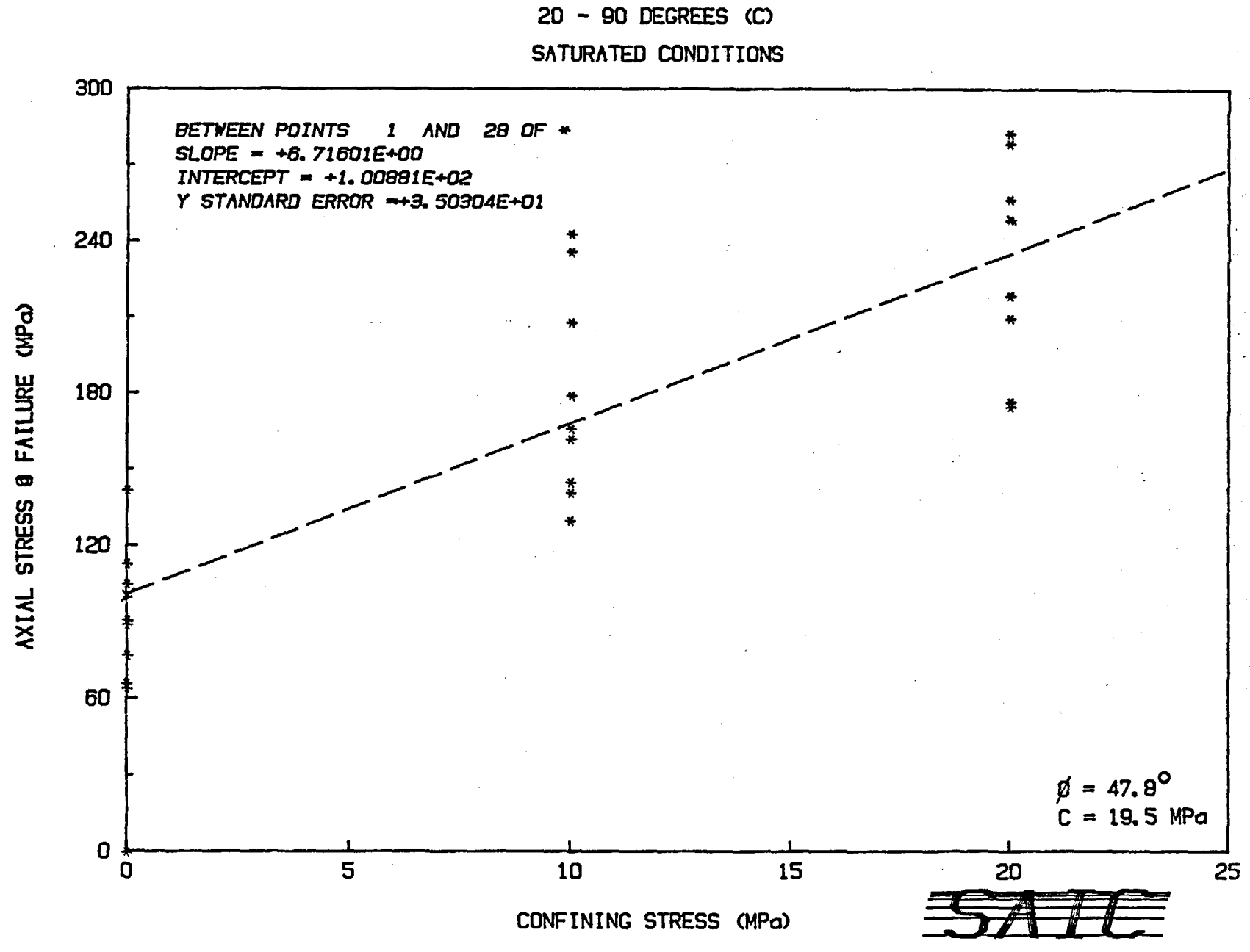

FIGURE 12. Compressive Strength versus Confining Pressure for Triaxial and Uniaxial Tests at 20 to 90°C, Saturated.

TABLE 8

MOHR-COULOMB PARAMETERS
FOR GROUSE CANYON WELDED TUFF AS
A FUNCTION OF TEMPERATURE AND MOISTURE CONTENT

TEMPERATURE (°C)	SATURATION	RANGE OF CONFINING PRESSURE (MPa)	COHESION (MPa)	INTERNAL FRICTION ANGLE (DEGREES)
20	DRY	0-20	26.5 (±4.0)*	45.1 (±3.9)*
20-90	SATURATED	0-20	19.5 (±2.7)	47.8 (±2.7)
120-220	DRY	0-20	44.0 (±26.9)	39.3 (±21.6)
ALL	DRY	0-20	28.3 (±6.5)	46.7 (±5.5)

* ± figures are standard deviations for cohesion and internal friction angle calculated from Equation 4.1 and from the standard deviation of the linear regression slopes and intercepts.

5.0 DIRECT SHEAR TESTING OF SAW-CUT JOINTS

A series of six direct shear tests were conducted on saw-cut samples under dry and saturated conditions at room temperature. In addition, five tests were run at elevated temperatures and dry conditions, and one test at elevated temperature and saturated conditions. This testing was originally to have been performed on naturally jointed specimens; however, none of the core received possessed natural joints suitable for testing. It was decided that saw-cut joints provided the best alternative under the circumstances.

When a direct shear test is conducted on a natural joint, a shear stress-shear displacement curve similar to that given in Figure 13 is obtained (Goodman, 1980, p 150). Peak shear strength is a function of the normal stress applied to the sample and of the roughness of the joint surface. Once the joint has sheared, the shear stress will approach a residual strength value. The corresponding peak shear stress-normal stress curve is given in Figure 14. Here, the initial slope of the curve is determined by the friction angle of the joint surface, ϕ_u, and the asperity angle, i, which is related to the joint roughness. The later slope is determined by the residual friction angle , ϕ_r. With a saw-cut joint, the cohesion will be small, and the frictional angle will approach the residual angle for natural fractures. A large literature base exists on tests of saw-cut joints and the effects of increasing roughness (Jaeger, 1959; Brace and Byerlee, 1968; and Hoskins, Jaeger, and Rosengren, 1968). These articles were referred to in the design and analysis of these tests.

5.1 Equipment and Procedure

The technique used for direct shear testing was taken after that described by Hoskins et al., (1968). All NQ core samples (47.6-mm diameter) were cut to produce three sections with joint surface asperities of less than 1/16 inch. The sections were than placed axially in a horizontal load frame (Figure 15) that used a 10-ton (90-kN) ram to deliver the normal load. The two outer halves of the core were supported with semicircular members in contact with the lower machine platen. The shear force was applied to the center core section by the large machine ram. The servo-controller was used under displacement control to load the sample at a prescribed rate. The normal load was kept constant during testing through the use of an accumulator on the axial ram load hydraulic circuit. Shear force was monitored by a load cell and shear displacement by a DCDT attached to the ram. Force and displacement were recorded on a analog X-Y plotter for later analysis.

A typical test was performed by assembling the sample along alignment marks made prior to the saw cutting. The assembled sample

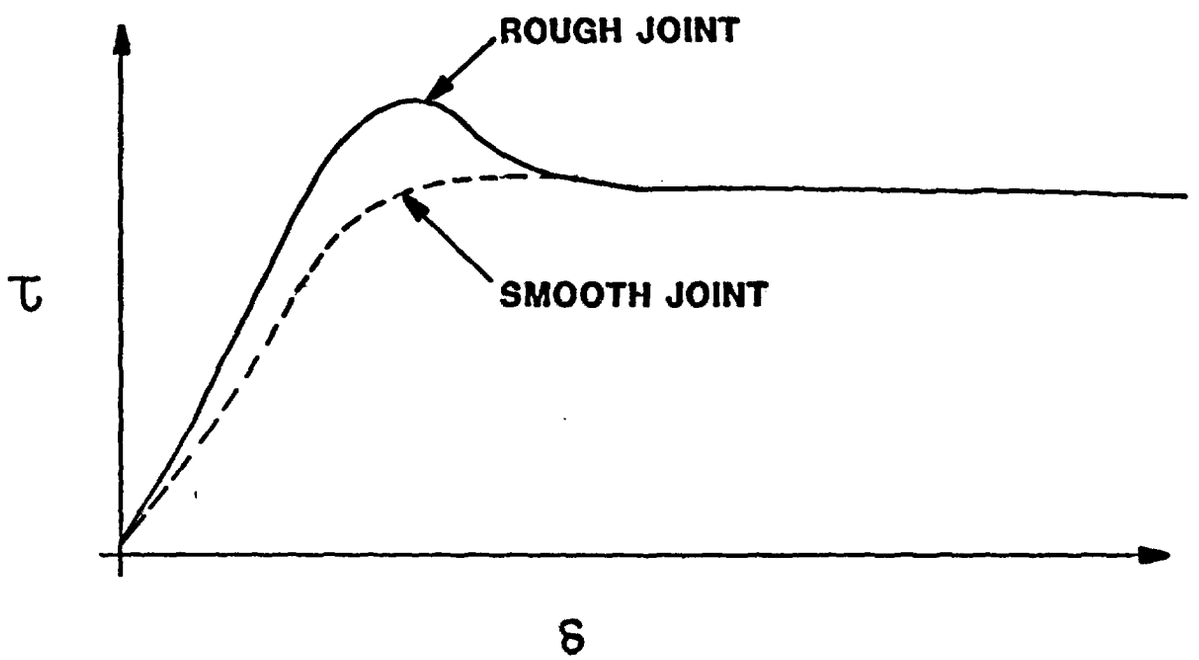

FIGURE 13. Shear Stress-Shear Displacement Curves for Rough and Smooth Joints. (After Goodman, 1980)

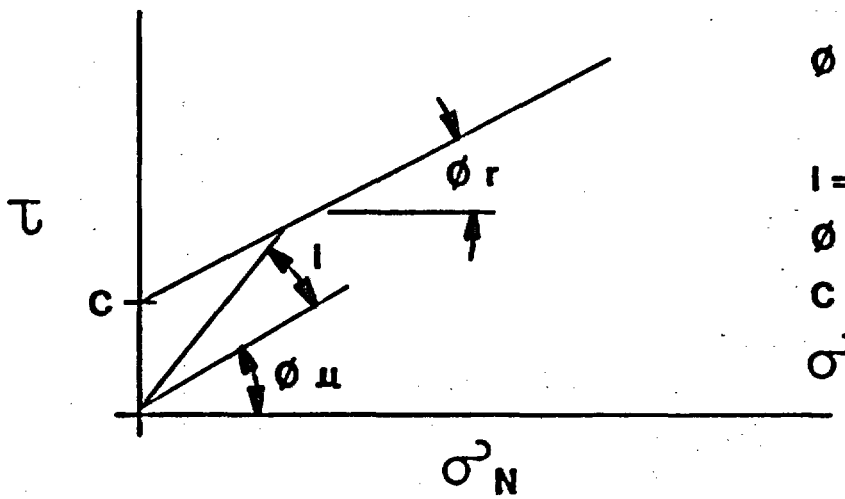

Ø μ = FRICTION ANGLE FOR SMOOTH JOINT

I = ASPERITY ANGLE

Ø r = RESIDUE FRICTION ANGLE

C = COHESION

σ_n = NORMAL STRESS

FIGURE 14. Bilinear Shear Strength Criterion Illustrating the Components of Friction (ϕ_μ and i) at Low Normal Stress and at High Normal Stress ($\phi_r = \phi\mu$). A saw-cut fracture will have essentially zero degree asperity angle, and low cohesion.

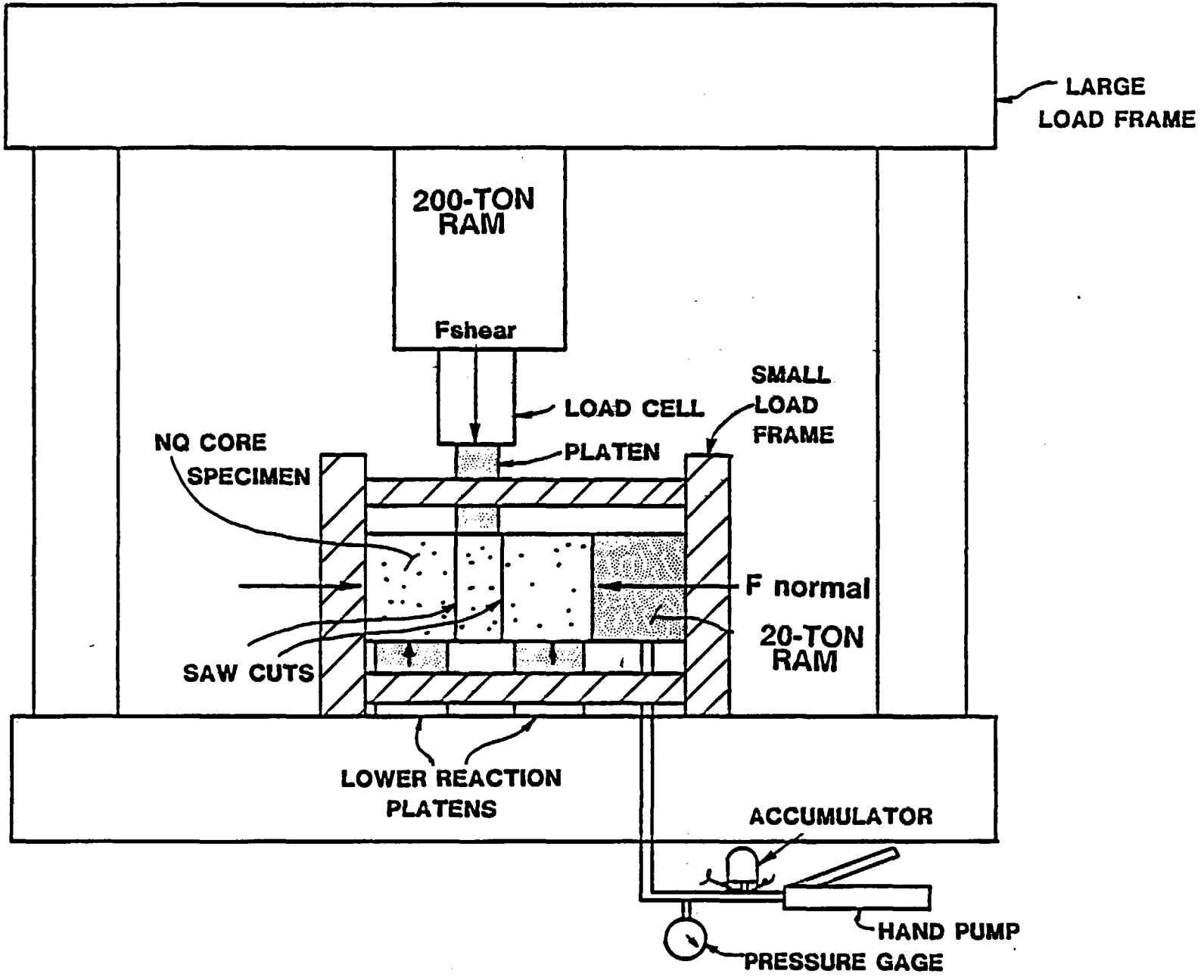

FIGURE 15. Direct Shear Testing Apparatus.

was placed horizontally in the small load frame and loaded axially to the designated normal stress. The outer sample supports were shimmed beneath the core until they were in intimate contact with the core. The large frame ram was brought just into contact with the center section, and the recorders and servo-controller zeroed. At this time, the shunt calibration resistors were activated to provide a load and displacement calibration on the analog recorder paper. A displacement ramp rate of 8.3×10^{-4} cm/s was used for shearing displacements. The test was terminated after significant displacement beyond peak strength. Normal stresses were varied from 2 to 10 MPa and temperature from 22° to 120°C. The surface of the fracture was either dry or saturated during testing. For saturated tests, the samples were submerged for several days before testing and wetted continuously for the duration of the test, which was approximately 5 min. For elevated temperature testing, the samples were heated to design levels slowly in an oven and loosely insulated during the testing. The temperature of an insulated sample was monitored while outside the oven, and minimal temperature loss was noted for the maximum test time (10 to 15 min).

5.2 Results

Figure 16 shows a typical plot of shear stress versus shear displacement. Initial nonlinearity occurs as minor surface irregularities close and seating of the loading platen occurs. This is followed by a relatively linear shear-stress-versus-displacement relationship. As the shear stress begins to overcome friction and shear through asperities, the curve becomes nonlinear and irregular. A peak stress is attained beyond which the stress remains relatively unchanged with increasing displacement as the central section of core slides along surfaces on which asperities have been sheared. The earliest peak stress is chosen as the peak shear stress. The slope of the loading portion of the curve represents the shear stiffness of the fracture. Table 9 summarizes the test conditions, peak shear stress, and shear stiffness for each test. The saturated samples appear to have a higher average shear stiffness, but there are insufficient data for an estimate of the significance of this result. The stiffness values obtained are of the same order as the typical ranges for natural joints, which have an average of approximately 3 GPa/m (Kulhawy, 1978).

The Mohr envelope for the peak shear stress-normal stress values obtained is shown in Figure 17. The plot indicates a dry friction angle of approximately 20 degrees and a saturated friction angle of 26 degrees. In both cases, the cohesion appears to be very small, or zero, as would be expected with smooth joints. Since the roughness of these artificial joints is less than might be expected in natural joints, the friction angles measured here give an estimate of the residual friction angles, ϕ_r (Figure 14). No particular temperature dependence was noted for any of the joint testing. This is not necessarily indicative of the behavior of natural in situ joints that may have infilling materials such as clays, which are temperature and moisture sensitive. It should also be noted that the envelope derived for saturated samples is based on only three data points.

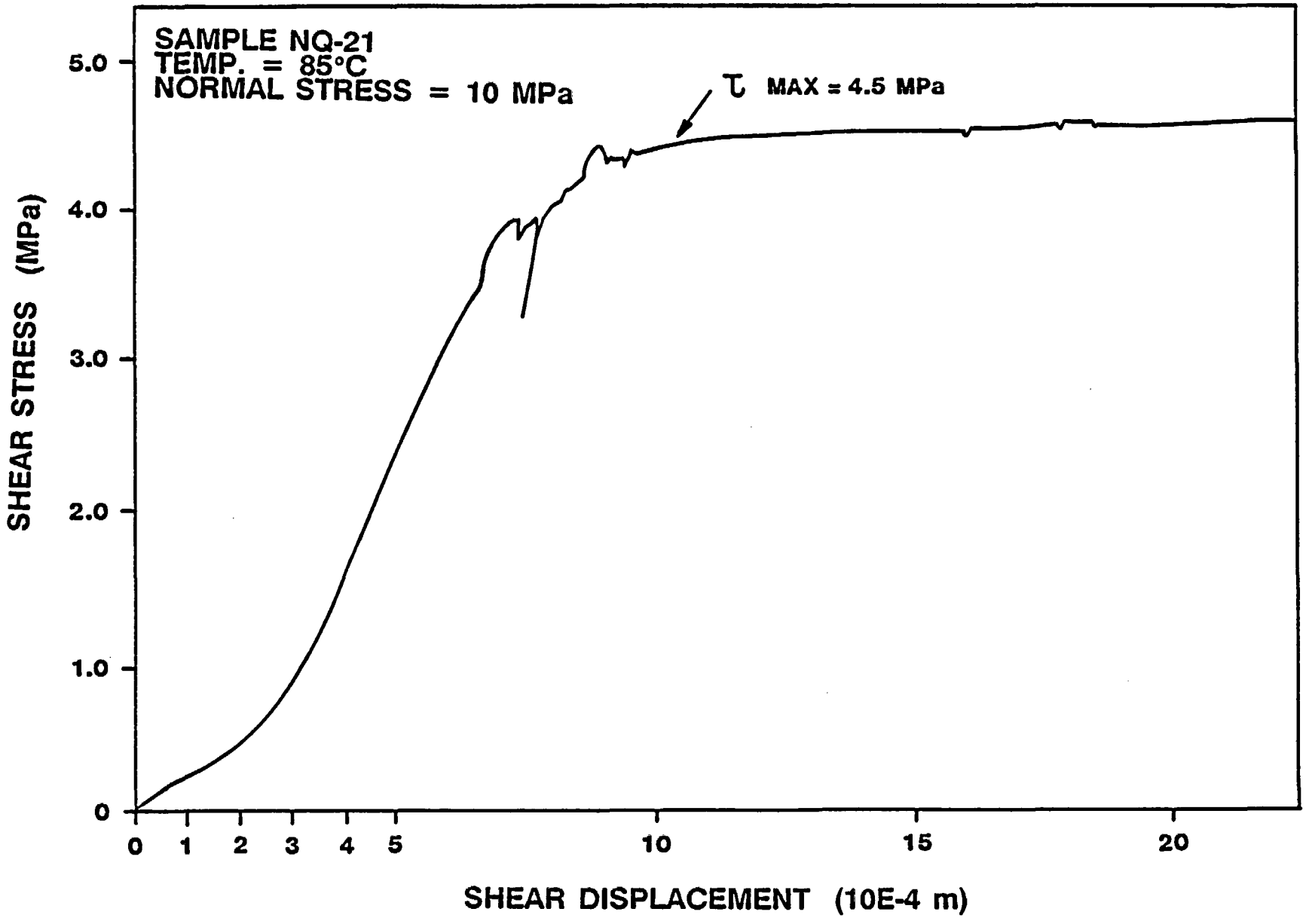

FIGURE 16. Typical Direct Shear Test Results; Shear-Stress-versus-Shear-Displacement plot.

TABLE 9

DIRECT SHEAR TESTING
OF SAW-CUT JOINTS,
GROUSE CANYON MEMBER WELDED TUFF

SAMPLE NO.	TEMPERATURE (°C)	SATURATION CONDITION	NORMAL STRESS (MPa)	PEAK SHEAR (MPa)	SHEAR STIFFNESS (GPa/m)
NQ-14	20	DRY	5	1.5	2.5
NQ-29	20	DRY	5	2.1	2.9
NQ-7	20	DRY	10	2.6	3.9
NQ-36	90	DRY	2	0.9	2.3
NQ-29	120	DRY	5	2.9	3.8
NQ-8	220	DRY	5	1.1	3.0
NQ-15	55	DRY	10	3.9	4.7
NQ-21	85	DRY	10	4.6	8.6
NQ-31	20	SATURATED	5	3.0	4.4
NQ-2	20	SATURATED	10	7.7	9.9
NQ-3	20	SATURATED	10	*	1.2
NQ-4	80	SATURATED	5	7.5	5.8
NQ-5	55	SATURATED	5	*	14.0

*Equipment problems before peak stress.

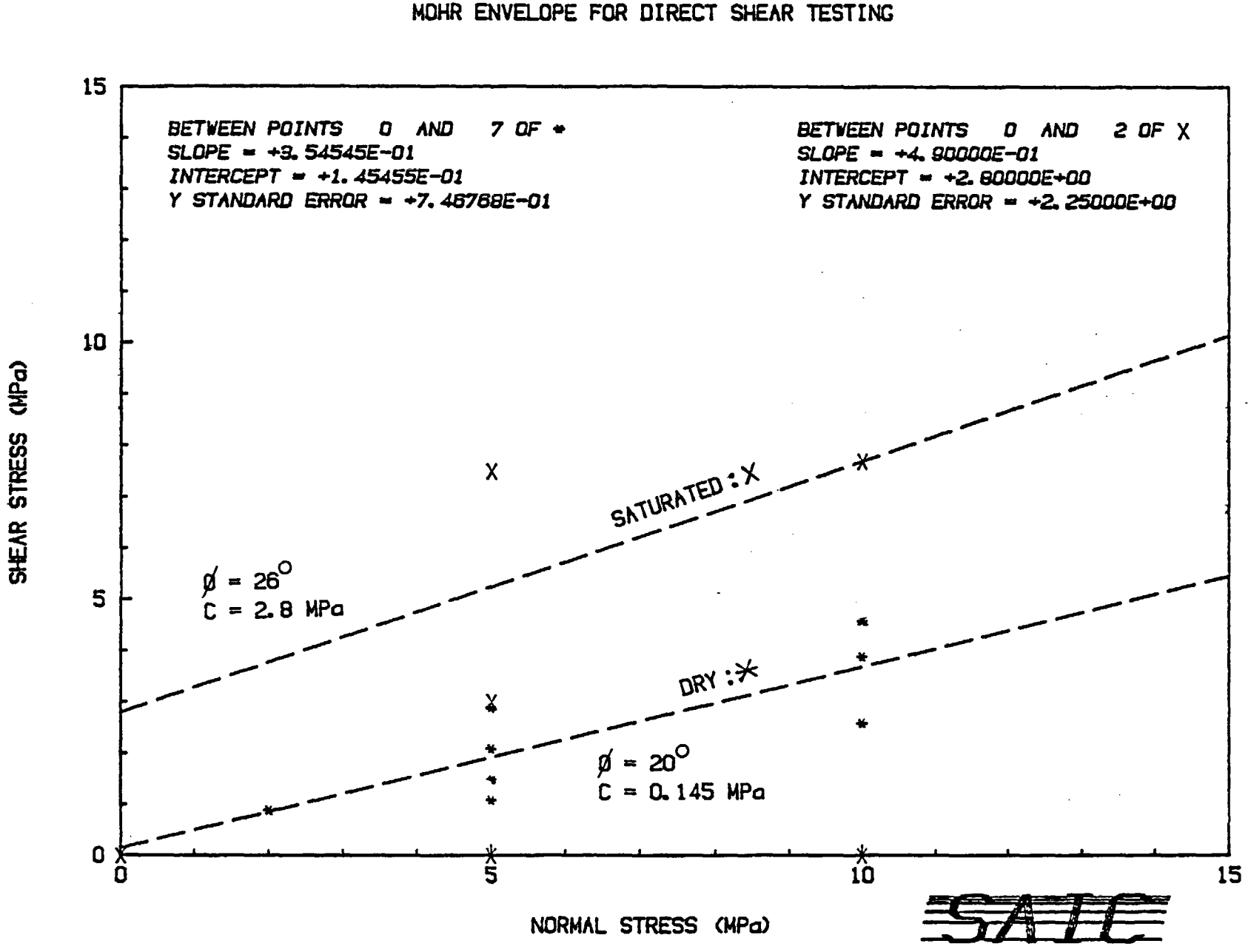

FIGURE 17. Mohr Envelope for Saw-Cut Joint Direct Shear Tests.

5.3 Normal Stiffness Testing

The normal stiffness of one joint was determined in a small loading frame (Figure 18). Here, a yoke with two Schaevitz DCDT transducers was clamped across a sample fractured perpendicular to the plug axis using a hammer and chisel. A hand pump was used to apply load to the NQ-sized sample using a 10-ton (90-kN) Enerpac hydraulic ram. Sample load was calculated from the ram pressure and effective piston area. Hydraulic pressure was determined from a 1/4%-accuracy 3D Instruments pressure gauge.

The joint was subjected to three load cycles to 27.5 MPa. A plot of normal stress versus normal displacement is shown in Figure 19. This curve represents the combined fracture and intact rock response. However, at the lower stress levels the fracture will be the softest element, so that the curve represents closing of the fracture in these regions, or the fracture normal stiffness. Fracture normal stiffness produces a nonlinear response of stress versus displacement, which becomes asymptotic to the intact rock stiffness as the joint closes. The normal stiffness is given by the tangent to the curve at any point. A plot of the normal stiffness versus normal stress is given in Figure 20. These values compare quite favorably with published data. For example, normal stiffness values typically range from 24 to 70 GPa/m (Kulhawy, 1978).

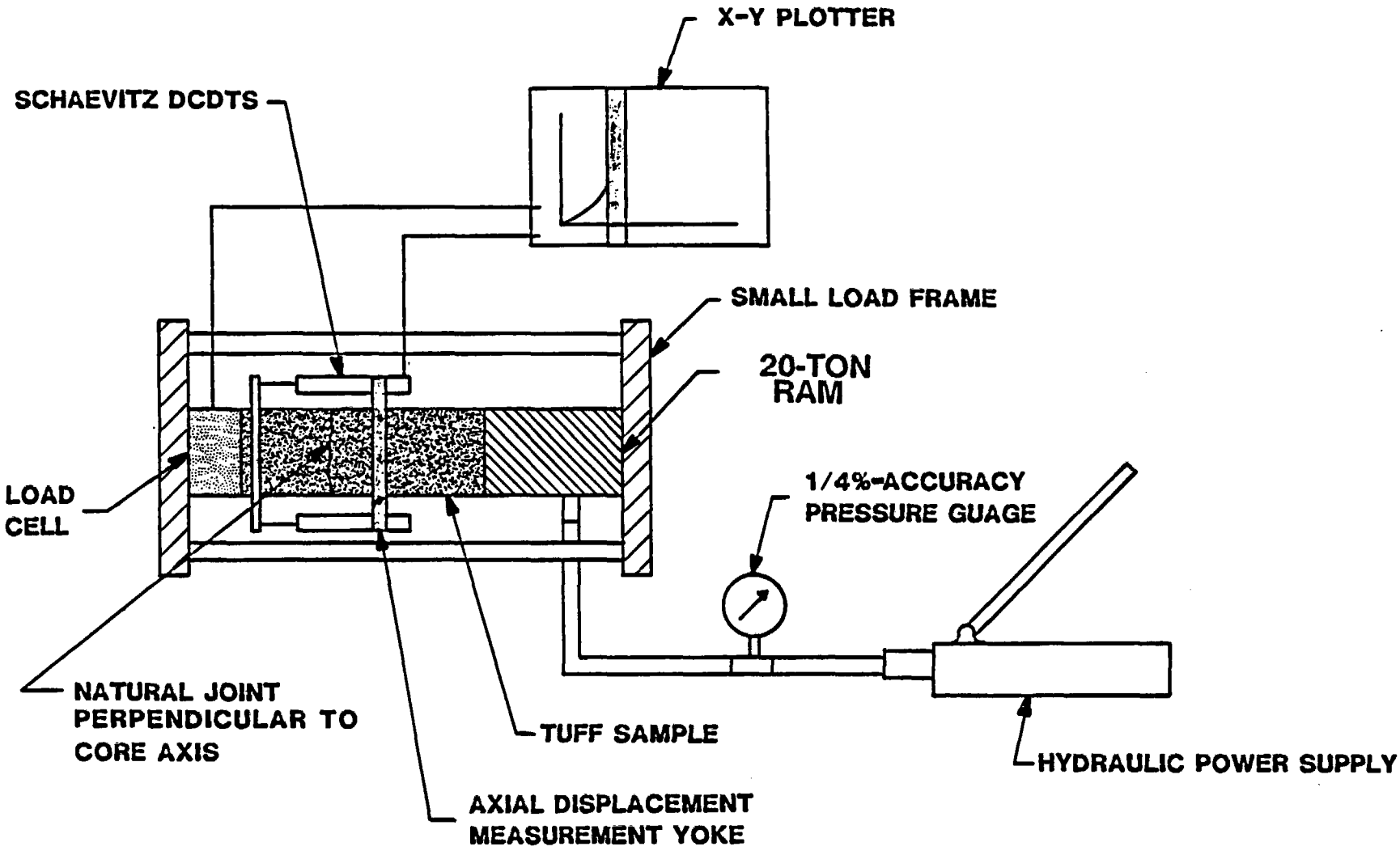

FIGURE 18. Set-up for Joint Normal Stiffness Measurement.

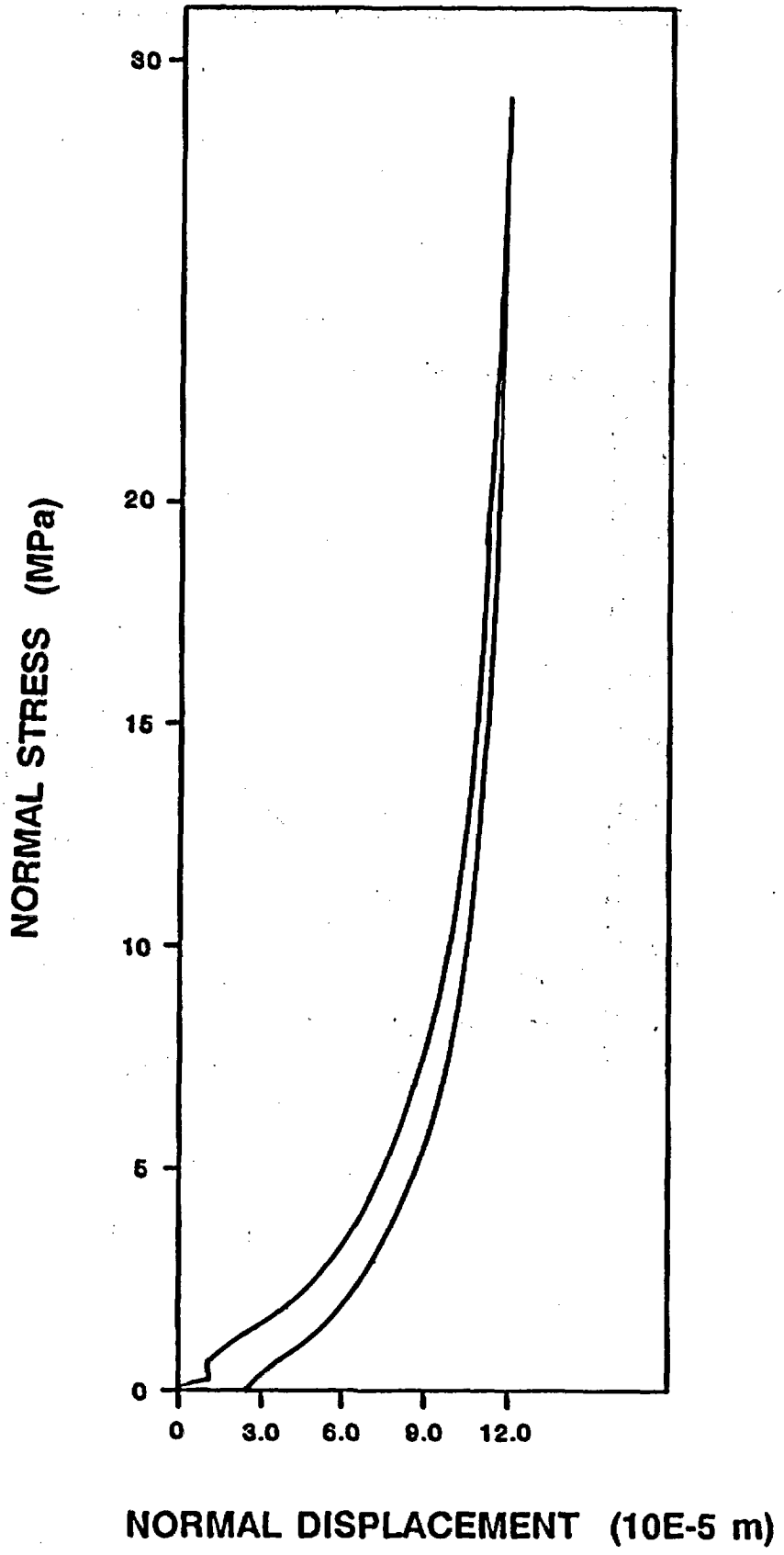

FIGURE 19. Normal Stress versus Normal Displacement for Determination of Joint Normal Stiffness.

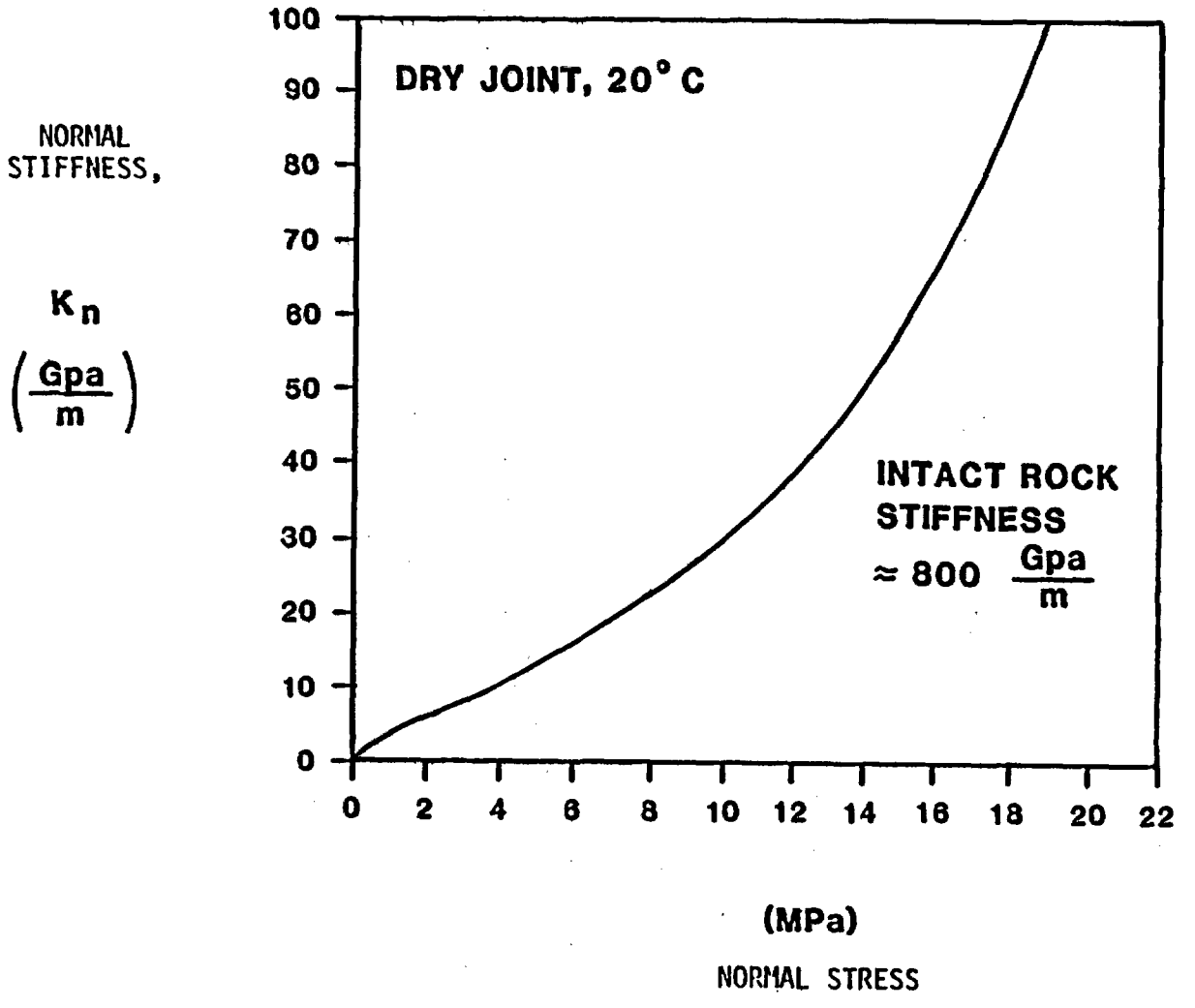

FIGURE 20. Variation of Joint Normal Stiffness with Applied Normal Stress.

6.0 ULTRASONIC VELOCITY MEASUREMENTS

Compressional and shear wave velocity data were acquired for six NQ-sized cores (47.6-mm diameter) that were drilled from the floor of the heated block test alcove. The core holes and acquisition depths for each of the NQ cores tests were given in Table 2 of this report. The cores tested for ultrasonic velocity were obtained from vertical holes; the cores were not oriented and were drilled using a single-tube core barrel. Cores for testing under saturated conditions were selected from core that was carefully wrapped in plastic immediately after recovery. Cores for unsaturated testing were exposed to ambient air during the several months between recovery and preparations for testing. The cores were prepared by grinding the ends flat and parallel to better than 0.025 mm. No couplant or adhesive was used.

Core saturation, varying between 80% and 99% based on weight, was accomplished by immersing the prepared cores in tap water and keeping them under vacuum for 30 days. Other cores were dried in a vacuum oven under similar vacuum conditions, at a temperature of 45°C, for 90 days.

6.1 Equipment and Procedures

The apparatus used for testing consisted of a pair of steel end caps each with an internal cavity containing a single piezoelectric transducer and a mechanism for constraining it (Figures 21 and 22). Transducers were varied to change the frequency of operation and to alternate between compressional and shear operation. The transducers used were of the single-element type, of PZT-5 material with uniform polarization direction. For the shear transducers, this direction was marked for consistency and reassembled. The polarization direction of each compressional element was determined statically and marked. In this way, the relative orientation of the transducers, end caps and the sample were maintained at all temperatures, even though the entire system was disassembled at each new temperature.

The system was calibrated by measuring the travel time through a cylinder of aluminum to determine the difference between observed and theoretical travel times (Tables 10 and 11). The difference was subsequently subtracted from all travel times measured in the rock. The delay time was sensitive to the configuration of the test system, necessitating exact reassembly whenever frequency or mode was changed. A measurement system consisting of a 5-MHz digitizer (Gould Biomation 2805) with a digital oscilloscope (Nicolet 2090) for display and storage was used to acquire signals. All received waveforms were saved on flexible discs for later inspection and analysis. Transmitter excitation was provided by a high-voltage pulse generator; the level and speed of each pulse could be adjusted so that approximately 400 V/mm of transducer thickness was applied at a rate of approximately 10 V/s.

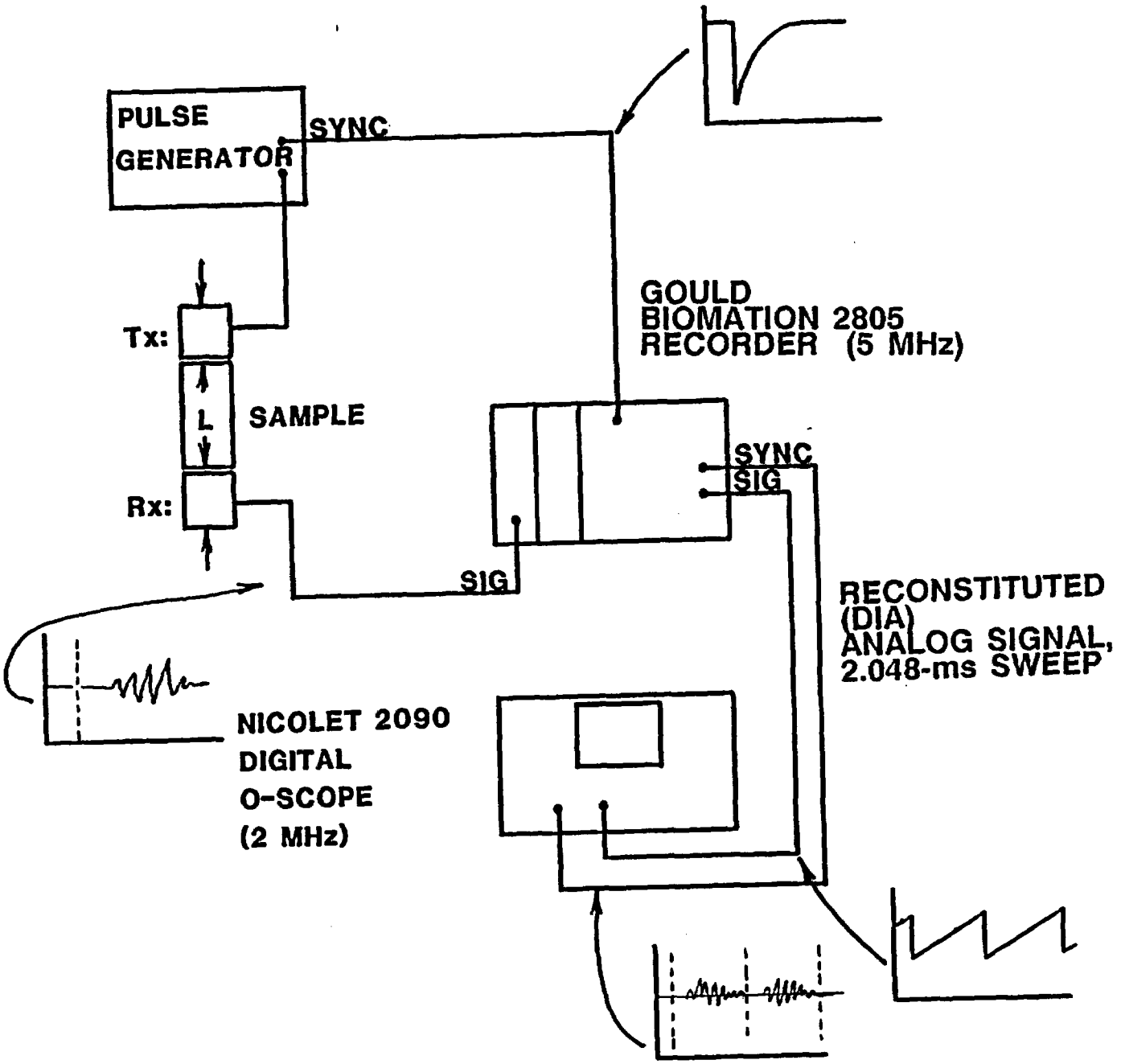

FIGURE 21. Laboratory Ultrasonics Apparatus.

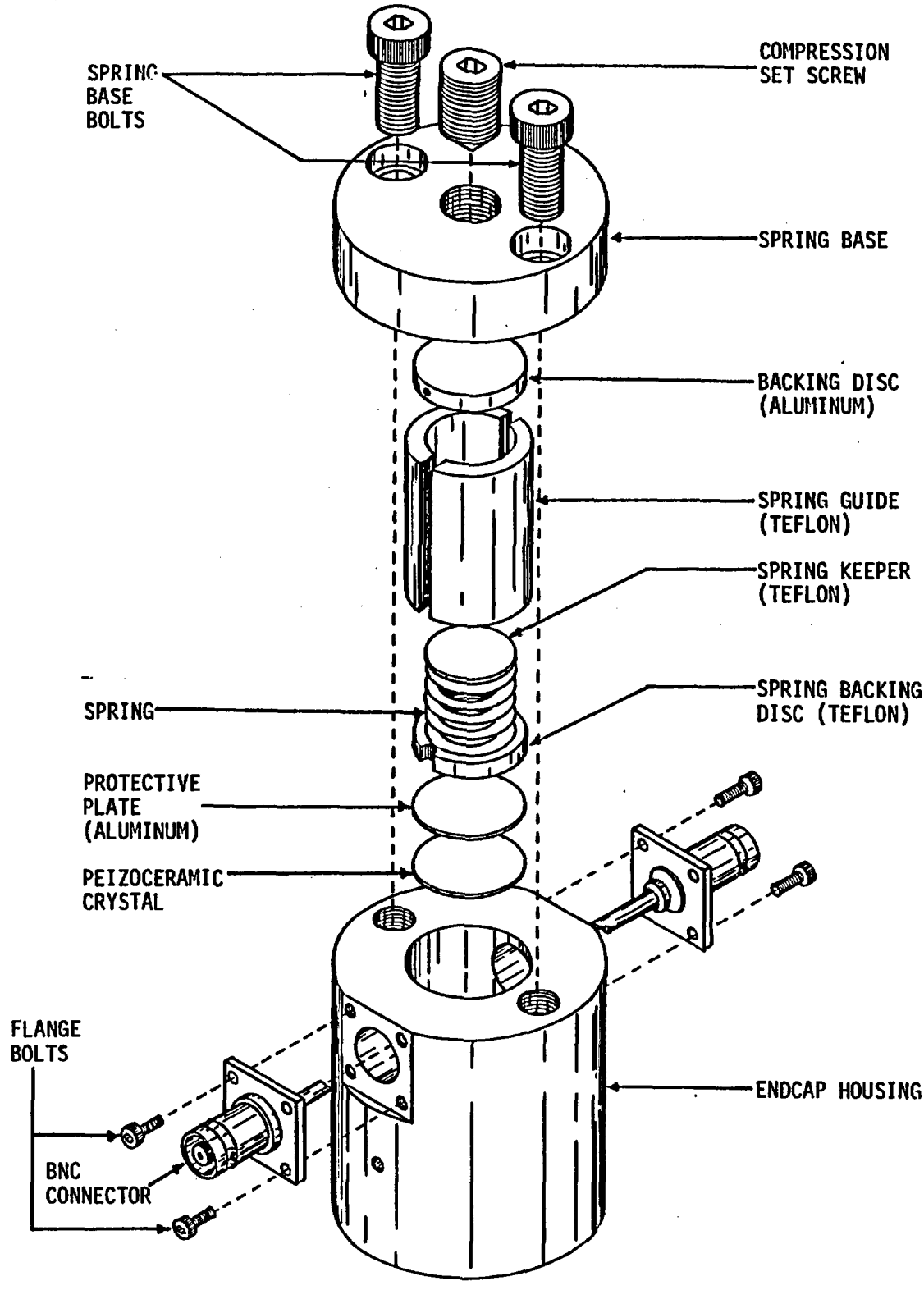

FIGURE 22. The End Cap Orthographic Projection.

TABLE 10

AMBIENT TEMPERATURE ULTRASONIC CALIBRATION TRIALS

	FREQUENCY (kHz)	OBS. TRAVEL TIME (μs) 1	2	3	MEAN, STD. DEV. (μs)	DELAY (μs)	ACCURACY (%) [see text]
P	250	25.6	24.7	24.6	24.9 ± 0.6	9.9 ± 0.6	2
P	500	23.5	22.4	22.8	22.6 ± 0.6	7.6 ± 0.6	2
P	1000	23.7	25.3	22.7	23.5 ± 0.5	8.5 ± 0.5	2
S	250	43.1	47.0	45.6	45.2 ± 2.0	13.5 ± 2.0	5
S	500	44.6	48.1	47.0	46.8 ± 2.1	15.1 ± 2.1	5
S	1000	51.1	51.6	52.4	51.7 ± 0.7	20.0 ± 0.7	2

TABLE 11

OBSERVED TRAVEL TIME IN ALUMINUM CYLINDER (μs)

	FREQUENCY (kHz)	20 °C	120 °C	220 °C
P	250	23.4	23.1	23.3
P	500	22.6	23.3	22.8
P	1000	22.5	24.5	25.4
S	250	43.0	44.8	47.0
S	500	44.6	45.6	47.2
S	1000	51.2	53.8	53.7

The test matrix (Tables 12 through 15) was designed so that all lower temperature measurements were made before elevating the specimen temperature, to avoid changes in the conflicting velocities because of thermal alteration. All measurements were conducted by first preparing the apparatus, bringing the sample and end caps to temperature in separate ovens, removing the end caps and specimen from the ovens, and acquiring the waveform as quickly as possible. Cooling of the specimen during the short period prior to acquisition was neglected. Since all measurements were performed with ambient confining pressure, it was necessary to limit the maximum temperature for saturated specimens to 90°C. No couplant or adhesive was used.

Accuracy of the system was estimated from the ambient temperature baseline tests of the aluminum cylinder. The standard deviation for successive measurements was determined for P-wave and S-wave velocities at each frequency (Tables 10 and 11). The end caps were disassembled and reassembled for each trial measurement. Using typical P-wave and S-wave travel times through rock cores of 25.0 and 40.0 μs, respectively, the accuracy at ambient temperature at each frequency was estimated. It is believed that errors were introduced by the following:

1. Inability to precisely repeat the orientation of piezoelectric crystal during reassembly of the end caps.

2. Nonuniform distortion of the specimens in response to the load required to seat the end caps.

3. Electronic drift in the triggering circuit which facilitated transfer of the data from digitizer to oscilloscope.

The time-scale resolution of the digitizer was 200 ns, corresponding to P-wave and S-wave velocity resolution for a typical rock specimen of ±0.030 and ±0.013 km/s, respectively.

6.2 Results

P-wave and S-wave velocities measured at each temperature for each specimen are given in Tables 12 through 15; these tables also give statistics summarizing the average velocity at each temperature, average of different specimens, and the average relative change in velocity between each two successive temperatures. Plots of P- and S-velocity versus temperature for saturated and unsaturated conditions, at the different frequencies, are presented as Figures 23 through 25 and 26 through 28. The data indicates the following relationships:

1. Saturated P-velocity tended to be slightly higher than unsaturated P-velocity.

TABLE 12

SATURATED SAMPLES
P-WAVE VELOCITY SUMMARY

SAMPLE	VELOCITY km/s 20°C	% CHANGE 20°-55°C	VELOCITY km/s 55°C	% CHANGE 55°-90°C	VELOCITY km/s 90°C
			FREQUENCY 250 kHz		
NQ-10	4.13	2.18	4.22	2.13	4.31
NQ-26	4.14	-0.24	4.13	1.45	4.19
NQ-27	4.14	3.14	4.27	-1.87	4.19
MEAN	4.14	1.69	4.21	0.57	4.23
STD.DEV.	±0.01	±1.74	±0.07	±2.14	±0.07
			FREQUENCY 500 kHz		
NQ-10	4.17	-1.20	4.12	-0.49	4.10
NQ-28	4.00	1.75	4.07	-0.98	4.03
NQ-27	4.11	1.95	4.19	0.48	4.21
MEAN	4.09	0.83	4.13	-0.33	4.11
STD.DEV.	±0.09	±1.76	±0.06	±0.74	±0.09
			FREQUENCY 1 MHz		
NQ-10	4.15	2.41	4.25	1.41	4.31
NQ-26	4.09	1.22	4.14	-1.21	4.09
NQ-27	4.21	1.43	4.27	-0.23	4.26
MEAN	4.15	1.69	4.22	-0.01	4.22
STD.DEV.	±0.06	±0.64	±0.07	±1.32	±0.12

TABLE 13

SATURATED SAMPLES
S-WAVE VELOCITY SUMMARY

SAMPLE	VELOCITY km/s 20°C	% CHANGE 20°-55°C	VELOCITY km/s 55°C	% CHANGE 55°-90°C	VELOCITY km/s 90°C
			FREQUENCY 250 kHz		
NQ-10	2.51	-1.99	2.46	0.81	2.48
NQ-26	2.46	1.22	2.49	-3.61	2.40
NQ-27	2.50	-0.40	2.49	0.40	2.50
MEAN	2.49	-0.39	2.48	-0.80	2.46
STD.DEV.	±0.03	±1.61	±.02	±2.44	±0.05
			FREQUENCY 500 kHz		
NQ-10	2.41	1.24	2.44	1.23	2.47
NQ-26	2.48	1.61	2.52	-5.16	2.39
NQ-27	2.49	2.01	2.54	-3.15	2.46
MEAN	2.46	1.62	2.50	-2.36	2.44
STD.DEV.	±0.04	±.39	±0.05	±3.27	±0.04
			FREQUENCY 1 MHz		
NQ-10	**	**	2.55	0.39	2.54
NQ-26	**	**	2.56	-6.25	2.40
NQ-27	2.46	-2.03	2.41	2.90	2.48
MEAN	2.46	-2.03	2.51	2.92	2.47
STD.DEV.			±0.08	±3.32	±0.07

**SHEAR ARRIVAL INDISTINCT

TABLE 14
UNSATURATED SAMPLES
P-WAVE VELOCITY SUMMARY

SAMPLE	VELOCITY km/s 20 C	PERCENT CHANGE 20 -70 C	VELOCITY km/s 70 C	PERCENT CHANGE 70 -120 C	VELOCITY km/s 120 C	PERCENT CHANGE 120 -170 C	VELOCITY km/s 170 C	PERCENT CHANGE 170 -220 C	VELOCITY km/s 220 C
P250 kHz									
NQ-17	3.95	3.04	4.07	-0.98	4.03	0.99	4.07	-0.49	4.05
NQ-24	4.01	-0.75	3.98	2.01	4.06	-0.49	4.04	1.73	4.11
NQ-25	3.82	2.88	3.93	-2.29	3.84	3.65	3.98	-1.26	3.93
Mean,	3.93	1.72	3.99	-0.42	3.98	1.38	4.03	-0.01	4.03
Std. Dev.	±0.10	±2.14	±0.07	±2.20	±0.12	±2.10	±0.05	±1.55	±0.09
P500 kHz									
NQ-17	3.95	-0.51	3.93	1.02	3.97	0.00	3.97	-1.76	3.90
NQ-24	3.98	-1.26	3.93	4.33	4.10	1.22	4.15	-1.20	4.10
NQ-25	3.79	0.53	3.81	0.79	3.84	0.00	3.84	0.52	3.86
Mean,	3.91	-0.41	3.89	2.05	3.97	0.41	3.99	-0.81	3.95
Std. Dev.	±0.10	±0.90	±0.07	±1.98	±0.13	±0.70	±0.16	±1.19	±0.13
P1 MHz									
NQ-17	4.03	0.99	4.07	-0.98	4.03	-0.74	4.00	1.25	4.05
NQ-24	4.03	2.23	4.12	0.73	4.15	0.48	4.17	-2.64	4.06
NQ-25	3.83	3.39	3.96	-1.52	3.90	0.26	3.91	-1.02	3.87

TABLE 15
UNSATURATED SAMPLES
S-WAVE VELOCITY SUMMARY

SAMPLE	VELOCITY km/s 20 C	PERCENT CHANGE 20 -70 C	VELOCITY km/s 70 C	PERCENT CHANGE 70 -120 C	VELOCITY km/s 120 C	PERCENT CHANGE 120 -170 C	VELOCITY km/s 170 C	PERCENT CHANGE 170 -220 C	VELOCITY km/s 220 C
S250 kHz									
NQ-17	2.36	2.12	2.41	-2.07	2.36	-1.27	2.33	3.86	2.42
NQ-24	**		2.41	3.32	2.49	-2.01	2.44	0.82	2.46
NQ-25	2.49	0.00	2.49	-0.40	2.48	0.00	2.48	-2.02	2.43
Mean, Std. Dev.	2.43 ±0.09	1.06 ±1.05	2.44 ±0.05	0.28 ±2.76	2.44 ±0.07	-1.09 ±1.02	2.42 ±0.08	0.89 ±2.94	2.44 ±0.02
S500 kHz									
NQ-17	**		2.45	-6.94	2.28	2.63	2.34	2.99	2.41
NQ-24	**		2.58	-4.65	2.46	-3.25	2.38	4.20	2.48
NQ-25	2.47	0.40	2.48	-1.61	2.44	-1.64	2.40	0.83	2.42
Mean, Std. Dev.	2.47	0.40	2.50 ±0.07	-4.40 ±2.68	2.39 ±0.10	-0.75 ±3.04	2.37 ±0.03	2.67 ±1.71	2.44 ±0.04
S1 MHz									
NQ-17	2.48	-0.40	2.47	-1.21	2.44	-1.23	2.41	-1.24	2.38
NQ-24	2.45	0.82	2.47	0.81	2.49	-0.40	2.48	-4.84	2.36
NQ-25	2.54	-2.36	2.48	4.44	2.59	-2.32	2.53	0.79	2.55

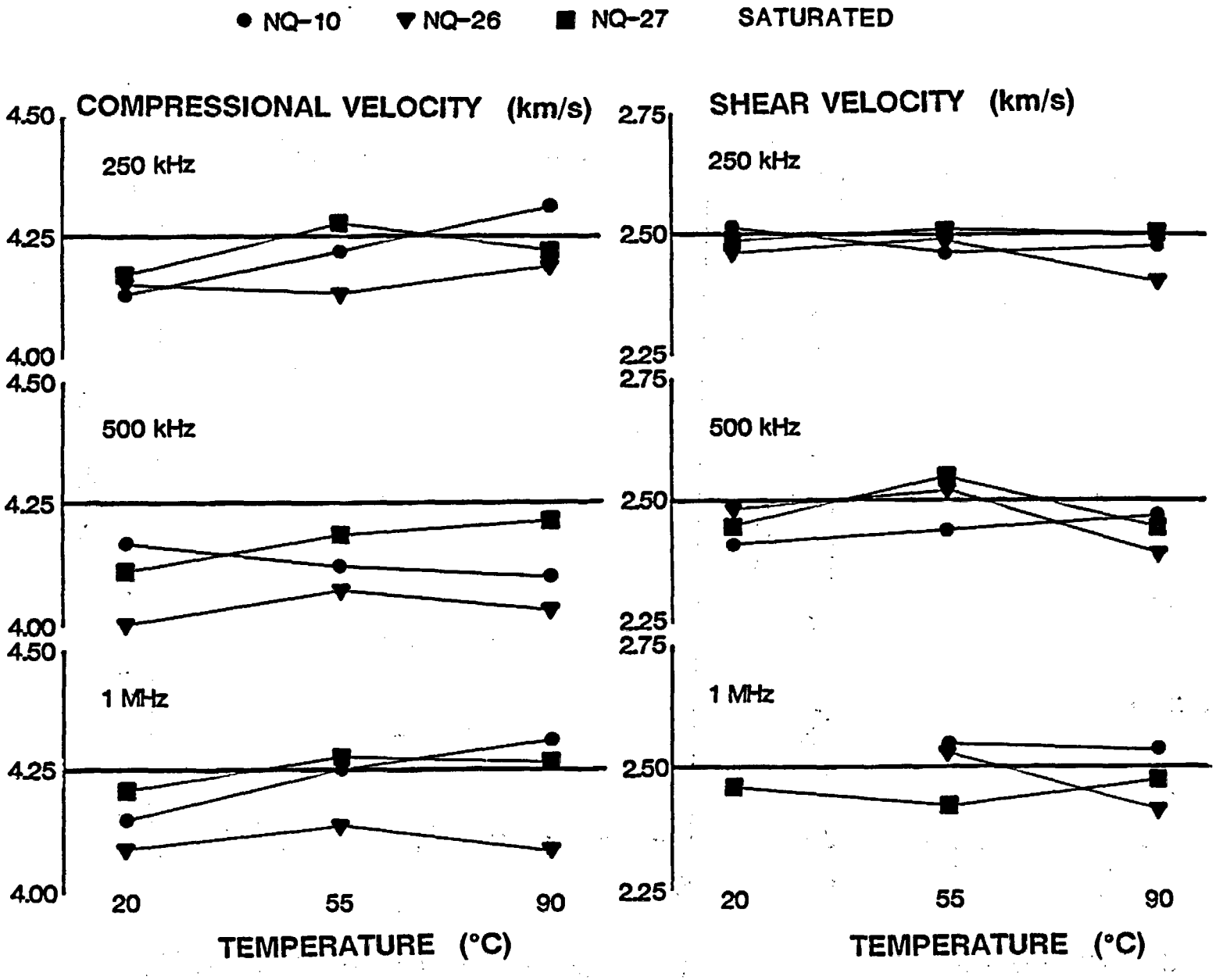

FIGURE 23. Compressional and Shear Wave Velocity versus Temperature for Saturated Samples (data of Tables 12 and 13)

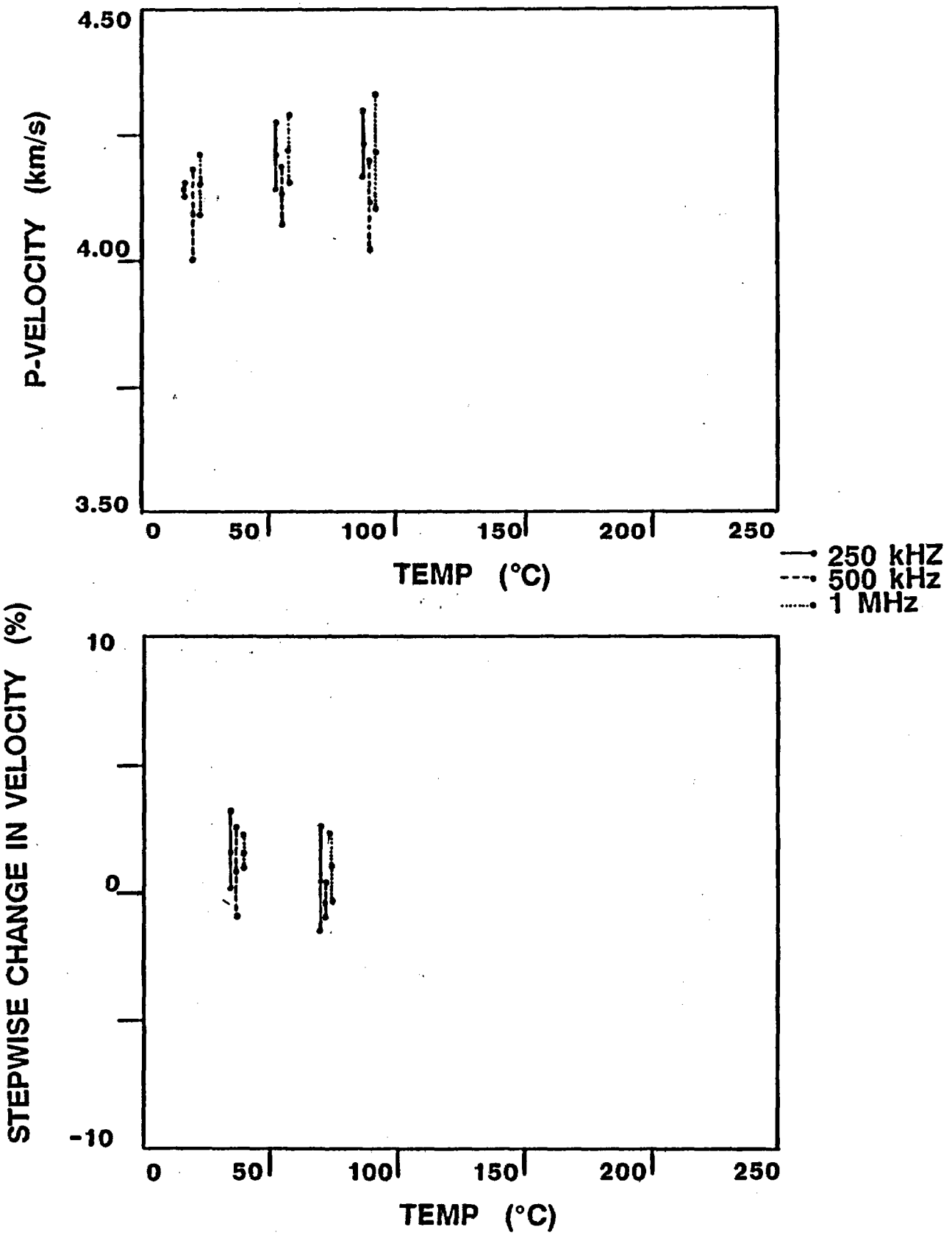

FIGURES 24. P-Wave Velocity Data for Saturated Samples.

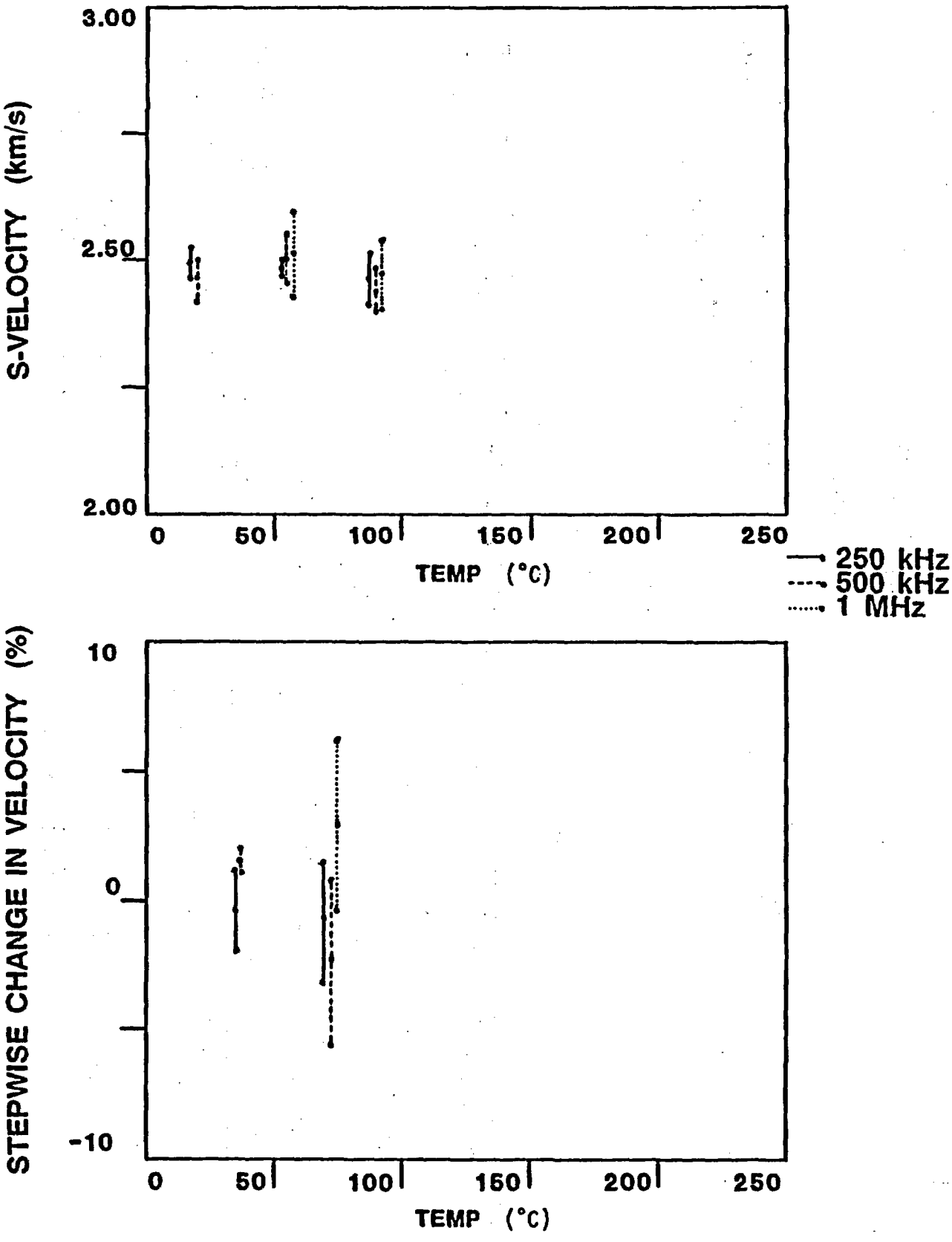

FIGURE 25. S-Wave Velocity Data for Saturated Samples.

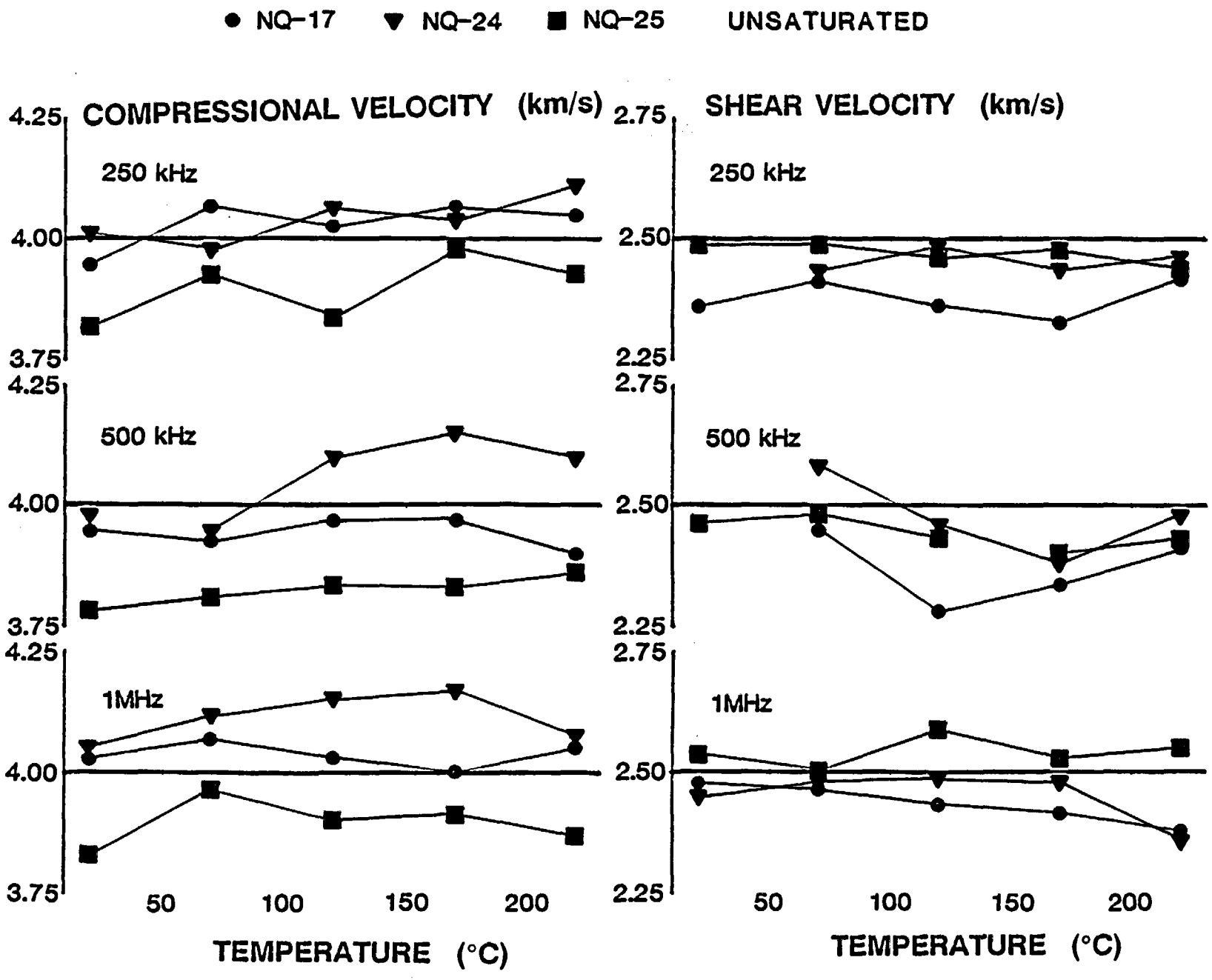

FIGURE 26. Compressional and Shear Wave Velocity versus Temperature for Saturated Samples (data of Tables 14 and 15)

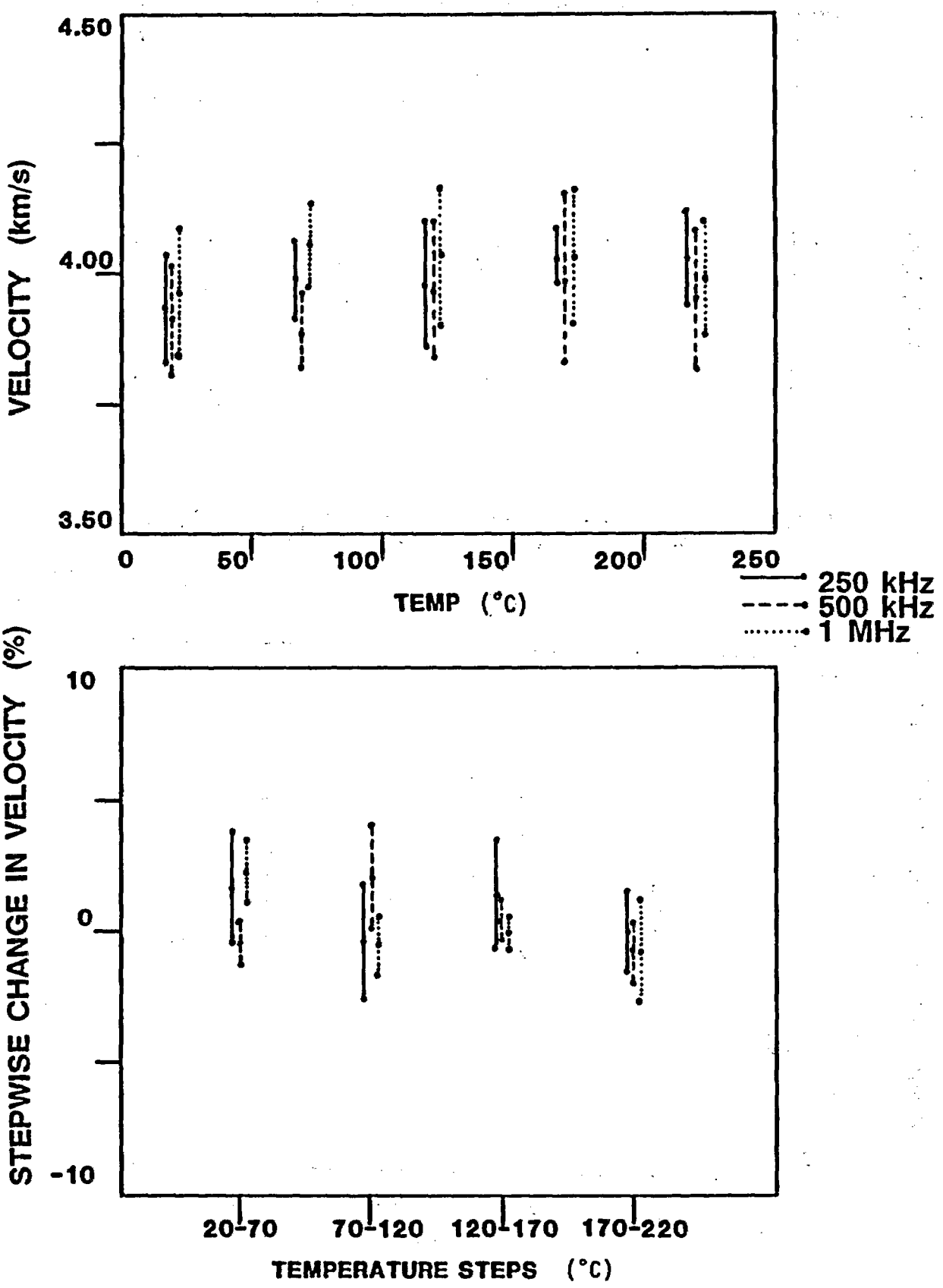

FIGURE 27. P-Wave Velocity Data for Unsaturated Samples.

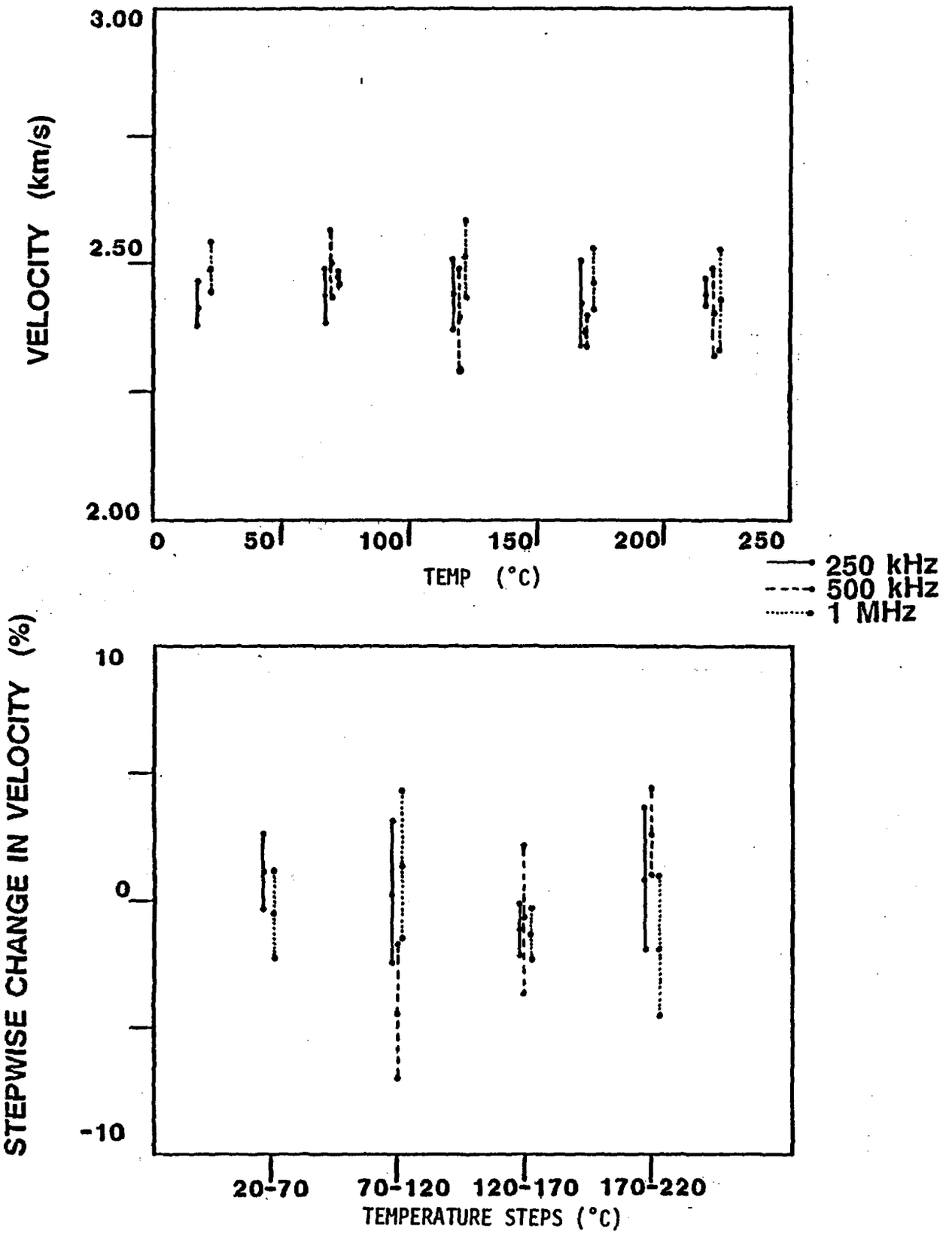

FIGURE 28. S-Wave Velocity Data for Unsaturated Samples.

2. S-velocity is significantly lower than P-velocities.

3. S-velocity shows little or no dependence on saturation.

4. Both P-wave and S-wave velocities appear to be independent of temperature within the range provided in these tests.

The independence of observed velocities from temperature effects suggests that the relatively large velocity change observed in cross-hole ultrasonic studies in the heated block (Bellman and Wilson, 1986) may be due to changes in saturation and fracture parameters and not because of thermal alteration in the lithology or material properties. However, it should be noted that these studies do not address the possible effects of scale or the possibility for velocity changes caused by lithologic alteration during long-term exposure to elevated temperatures.

The possible increase in P-wave velocity with saturation may be due to the increased bulk modulus and intact rock stiffness associated with the presence of water in the pore structure. It has been shown (Kuster and Toksoz, 1974) that this relationship is also sensitive to the aspect ratio of pores in the transmission path. This model is derived by expressing the scattered wavefield from a single pore-scatterer as a series expansion and equating this term-by-term with the expansion for the scattered wavefield in the composite medium. The resulting equations express relationships between the geometry and physical properties of a single pore and the bulk properties of the composite, which can be manipulated to determine pore structure from measured velocity. The wavelength should be much greater than the limiting pore dimension, and the bulk modulus of the matrix material and pore fluid must be known. A nonuniqueness condition exists in the same model. However, most rocks have multiple populations of pores with different aspect ratios, so a more complicated model is often needed to obtain a good fit to velocity data. On the other hand, if we assume that the pores are randomly oriented, this simplifies the model considerably by allowing the effective medium to be isotropic. The composition law for the bulk modulus is then (Kuster and Toksoz, 1974):

$$\frac{K^* - K}{3K^* + 4\mu} = C\,\frac{K^+ - K}{3k + 4\mu} \cdot \frac{1}{3} \cdot T_{iijj}$$

where: K^* = effective bulk modulus
K = matrix bulk modulus
K^+ = inclusion (pore fluid) bulk modulus
μ = matrix shear modulus
C = pore concentration (porosity)
T_{iijj} = 4th-order tensor, (dependent upon matrix and inclusion properties)

The concentration of pores (porosity) of a given aspect ratio is limited to a value no greater in magnitude than the aspect ratio to prevent overlapping pores. Using a porosity estimate of 15%, and assuming values of 50.0 GPa and 0.2 for the bulk modulus and Poisson's ratio of the tuff matrix (vitreous silica), respectively, an explicit relationship between pore aspect ratio and velocity, for both saturated and dry conditions, can be calculated.

For the welded tuff at ambient stress and temperature, a dual distribution of nearly spherical pores and small, flat cracks provided much better agreement to the measured velocities than a single aspect ratio. This is because flat pores are required to obtain increased velocity with saturation, and more spherical pores are needed to obtain the total porosity. For this simple analysis, a flat pore aspect ratio of 0.2% of the "spherical," or principal ratio and a concentration of flat pores of 0.2% of total porosity were determined. The principal aspect ratio was then varied over a wide range to investigate velocity behavior (Figure 29). The result shows a reasonable agreement between the model results and the measured data. However, it is important to note that this is a nonunique solution since other pore descriptions yield similar dry and saturated velocities, although at different values of the principal aspect ratio.

The nonuniqueness issue for this model could be resolved by incorporating data from additional tests into the model. Thus, velocity and bulk moduli measured at confining pressures up to 1 kbar can constrain the model by forcing the flat pores to close, thereby simplifying the velocity mechanism, and the inversion of the model for pregeometry. Also, this data would resolve the degree of anisotropy of the intact rock. It is unlikely, however, that any change in pore geometry resulted from stress levels attained in the heated block test.

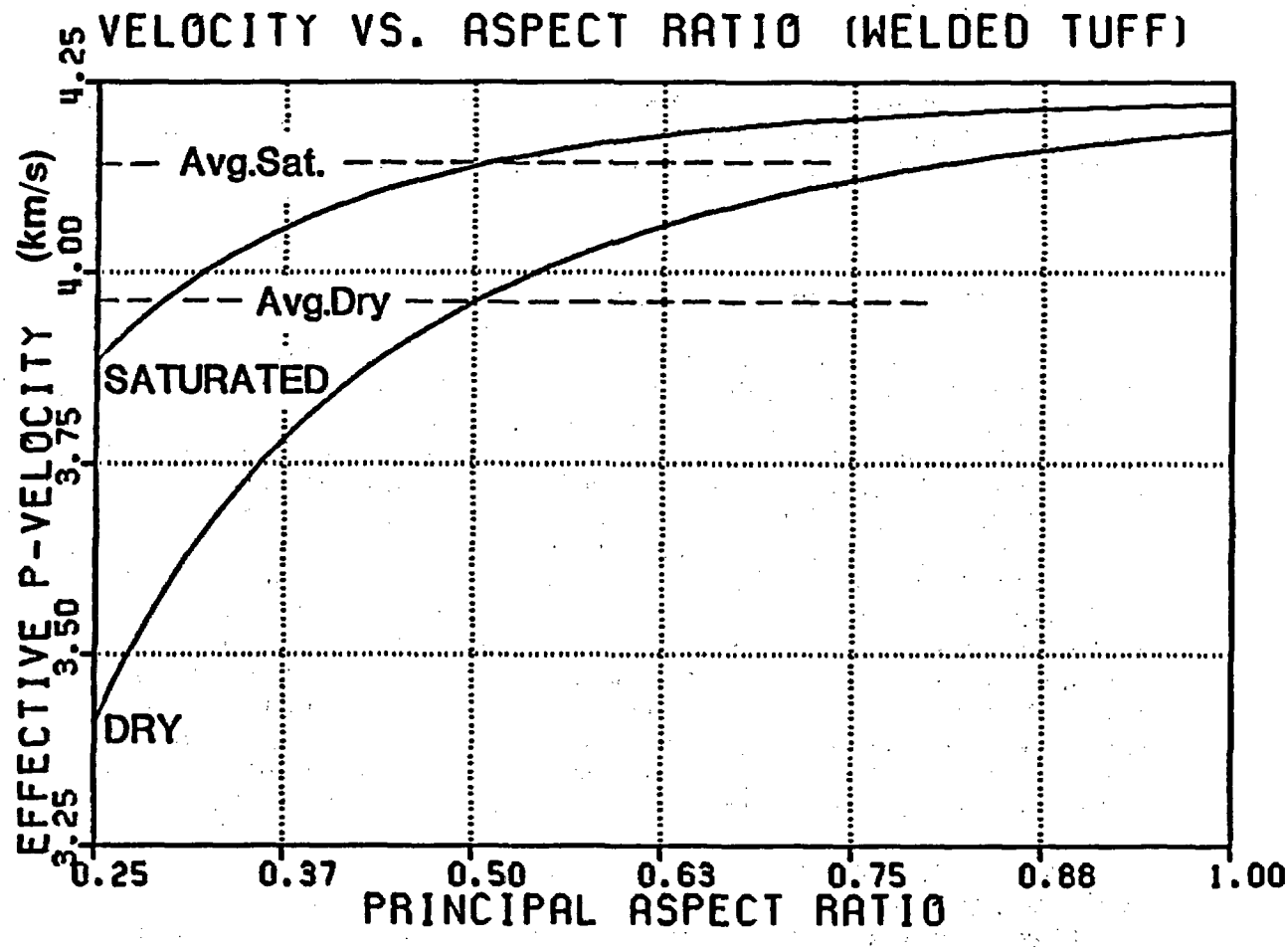

FIGURE 29. P-Velocity versus Principal Aspect Ratio. Using the Kuster-Toksoz model, the welded tuff is modeled as having total porosity of 15%, a homogeneous matrix, a Young's modulus of 50 GPa, and a Poisson's ratio of .2. Pores of two different aspect ratios are present. The principal pores, principal aspect ratio, comprise most of the porosity, and the flat pores, aspect ratio 0.2% of principal ratio, porosity 0.2% of total, cause the observed dry-versus-saturated P-velocity response. The curves converge with increasing principal ratio since spherical pores have little effect on modulus but increase bulk density when saturated. Shear velocity increases very slightly with increasing saturation and principal aspect ratio in this model.

7.0 PERMEABILITY

The permeability of welded tuff samples was determined over a range of temperatures and pressures using an axial steady-state technique, as described by Brace and others (1982).

7.1 Equipment and Procedures

The apparatus used for this testing is shown in Figure 30. An NQ core sample of welded tuff (25.4 x 47.6-mm diameter) with ends ground flat and parallel to within 0.025 mm, was placed between two porous injection end caps. The sample and end caps were placed in a urethane confinement jacket in a Hoek-style triaxial cell. Axial load to the sample was delivered by a servo-controlled 200-ton (1780-kN) ram and confining pressure was supplied by a hand pump with a 0.5-gal (1.9-l) accumulator. Axial load was monitored by a calibrated Terrametrics load cell and confining pressure by a 1/4%-accuracy 3D Instruments pressure gauge. The permeant chosen for these tests was argon gas because its stability at high temperatures. A nitrogen gas bottle was used to charge the bladder accumulator, whose volume was such that pressure decreases during testing were negligible. A pressure transducer was used to monitor permeant pressure, and a series of calibrated bubble flowmeters were used to indicate permeant flow rate.

Once the sample was placed in the triaxial chamber, a small confining pressure was applied to hold the sample-end cap assembly in position. The chamber was then placed in the load frame, and the axial load and confining pressure applied to designated stress levels. The permeant pressure was next applied to the sample by opening the gas bottle and adjusting a pressure regulator. With the pressure gradient across the sample constant, the rate of flow through the sample was determined at steady state and the permeability calculated from Darcy's Law for compressible flow.

For elevated temperature testing, the high-temperature Hoek cell apparatus described in the triaxial testing section was used with silicone-rubber jackets. The samples were heated to the designated temperature level in an oven adjacent to the testing apparatus. The sample was quickly transferred to the triaxial cell and tested. The permeability test was completed within 15 minutes. Temperature monitoring of the sample confirmed minimal temperature loss during this time period.

7.2 Results

Four core samples were used to examine permeability as a function of confining pressure and temperature. For each sample, the

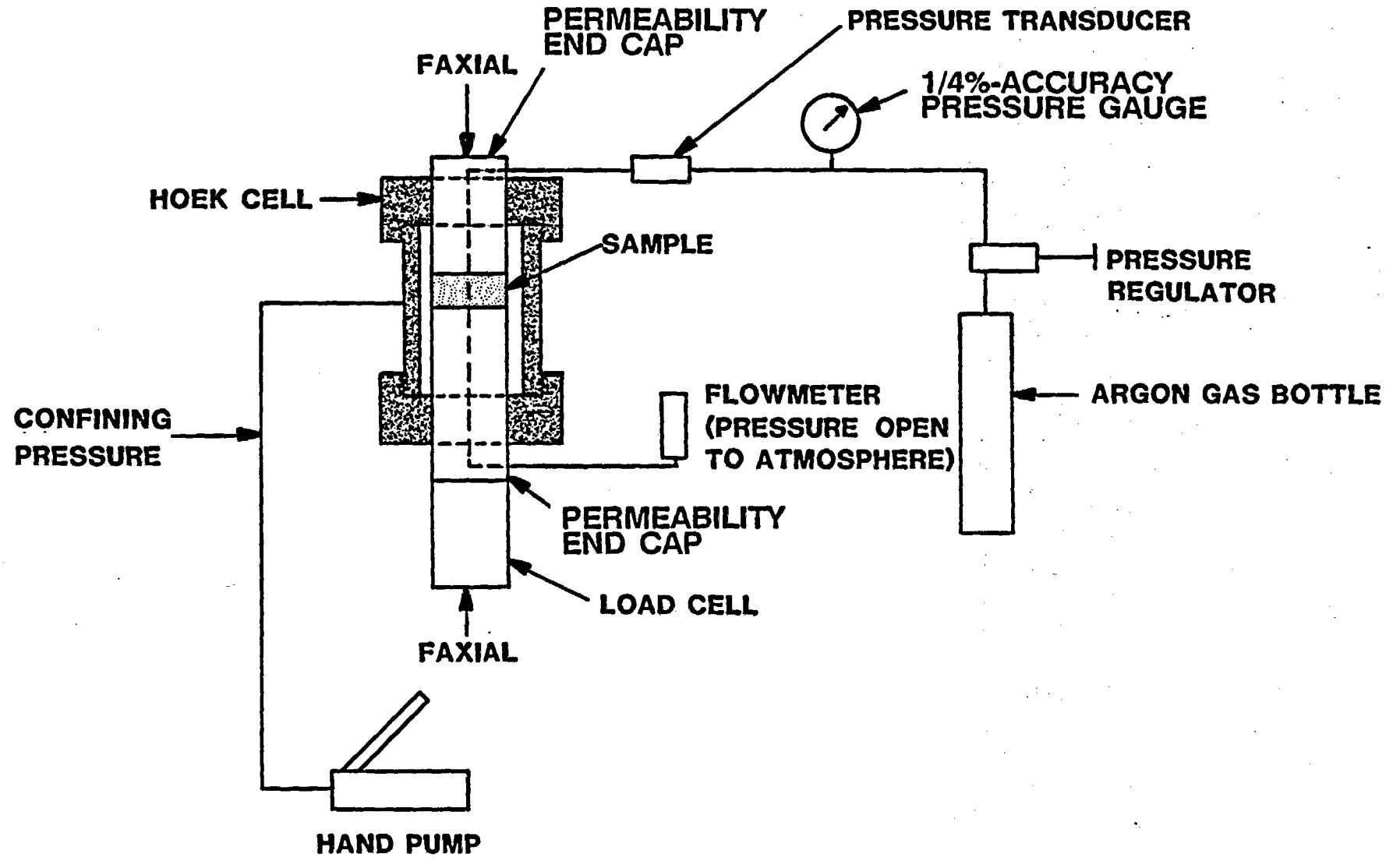

FIGURE 30. Steady State Permeability Apparatus.

designated temperature was established, and tests were conducted at a succession of increasing confining pressures. All samples were thoroughly dried prior to testing to avoid possible problems of two-phase gas-liquid flow. The results of the testing are given in Table 16 and illustrated graphically in Figures 31 through 37.

Figures 31 to 34 show permeability as a function of temperature and confining pressure for individual samples, and Figures 35 through 37 provide composite plots of all samples at a given temperature. Sample 1 shows a tendency to reduction of permeability with an increase in temperature. Samples 1 and 2 indicated little variability of the permeability with confining pressure, averaging approximately 2.5 to 3.0 x $10^{-13}cm^2$. Samples 3 and 4, however, showed a marked reduction in permeability of between 30% and 50% until a confining pressure of approximately 5 MPa was reached. The average permeability of the four samples at given confining pressure and temperatures is given in Table 17.

TABLE 16

PERMEABILITY OF GROUSE CANYON WELDED TUFF
TO ARGON GAS
AT VARIOUS CONFINING PRESSURES AND TEMPERATURES

TEST ID	CONFINING PRESSURE (MPa)	TEMPERATURE (°C)	GAS PERMEABILITY ($\times 10^{-13}$ cm^2)
1A-1	1.38	20	2.57
-2	3.45	20	2.74
-3	3.45	20	3.30
-4	9.96	20	2.66
-5	9.96	20	3.22
-6	13.79	20	3.22
-7	20.62	20	3.22
1B-1	1.72	53	2.38
-1A	1.72	53	2.43
-2	1.72	53	2.99
-3	3.45	53	2.81
-4	6.89	53	2.90
-5	9.96	53	2.78
-6	13.79	53	2.79
-7	20.62	53	2.82
1C-1	1.72	93	2.05
-2	3.45	93	2.00
-3	6.89	93	2.43
-3A	6.89	93	2.05
-4	9.96	93	2.37
-5	20.60	90	2.43
2A-1	1.72	20	1.73
-2	9.96	20	2.14
-3	9.96	20	2.50
-4	20.61	20	2.25
2B-1	1.37	50	3.11
3B-1	1.72	50	4.45
-2	9.99	50	1.38
-3	20.62	50	1.26
3C-1	20.62	90	1.28
-2	9.96	90	1.32
-3	1.72	90	2.44*

*Crack was observed in the sample upon removal from the chamber.

TABLE 16 (Cont.)

PERMEABILITY OF GROUSE CANYON WELDED TUFF
TO ARGON GAS
AT VARIOUS CONFINING PRESSURES AND TEMPERATURES

TEST ID	CONFINING PRESSURE (MPa)	TEMPERATURE (°C)	GAS PERMEABILITY (X 10^{-13} cm^2)
4A-1	1.72	20	4.60
-2	9.99	20	1.41
-3	20.62	20	1.30
-3A	20.62	20	1.00
4B-1	1.72	50	2.24
-2	9.96	50	1.27
-3	20.62	50	1.17
4C-1	20.62	90	1.14
-2	9.96	90	1.28
-3	1.72	90	5.46

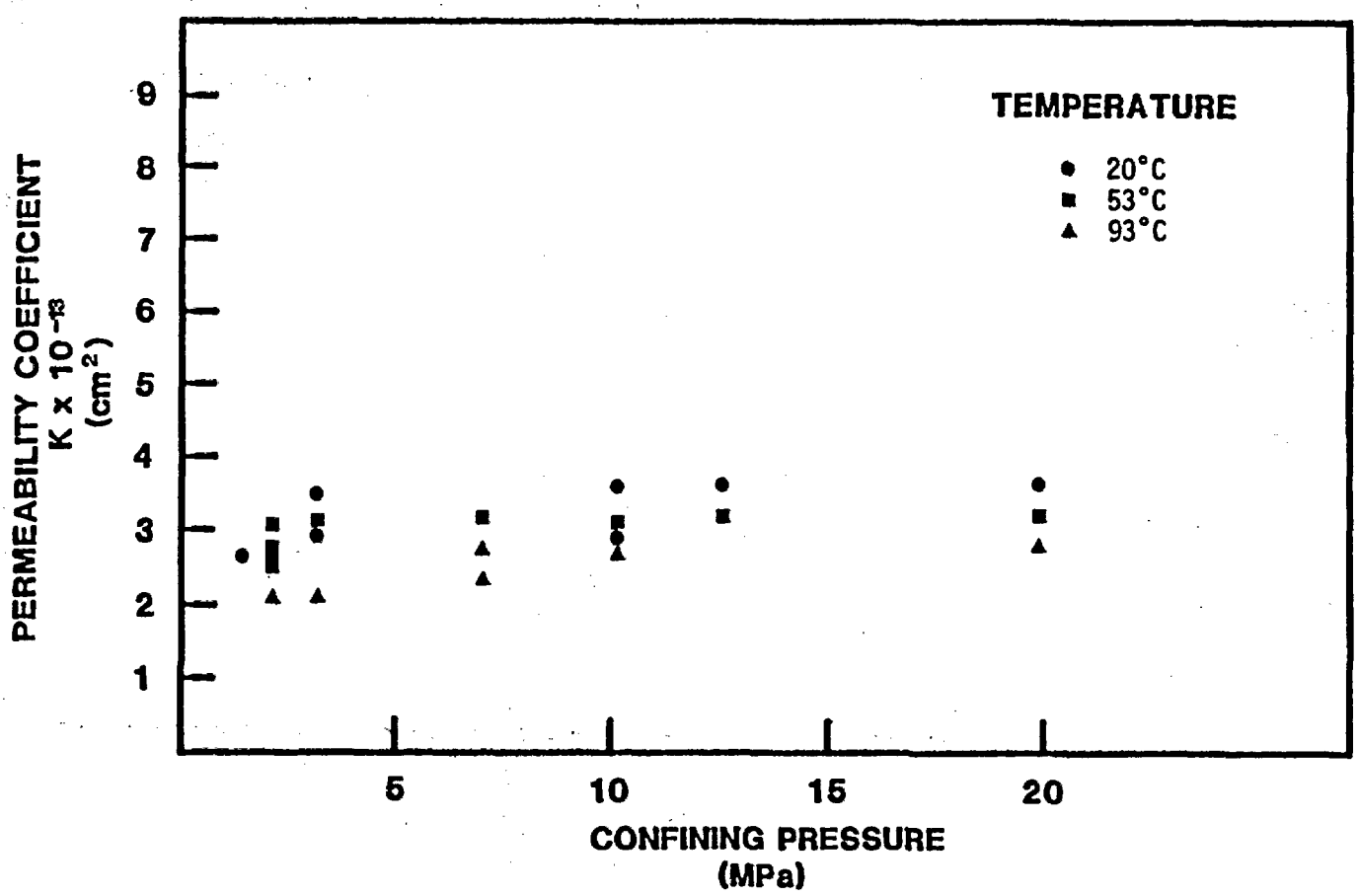

FIGURE 31. Permeability Coefficient, Sample 1.

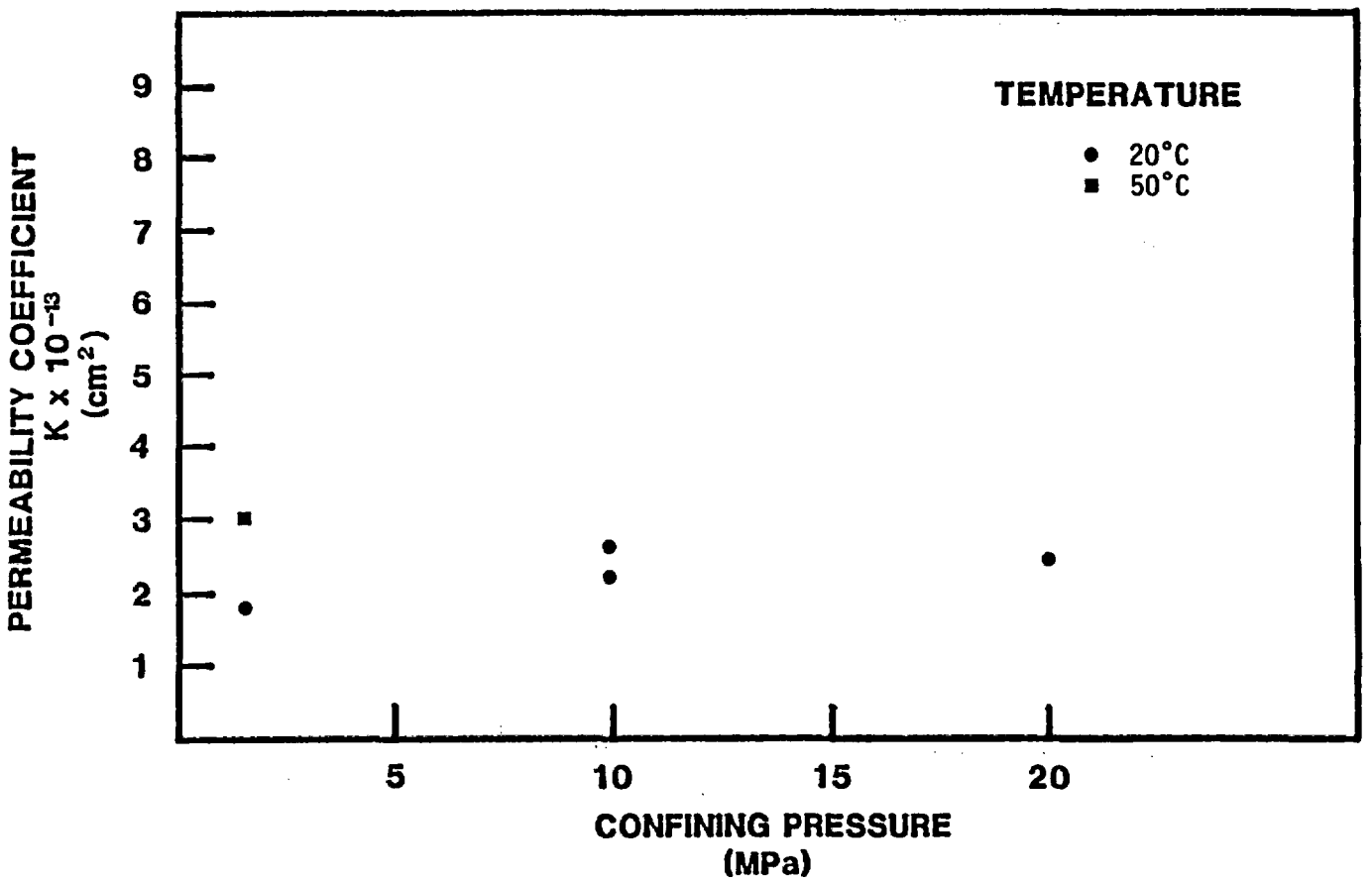

FIGURE 32. Permeability Coefficient, Sample 2.

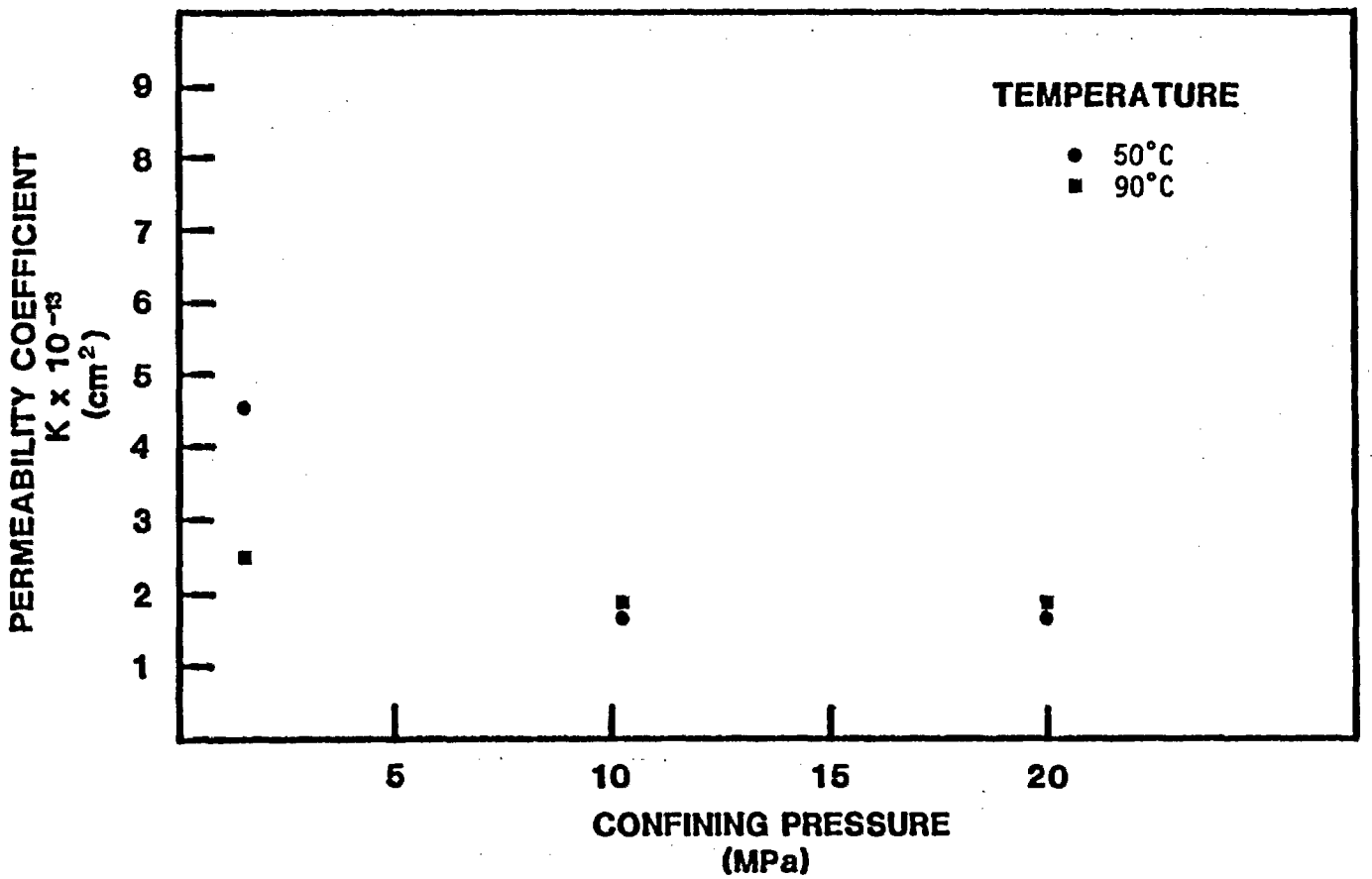

FIGURE 33. Permeability Coefficient, Sample 3.

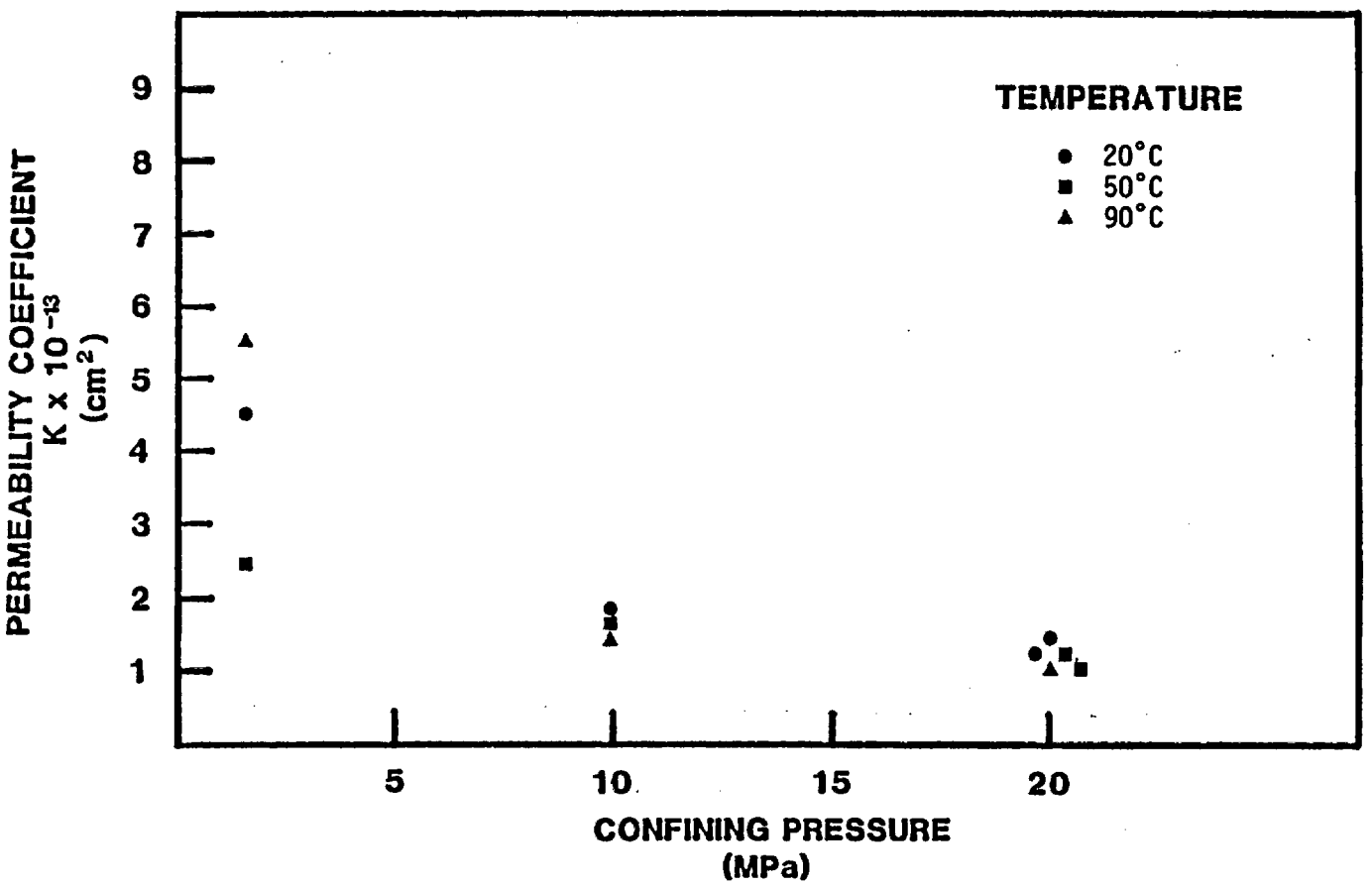

FIGURE 34. Permeability Coefficient, Sample 4.

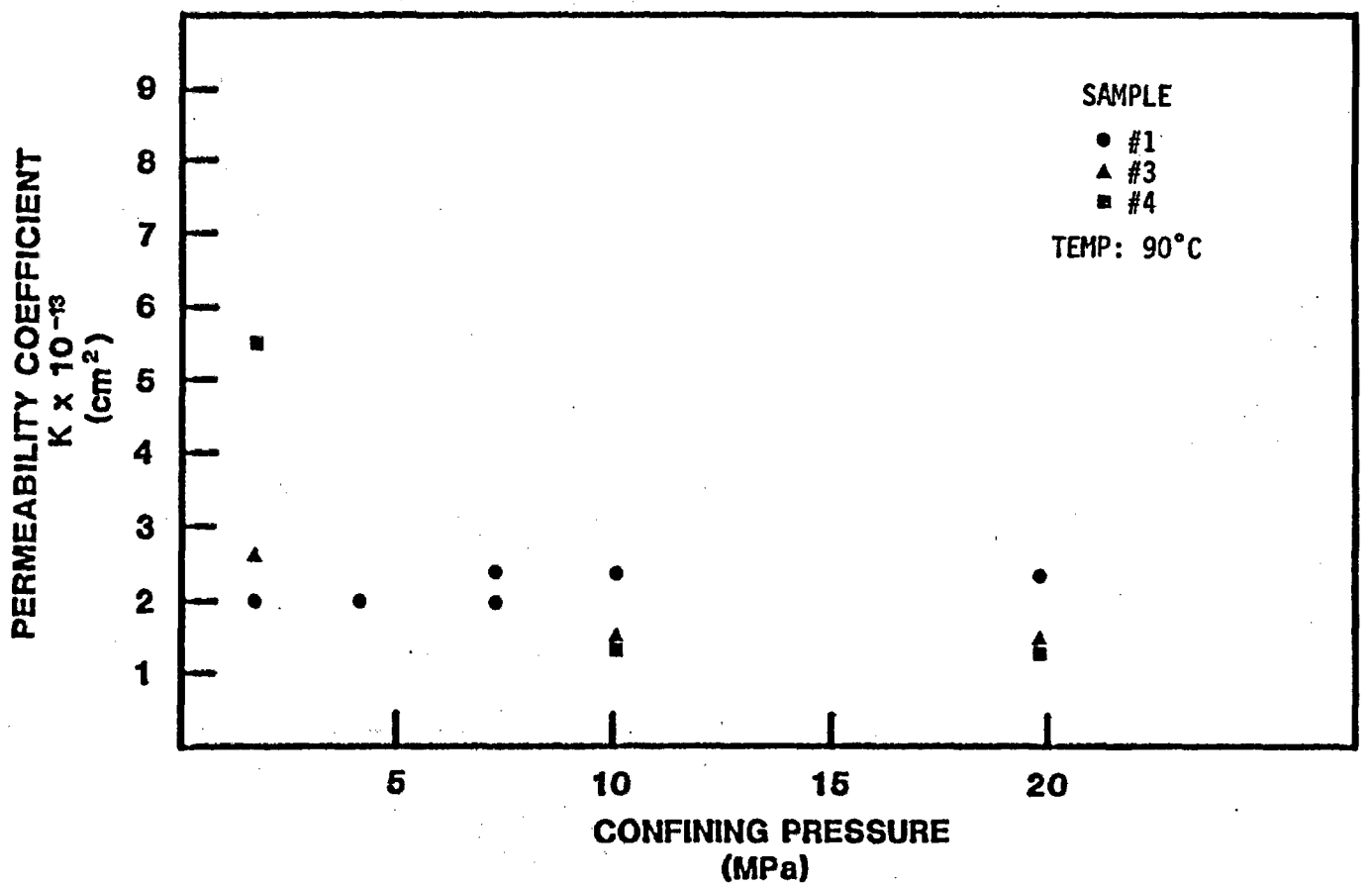

FIGURE 35. Composite Plot of Permeability Coefficients for All Tests at Approximately 90°C.

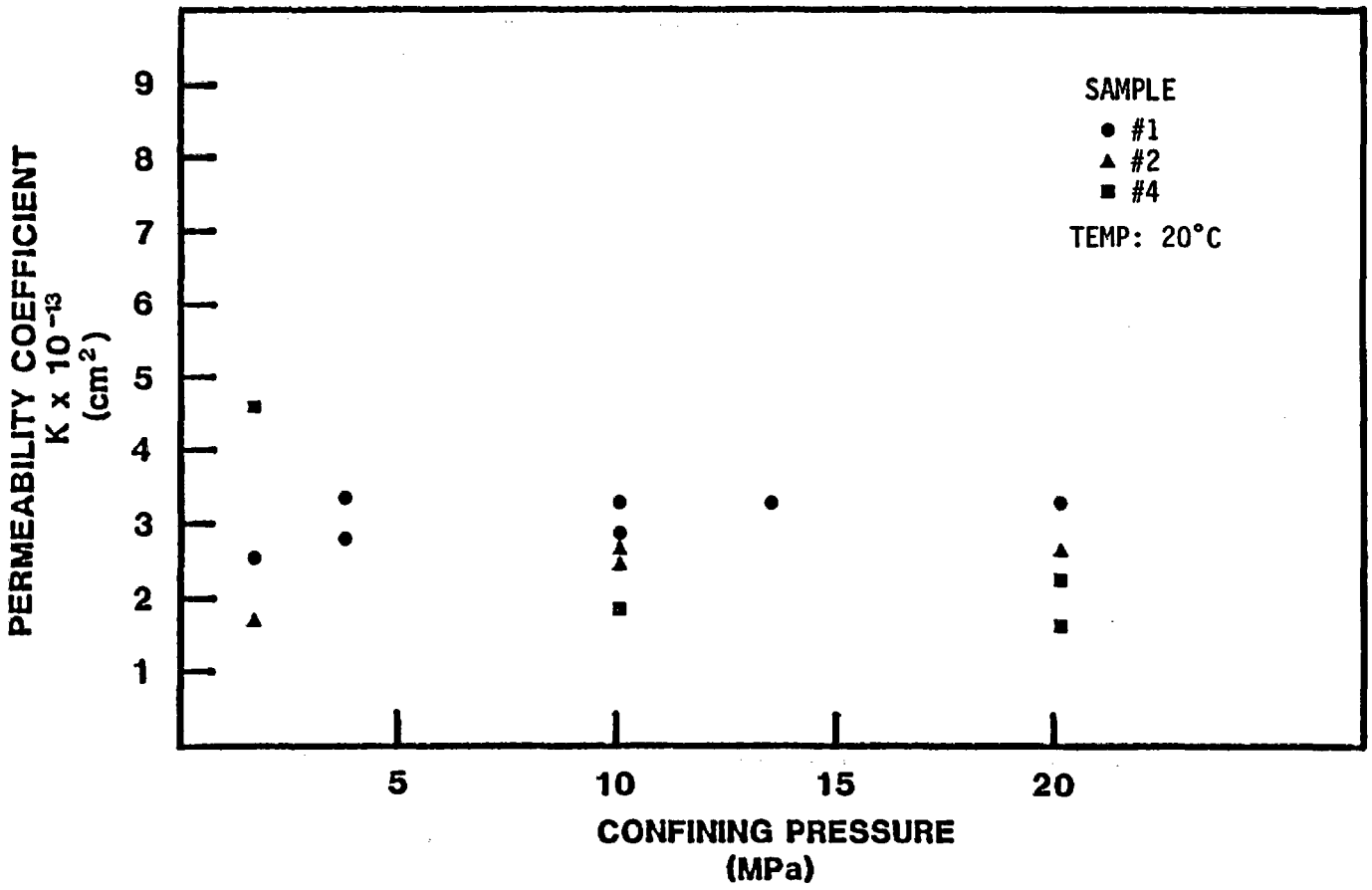

FIGURE 36. Composite Plot of Permeability Coefficients for All Tests at 20°C.

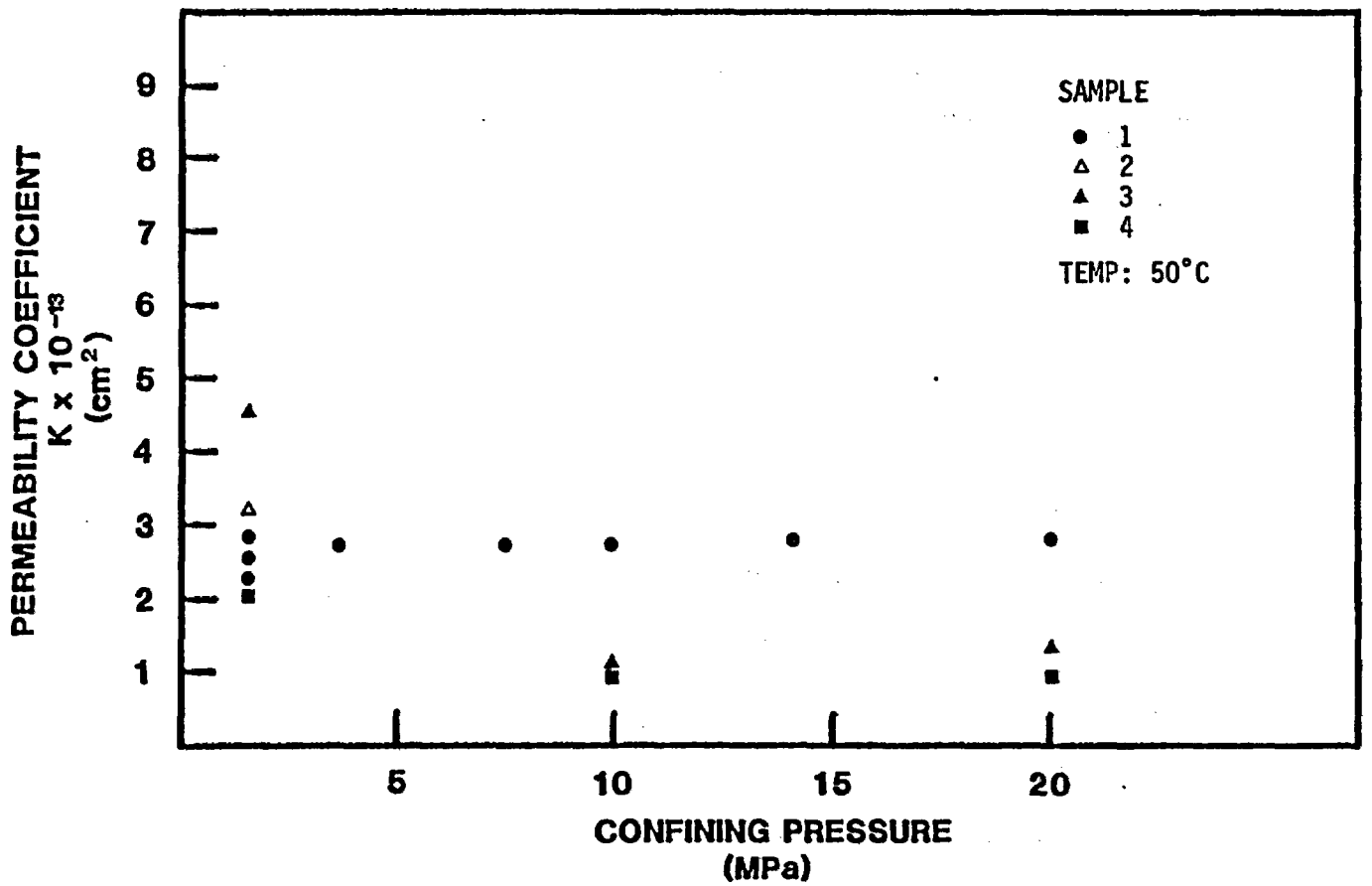

FIGURE 37. Composite Plot of All Permeability Tests at Approximately 50°C.

TABLE 17

SUMMARY OF THE PERMEABILITIES
FOR
GROUSE CANYON WELDED TUFF

CONFINING PRESSURE (MPa)	TEMPERATURE (°C)	NUMBER OF TESTS	PERMEABILITY ($\times 10^{-13}$ cm^2)
1.72	20	2	3.17 ± 2.03
9.96	20	5	2.39 ± 0.67
20.62	20	4	1.94 ± 1.00
1.72	50-53	5	2.89 ± 0.91
9.96	50-53	3	1.81 ± 0.84
20.62	50-53	3	1.75 ± 0.92
1.72	90-93	3	3.32 ± 1.87
9.96	90-93	3	1.66 ± 0.62
20.62	90-93	3	1.62 ± 0.71

APPENDIX A

RIB/SEPDB DATA

Candidate data for the RIB are contained in Table 1.

Candidate data for the SEPDB are contained in Tables 3 through 9 and Tables 12 through 16.

APPENDIX B

CALIBRATION OF TESTING EQUIPMENT

B.0 CALIBRATION OF TESTING EQUIPMENT

B.1 Ram DCDT Stroke

Prior to each series of compression tests using the system shown in Figure 1 of the text, the 6-inch (15.24-cm) stroke Schaevitz DCDT that senses the 200-ton (1780-kN) ram displacement was calibrated. To perform this calibration, the DCDT was connected through the entire servo-control system, and its output was monitored on an X-Y plotter and digital voltmeter. A 0.025-mm-accuracy dial indicator on a universal mount magnetic base was attached to the lower machine platen, with an indicator sensing the motion of the bottom surface of the ram (Figure B1). The ram was then displaced downward to provide a relationship between DCDT voltage output and actual displacement read from the dial gauge. The servo-controller gain setting was adjusted and the displacement procedure repeated until a desired output voltage/displacement ratio was produced. The X-Y recorder was then used to record the calibration curve since the ram was again displaced through the range of displacement available with this DCDT.

B.2 Elastic Moduli Measurement Apparatus

The device used to determine Young's modulus and Poisson's ratio was calibrated prior to each series of measurements. Cylinders of 304 stainless steel and 6061-T6 aluminum were placed in the measurement apparatus and a series of load-unload cycles made to determine the calibration (in/volt) of the axial displacement and lateral strain measurement devices. A calibrated load cell, either a Terrametrics 100-ton (890-kN) or Sensotec 200-ton (1780-kN) load cell, was used to provide correct load values, and the displacement/voltage calibrations were computed from this load, the known elastic properties of the calibration materials and the voltage outputs of the sensing instruments. Figure B2 shows an example of the computer printout from the elastic moduli apparatus calibration of the aluminum cylinder. The program uses known values of E and ν for aluminum of 68.97 GPa and 0.34, respectively, in this case, and determines the axial and two transverse calibration factors every 10 s during loading. The calibration factors are averaged for use in subsequent measurements.

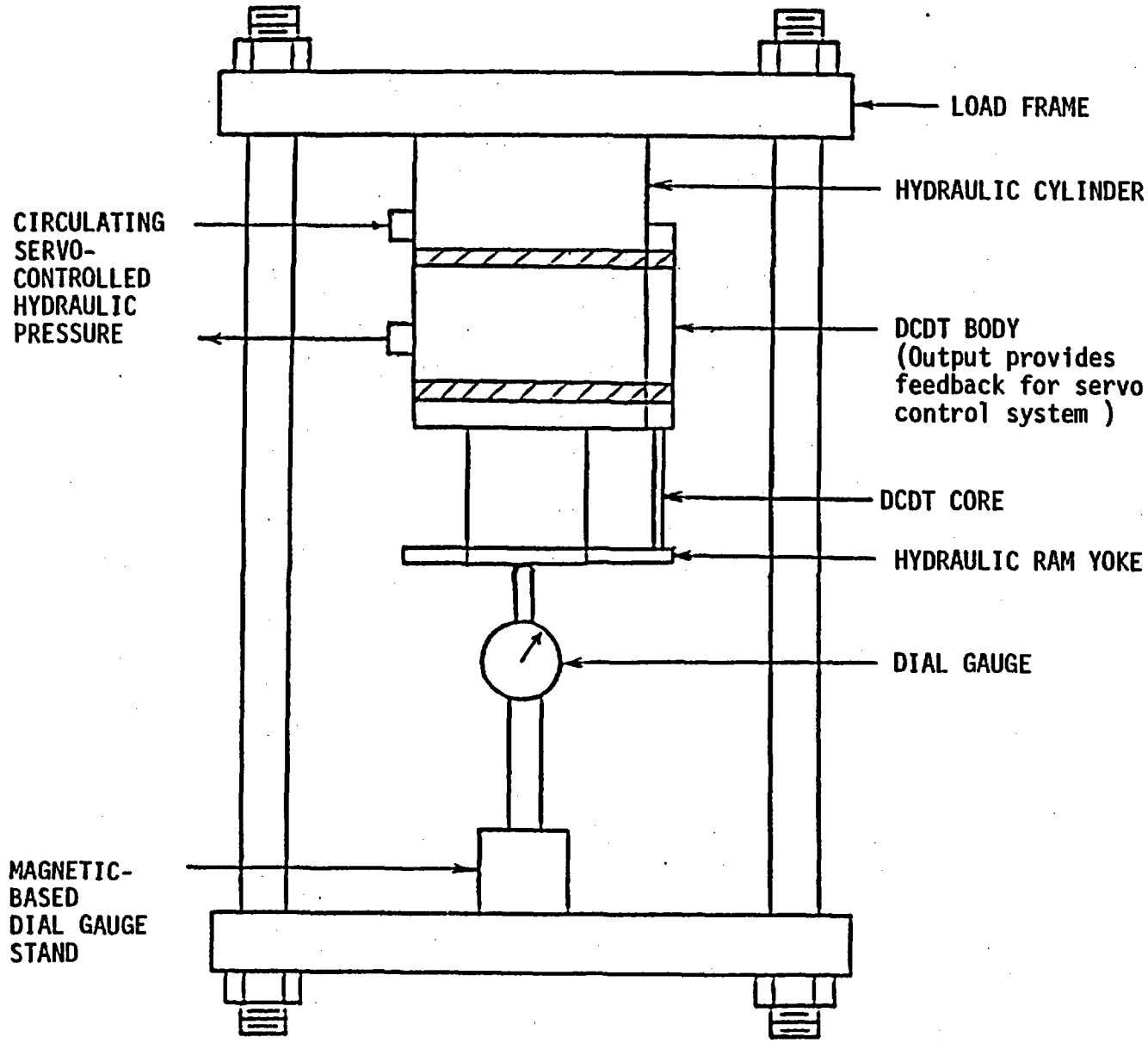

FIGURE B1. Compression Testing System Calibration Assembly.

CALIBRATION/CHECKOUT ROUTINE FOR MODULUS AND POISSON'S. UNCONFINED

SAMPLE HEIGHT = 3.790
DIAMETER = 1.888 (in.)
MODULUS (x1E6 psi) = 10.000
POISSON'S = .340

CALIBRATION FACTORS:

LOAD CELL (ksi/V) = 10.000

DCDT #1 (in/V) = -.02463
#2 = -.02387

DATA CHNL #'S ARE 40 THRU 44
DCDT EXCITATION (-) CHNK # = 45
DCDT EXCITATION (+) CHNL # = 46
CANTILEVER EXCITATION CHNL # = 47

DCDT EXCITATION (-) = -15.02500 (V)
DCDT EXCITATION (+) = 15.05600 (V)
CANTILEVER EXCITATION = 5.00790 (V)

ELAPSED TIME (sec)	STRESS (ksi)	AXIAL VOLTAGE AVG	FIXTURE DISP. (in/ksi)	AXIAL CALIB. FACTOR	TRANSVERSE CALIB. FACTOR 1	TRANSVERSE CALIB. FACTOR 2
0.00	0.000	0.0000	0.000	0.0000	0.000	0.000
10.00	.703	.0185	0.000	-.0144	1.504	1.455
20.27	1.699	.0211	0.000	-.0179	1.998	1.560
30.25	2.700	.0196	0.000	-.0194	2.073	1.606
40.15	3.754	.0197	0.000	-.0203	2.114	1.537
50.15	4.846	.0201	0.000	-.0206	2.062	1.558
60.15	5.962	.0207	0.000	-.0205	2.108	1.558
70.15	7.102	.0209	0.000	-.0207	1.976	1.523
80.15	8.275	.0211	0.000	-.0211	2.151	1.569
90.15	9.473	.0217	0.000	-.0209	2.024	1.570
100.14	10.679	.0218	0.000	-.0210	2.093	1.518
110.14	11.904	.0219	0.000	-.0212	2.016	1.573
120.14	13.138	.0224	0.000	-.0209	2.085	1.523
130.14	14.393	.0227	0.000	-.0210	2.066	1.580
140.14	15.547	.0223	0.000	-.0213	2.012	1.548
150.14	15.867	.0217	0.000	-.0214	2.117	1.598
160.14	15.711	-.0206	0.000	-.0213	1.903	1.514
170.14	14.392	-.0234	0.000	-.0214	2.016	1.568
180.14	13.079	-.0233	0.000	-.0214	2.056	1.561
190.14	11.781	-.0232	0.000	-.0212	1.984	1.543
200.14	10.491	-.0228	0.000	-.0214	2.123	1.562
210.14	9.228	-.0228	0.000	-.0210	2.027	1.559
220.14	7.984	-.0224	0.000	-.0210	2.158	1.566
230.14	6.788	-.0218	0.000	-.0208	2.020	1.567
240.14	5.647	-.0206	0.000	-.0210	2.098	1.592
250.13	4.528	-.0207	0.000	-.0205	2.114	1.529
260.25	3.441	-.0202	0.000	-.0204	2.052	1.550
270.25	2.403	-.0198	0.000	-.0199	2.083	1.550
280.25	1.430	-.0197	0.000	-.0188	2.014	1.523
290.25	.474	-.0210	0.000	-.0173	1.860	1.534
300.38	-.308	-.0249	0.000	-.0119	1.287	1.521

AVG. AXIAL CALIB. FACTOR = -.0201 STD. DEV. = .0022
AVG. TRANSVERSE CALIB. FACTOR #1 = 2.0062 STD. DEV. = .1811
AVG. TRANSVERSE CALIB. FACTOR #2 = 1.5505 STD. DEV. = .0330

FIGURE B2. Elastic Moduli Apparatus Calibration.

TABLE B1.

TRAVEL TIME MEASUREMENTS IN AN ALUMINUM CYLINDER

FREQUENCY (kHz)	ORIENTATION ANGLE (deg)	TEMPERATURE (°C)	DATE	OBSERVED TRAVEL TIME RAW	CONVERTED	LOAD NO	SAVED
P250		20	8-30	117.0	23.4	600	D4Q3
		120	8-30	115.5	23.1	600	D6Q1
		220	9-01	116.5	23.3	600	F7Q3
P500		20	8-30	113.0	22.6	600	D2Q2
		120	8-30	116.5	23.3	600	D7Q4
		220	9-01	114.0	22.8	600	F8Q3
P1000		20	8-29	113.5	22.7	600	C8Q4
		120	8-30	122.5	24.5	600	E1Q2
		220	9-01	127.0	25.4	600	G1Q3
S250		20	8-29	215.0	43.0	400	87Q3
		120	8-31	224.0	44.8	400	E3Q3
		220	9-01	235.0	47.0	400	G2Q3
S500		20	8-29	223.0	44.6	400	C5Q2
		120	8-31	228.0	45.6	400	E5Q1
		220	9-01	236.0	47.2	400	G3Q3
S1000		20	8-29	256.0	51.2	400	C2Q3
		120	8-31	269.0	53.8	400	E6Q4
		220	9-01	268.5	53.7	400	G4Q3

B.3 Ultrasonics Testing System

The effect of the interfaces involved in the application of an ultrasonics pulse to a sample were determined using a cylinder of known wave propagation speed. The difference between the measured and known wave speeds gives the additional travel time resulting from less than perfect coupling of the transducers to the sample. Table B1 shows a sample aluminum cylinder calibration for various input frequencies and temperatures. The average percent differences between reference travel time for 6061-T6 aluminum and tested travel times are 6% for P-wave velocities and 7% for S-wave velocities.

B.4 Miscellaneous

All other instrumentation used in the testing program for measurement of time, fluid flow rate, temperature, displacement, pressure, and load possesses current calibration records traceable to the National Bureau of Standards. The techniques and rates of calibration are detailed in SAIC's Manual of Technical Practice, which is maintained in the Las Vegas Laboratory. In general, SAIC maintains a number of calibration instruments that are traceable to the National Bureau of Standards and are regularly certified by calibration instruments used in the testing program. The standards used in the present system include:

1. Certified Gauge Block Set, Mitutoyo, Inc., Serial Number 099256 #BE1-35-3.

2. Platinum Resistance Temperature Device, Omega Engineering, Inc.

3. Time Base, Nicolet Explorer II Digital Oscilloscope.

4. Dead Weight Pressure Calibrator, Budenburg Gauge Co., Serial Number Base 13653, Piston L957.

5. Calibrated Flow Meter, Flow Technology, Type FTO-NS-LJS, Serial Number 8550668.

6. DC Voltage/Current Standard, Yokagawa Electric Corp., Type 2554, Serial Number 04555.

REFERENCES

Bellman, R. A., and M. L. Wilson: "G-Tunnel Heated Block Ultrasonic Velocity Measurement Results", Unpublished Report (SAIC Contract #1-209-07-588-00), Sept. 15, 1986.

Brace, W. F., and J. D. Byerlee: "Stick-Slip as a Mechanism for Earthquakes," Science 153, pp. 990-992, 1966.

Brace, W. F., M. D. Voegele, and H. R. Pratt: "Porosity, Permeability and Their Relationship in Granite, Basalt and Tuff" Science Applications Report to INTERAK Environmental Consultants, Inc., Feb. 1982.

Brown, E. T.: "Rock Characterization Testing and Monitoring". ISRM suggested methods. Pergamon Press. Oxford, 1981.

Goodman, R. E.: "Introduction to Rock Mechanics," John Wiley and Sons, 1980.

Hoskins, E. R., J. C. Jaeger, and K. J. Rosengren: "A Medium/Scale Direct Friction Experiment," Int. Journal Rock Mechanics Mining Sciences, Colt. 5, pp. 143-154, 1968.

Jaeger, J. C.: "The Frictional Properties of Joints in Rock," Geophysics. pura appl. 43, pp. 148-158, 1959.

Kulhawy, F. H.: "Geomechanical Model for Rock Foundation Settlement," J. Geo. Engr. Div. (ASCE), 104, pp. 211-227, 1978.

Kuster, G. T., and M. N. Toksoz: "Velocity and Attenuation of Seismic Waves in Two-Phase Media: Part 1, Theoretical Formulations," Geophysics, Vol. 39, No. 5, pp. 587-606, Oct. 1974.

Manual of Technical Practice, Foundation Sciences, Inc., Portland, Oregon.

Vogler, U. W., and K. Kovari: "Suggested Methods for Determining the Strength of Rock Materials in Triaxial Compression," in: Brown, E. T. (Editor): "Rock Characterization Testing and Monitoring, ISRM Suggested Methods." Pergamon Press, Oxford, Eng., 1981.

Zimmerman, R. M., Schuch, R. L., Mason, D. S., Wilson, M. L., Hall, M. E., Board, M. P., Bellman, R. P., and Blanford, M. P.: "Final Report: G-Tunnel Heated Block Experiment," SAND84-2620, Sandia National Laboratories, Albuquerque, NM, May 1986.

DISTRIBUTION LIST

B. C. Rusche (RW-1)
Director
Office of Civilian Radioactive
Waste Management
U.S. Department of Energy
Forrestal Building
Washington, DC 20585

Ralph Stein (RW-23)
Office of Civilian Radioactive
Waste Management
U.S. Department of Energy
Forrestal Building
Washington, DC 20585

J. J. Fiore, (RW-221)
Office of Civilian Radioactive
Waste Management
U.S. Department of Energy
Forrestal Building
Washington, DC 20585

M. W. Frei (RW-231)
Office of Civilian Radioactive
Waste Management
U.S. Department of Energy
Forrestal Building
Washington, DC 20585

M. P. Kunich, Director (4)
Waste Management Project Office
U.S. Department of Energy
Post Office Box 98518
Las Vegas, NV 89193-8518

Chief, Repository Projects Branch
Division of Waste Management
U.S. Nuclear Regulatory Commission
Washington, D.C. 20555

NTS Section Leader
Repository Project Branch
Division of Waste Management
U.S. Nuclear Regulatory Commission
Washington, D.C. 20555

B. G. Gale (RW-223)
Office of Civilian Radioactive
Waste Management
U.S. Department of Energy
Forrestal Building
Washington, DC 20585

R. W. Gale (RW-40)
Office of Civilian Radioactive
Waste Management
U.S. Department of Energy
Forrestal Building
Washington, D.C. 20585

J. O. Neff, Manager
Salt Repository Project Office
U.S. Department of Energy
110 North 25 Mile Avenue
Hereford, TX 79045

V. J. Cassella (RW-222)
Office of Civilian Radioactive
Waste Management
U.S. Department of Energy
Forrestal Building
Washington, DC 20585

S. A. Mann, Manager
Crystalline Rock Project Office
U.S. Department of Energy
9800 South Cass Avenue
Argonne, IL 60439

K. Street, Jr.
Lawrence Livermore National
Laboratory
Post Office Box 808
Mail Stop L-209
Livermore, CA 94550

L. D. Ramspott (3)
Technical Project Officer for NNWSI
Lawrence Livermore National
Laboratory
P.O. Box 808
Mail Stop L-204
Livermore, CA 94550

Document Control Center
Division of Waste Management
U.S. Nuclear Regulatory Commission
Washington, D.C. 20555

D. T. Oakley (4)
Technical Project Officer for NNWSI
Los Alamos National Laboratory
N-5, Mail Stop J521
P.O. Box 1663
Los Alamos, NM 87545

V. M. Glanzman
U.S. Geological Survey
Post Office Box 25046
913 Federal Center
Denver, CO 80225

L. R. Hayes (6)
Technical Project Officer for NNWSI
U.S. Geological Survey
Post Office Box 25046
421 Federal Center
Denver, CO 80225

P. T. Prestholt
NRC Site Representative
1050 East Flamingo Road
Suite 319
Las Vegas, NV 89109

C. H. Johnson, Technical
Program Manager
Nuclear Waste Project Office
State of Nevada
Evergreen Center, Suite 252
1802 North Carson Street
Carson City, NV 89701

M. E. Spaeth
Technical Project Officer for NNWSI
Science Applications
International Corporation
Suite 407
101 Convention Center Drive
Las Vegas, NV 89109

ONWI Library
Battelle Columbus Laboratory
Office of Nuclear Waste Isolation
505 King Avenue
Columbus, OH 43201

SAIC-T&MSS Library (2)
Science Applications
International Corporation
Suite 407
101 Convention Center Drive
Las Vegas, NV 89109

W. M. Hewitt, Program Manager
Roy F. Weston, Inc.
955 L'Enfant Plaza, Southwest, Suite 800
Washington, DC 20024

W. S. Twenhofel, Consultant
Science Applications
International Corp.
820 Estes Street
Lakewood, CO 89215

H. D. Cunningham
General Manager
Reynolds Electrical &
Engineering Co., Inc.
Post Office Box 14400
Mail Stop 555
Las Vegas, NV 89114

A. E. Gurrola
General Manager
Energy Support Division
Holmes & Narver, Inc.
Mail Stop 580
Post Office Box 93838
Las Vegas, NV 89193-3838

T. Hay, Executive Assistant
Office of the Governor
State of Nevada
Capitol Complex
Carson City, NV 89710

J. A. Cross, Manager
Las Vegas Branch
Fenix & Scisson, Inc.
Mail Stop 514
Post Office Box 93265
Las Vegas, NV 89193-3265

John Fordham
Desert Research Institute
Water Resources Center
Post Office Box 60220
Reno, NV 89506

Department of Comprehensive Planning
Clark County
225 Bridger Avenue, 7th Floor
Las Vegas, NV 89155

Lincoln County Commission
Lincoln County
Post Office Box 90
Pioche, NV 89043

Community Planning and Development
City of North Las Vegas
Post Office Box 4086
North Las Vegas, NV 89030

City Manager
City of Henderson
Henderson, NV 89015

Timothy G. Barbour
Science Applications International Corporation
1626 Cole Boulevard, Suite 270
Golden, CO 80401

E. P. Binnall
Field Systems Group Leader
Building 50B/4235
Lawrence Berkeley Laboratory
Berkeley, CA 94720

R. R. Loux, Jr., Executive Director (3)
Nuclear Waste Project Office
State of Nevada
Evergreen Center, Suite 252
1802 North Carson Street
Carson City, NV 89701

Dr. Martin Mifflin
Desert Research Institute
Water Resources Center
Suite 1
2505 Chandler Avenue
Las Vegas, NV 89120

Planning Department
Nye County
Post Office Box 153
Tonopah, NV 89049

Economic Development Department
City of Las Vegas
400 East Stewart Avenue
Las Vegas, NV 89101

Director of Community Planning
City of Boulder City
Post Office Box 367
Boulder City, NV 89005

Commission of the European Communities
200 Rue de la Loi
B-1049 Brussels
BELGIUM

Technical Information Center
Roy F. Weston, Inc.
955 L'Enfant Plaza, Southwest, Suite 800
Washington, DC 20024

Gerald Parker (RW-241)
Office of Civilian Radioactive Waste Management
U.S. Department of Energy
Forrestal Building
Washington, DC 20585

T. H. Isaacs (RW-20)
Office of Civilian Radioactive
Waste Management
U.S. Department of Energy
Forrestal Building
Washington, DC 20585

J. P. Knight (RW-24)
Office of Civilian Radioactive
Waste Management
U.S. Department of Energy
Forrestal Building
Washington, DC 20585

D. H. Alexander (RW-232)
Office of Civilian Radioactive
Waste Management
U.S. Department of Energy
Forrestal Building
Washington, DC 20585

Allen Jelacic (RW-233)
Office of Civilian Radioactive
Waste Management
U.S. Department of Energy
Forrestal Building
Washington, DC 20585

B. J. King, Librarian (2)
Basalt Waste Isolation Project
Library
Rockwell Hanford Operations
Post Office Box 800
Richland, WA 99352

J. R. Rollo
Deputy Assistant Director
for Engineering Geology
U.S. Geological Survey
106 National Center
12201 Sunrise Valley Drive
Reston, VA 22092

D. L. Fraser, General Manager
Reynolds Electrical & Engineering
Co., Inc.
Mail Stop 555
Post Office Box 98521
Las Vegas, NV 89193-8521

Vincent Gong
Technical Project Officer for NNWSI
Reynolds Electrical & Engineering
Co., Inc.
Mail Stop 615
Post Office Box 98521
Las Vegas, NV 89193-8521

J. P. Pedalino
Technical Project Officer for NNWSI
Holmes & Narver, Inc.
101 Convention Center Drive,
Suite 860
Las Vegas, NV 89109

S. D. Murphy
Technical Project Officer for NNWSI
Fenix & Scisson, Inc.
Mail Stop 514
Post Office Box 15408
Las Vegas, NV 89114

Eric Anderson
Mountain West Research-Southwest, Inc.
Phoenix Gateway Center
432 North 44 Street
Suite #400
Phoenix, AZ 85008-6572

S. H. Kale (RW-20)
Office of Civilian Radioactive
Waste Management
U.S. Department of Energy
Forrestal Building
Washington, DC 20585

Judy Foremaster (5)
City of Caliente
Post Office Box 158
Caliente, NV 89008

J. H. Anttonen, Deputy Assistant
Manager for Commercial
Nuclear Waste
Basalt Waste Isolation Project
Office
U.S. Department of Energy
P.O. Box 550
Richland, WA 99352

J. C. Bresee (RW-22)
Office of Civilian Radioactive
Waste Management
U.S. Department of Energy
Forrestal Building
Washington, DC 20585

J. L. Fogg (12)
Technical Information Office
Nevada Operations Office
U.S. Department of Energy
P.O. Box 98518
Las Vegas, NV 89193-8518

R. L. Bullock
Technical Project Officer for NNWSI
Fenix & Scisson, Inc.
Mail Stop 514
P.O. Box 93265
Las Vegas, NV 89193-3265

Robert A. Bellman, Jr.
Science Applications International
Corporation
3349 So. Highland Drive
Suite 403
Las Vegas, Nevada 89109

C. L. West, Acting Director
Office of External Affairs
Nevada Operations Office
U.S. Department of Energy
P.O. Box 98518
Las Vegas, NV 89193-8518

P. K. Fitzsimmons, Director
Health Physics and Environmental
Division
Nevada Operations Office
U.S. Department of Energy
P.O. Box 98518
Las Vegas, NV 89193-8518

Prof. S. W. Dickson
Department of Geological Sciences
Mackay School of Mines
University of Nevada, Reno
Reno, Nevada 89557

Mark P. Board
ITASCA Consulting Group
1313 Fifth Street, SE
Minneapolis, MN 55414

6300 R. W. Lynch
6310 T. O. Hunter
6310 22/124212/47-7694/REP-II/Q3
6310 55/F03.A-2/1/82 (2)
6310 NNWSI CF
6311 A. L. Stevens
6311 C. Mora
6311 V. Hinkel (2)
6312 F. W. Bingham
6313 T. E. Blejwas
6313 B. M. Schwartz
6313 R. M. Zimmerman (5)
6314 J. R. Tillerson
6315 S. Sinnock
6316 R. B. Pope
6332 WMT Library (20)
6430 N. R. Ortiz
3141 S. A. Landenberger (5)
3151 W. L. Garner (3)
8024 P. W. Dean
3154-3 C. H. Dalin (28)
for DOE/OSTI